

The Pennsylvania State University

The Graduate School

Department of Civil and Environmental Engineering

**PHYSICS BASED, INTEGRATED MODELING OF
HYDROLOGY AND HYDRAULICS AT WATERSHED SCALES**

A Thesis in

Civil Engineering

by

Guobiao Huang

© 2006 Guobiao Huang

Submitted in Partial Fulfillment
of the Requirements
for the Degree of

Doctor of Philosophy

August 2006

The thesis of Guobiao Huang was reviewed and approved* by the following:

Gour-Tsyh (George) Yeh
Provost Professor of Civil Engineering
Thesis Co-Advisor
Co-Chair of Committee

Arthur C. Miller
Distinguished Professor of Civil Engineering
Thesis Co-Advisor
Co-Chair of Committee

Christopher J. Duffy
Professor of Civil Engineering

Derek Elsworth
Professor of Geo-Environmental Engineering

Peggy A. Johnson
Professor of Civil Engineering
Head of the Department of Civil and Environmental Engineering

*Signatures are on file in the Graduate School

ABSTRACT

This thesis presents the major findings in the development of the hydrology and hydraulics modules of a first principle, physics-based watershed model (WASH123D Version 1.5). The numerical model simulates water movement in watersheds with individual water flow components of one-dimensional stream/channel network flow, two-dimensional overland flow and three-dimensional variably saturated subsurface flow and their interactions.

Firstly, the complete Saint Venant equations/2-D shallow water equations (dynamic wave equations) and the kinematic wave or diffusion wave approximations were implemented as three solution options for 1-D channel network and 2-D overland flow. Different solution techniques are considered for the governing equations based on physical reasoning and their mathematical property. A characteristic based finite element method is chosen for the hyperbolic-type dynamic wave model. And the Galerkin finite element method is used to solve the diffusion wave model. Careful choice of numerical methods is needed even for the simple kinematic wave model. Since the kinematic wave equation is of pure advection, the backward method of characteristics is used for kinematic wave model. Diffusion wave and kinematic wave approximations are found in many surface runoff routing models. The error in these models has been characterized for some cases of overland flow over simple geometry. However, the nature and propagation of these approximation errors under more complex 2-D flow conditions are not well known. These issues are evaluated within WASH123D with comparison of simulation

results of several example problems. The accuracy of the three wave models for 1-D channel flow was evaluated with several non-trivial (trans-critical flow; varied bottom slopes with frictions and non-prismatic cross-section) benchmark problems (MacDonnell et al., 1997). The test examples for 2-D overland flow include: (1) a simple rainfall-runoff process on a single plane with constant rainfall excess that has a kinematic analytical solution under steep slope condition. A range of bottom slopes (mild, average and steep slope) are numerically solved with the three wave models and compared; (2) Iwagaki (1955) overland flow experiments on a cascade of three planes with shock waves; (3) overland flow in a hypothetical wetland. The applicability of dynamic-wave, diffusion-wave and kinematic-wave models to real watershed modeling is discussed with simulation results from these numerical experiments. It was concluded that kinematic wave model could lead to significant errors in most applications. On the other hand, diffusion wave model is adequate for modeling overland flow in most natural watersheds. The complete dynamic wave equations are required in low-terrain areas such as flood plains or wetlands and many transient fast flow situations.

Secondly, issues about the coupling between surface water and subsurface flow are investigated. In the core of an integrated watershed model is the coupling among surface water and subsurface water flows. Recently, there is a tendency of claiming the fully coupled approach for surface water and groundwater interactions in the hydrology literature. One example is the assumption of a gradient type flux equation based on Darcy's Law (linkage term) and the numerical solution of all governing equations in a single global matrix. We argue that this is only a special case of all possible coupling

combinations and if not applied with caution, the non-physical interface parameter becomes a calibration tool. Generally, there are two cases based on physical nature of the interface: continuous or discontinuous assumption, when a sediment layer exists at the interface, the discontinuous assumption may be justified. As for numerical schemes, there are three cases: time-lagged, iterative and simultaneous solutions. Since modelers often resort to the simplest, fastest schemes in practical applications, it is desirable to quantify the potential error and performance of different coupling schemes. We evaluate these coupling schemes in a finite element watershed model, WASH123D. Numerical experiments are used to compare the performance of each coupling approach for different types of surface water and groundwater interactions. These are in terms of surface water and subsurface water solutions and exchange fluxes (e.g. infiltration/seepage rate). It is concluded that different coupling approaches are justified for flow problems of different spatial and temporal scales and the physical setting of the interface.

Thirdly, The Method of Characteristics (MOC) in the context of finite element method was applied to the complete 2-D shallow water equations for 2-D overland flow. For two-dimensional overland flow, finite element or finite volume methods are more flexible in dealing with complex boundary. Recently, finite volume methods have been very popular in numerical solution of the shallow water equations. Some have pointed out that finite volume methods for 2-D flow are fundamentally one-dimensional (normal to the cell interface). The results may rely on the grid orientation. The search for genuinely multidimensional numerical schemes for 2-D flow is an active topic. We consider the Method of Characteristics (MOC) in the context of finite element method as a good

alternative. Many researchers have pointed out the advantage of MOC in solving 2-D shallow water equations that are of the hyperbolic type that has wave-like solutions and at the same time, considered MOC for 2-D overland flow being non-tractable on complex topography. The intrinsic difficulty in implementing MOC for 2-D overland flow is that there are infinite numbers of wave characteristics in the 2-D context, although only three independent wave directions are needed for a well-posed solution to the characteristic equations. We have implemented a numerical scheme that attempts to diagonalize the characteristic equations based on pressure and velocity gradient relationship. This new scheme was evaluated by comparison with other choice of wave characteristic directions in the literature. Example problems of mixed sub-critical flow/super-critical flow in a channel with approximate analytical solution was used to verify the numerical algorithm. Then experiments of overland flow on a cascade of three planes (Iwagaki 1955) were solved by the new method. The circular dam break problem was solved with different selections of wave characteristic directions and the performance of each selection was evaluated based on accuracy and numerical stability. Finally, 2-D overland flow over complex topography in a wetland setting with very mild slope was solved by the new numerical method to demonstrate its applicability.

Finally, the physics-based, integrated watershed model was tested and validated with the hydrologic simulation of a pilot constructed wetland in South Florida. For this field problem strong surface water and groundwater interactions are a key component of the hydrologic processes. The site has extensive field measurement and monitoring that provide point scale and distributed data on surface water levels, groundwater levels and

physical range of hydraulic parameters and hydrologic fluxes. The uniqueness of this modeling study includes (1) the point scale and distributed comparison of model results with observed data, for example, the spatial distribution of measured vertical flux in the wetland is available; (2) model parameters are based on available field test data; and (3) water flows in the study area consist of 2-D overland flow, hydraulic structures/levees, 3-D subsurface flow and 1-D canal flow and their interactions. This study demonstrates the need and the utility of a physics-based modeling approach for strong surface water and groundwater interactions.

TABLE OF CONTENTS

LIST OF FIGURES.....	xi
LIST OF TABLES.....	xv
ACKNOWLEDGEMENTS	xvi
Chapter 1 Introduction	1
1.1 Overview of the Mathematical Modeling of Watersheds	1
1.2 Physics-based, integrated watershed models	4
1.3 Motivation and Objectives.....	5
1.4 Format.....	8
References.....	9
Chapter 2 On simulating surface water flows with dynamic, diffusion and kinematic waves.....	14
Abstract.....	14
2.1 Introduction.....	15
2.2 Governing Equations	17
2.2.1 Dynamic wave equations	18
2.2.2 Diffusion wave equation.....	20
2.2.3 Kinematic wave equation	21
2.3 Numerical Methods	22
2.3.1 Dynamic wave model	22
2.3.2 Diffusion wave model	27
2.3.3 Kinematic wave model	28
2.4 Comparative examples.....	29
2.4.1 Verification and comparison of steady flow in one-dimensional channels.....	30
2.4.2 Rainfall-runoff over a plane	37
2.4.3 Two-dimensional partial dam break with friction	40
2.4.4 Two-dimensional unsteady flow in a treatment wetland.....	44
2.4.5 Two-dimensional river flow at a river bend	51
2.5 Discussions	54
2.6 Summary and Conclusions	55
Acknowledgements.....	55
References.....	56
Chapter 3 Dynamic Wave Modeling of Two-dimensional Overland Flow using Characteristics-based Finite Element Method	60

Abstract.....	60
3.1 Introduction.....	61
3.2 Governing Equations	65
3.3 Numerical Methods	71
3.3.1 Backward Tracking approach.....	73
3.3.2 Characteristic wave directions.....	73
3.4 Verification and Validation Examples.....	76
3.4.1 Example 1: non-uniform steady flow in a straight channel.....	76
3.4.2 Example 2: Rainfall-runoff on a sloping plane	79
3.4.3 Example 3: Two-dimensional Circular dam break problem	81
3.4.4 Example 4: rainfall-runoff process over a three-plane cascade surface	86
3.4.5 Example 5: Overland flow in a hypothetical wetland	89
3.5 Discussions	97
3.6 Summary and Conclusions	98
Acknowledgements.....	99
References.....	99
 Chapter 4 A Comparative Study of coupling Approaches for Surface water and groundwater interactions.....	 104
Abstract.....	104
4.1 Introduction.....	103
4.2 Governing equations and Interface Conditions.....	107
4.2.1 Channel Network Flow.....	107
4.2.2 Overland Flow	109
4.2.3 Subsurface Flow	111
4.2.4 Interface Conditions	113
4.3 Numerical Schemes for Surface and Subsurface Flow Coupling.....	115
4.3.1 Coupling between overland flow and subsurface flow.....	120
4.3.2 Coupling between channel flow and subsurface flow	121
4.3.3 Coupling Procedure	122
4.4 Numerical Examples.....	125
4.4.1 Coupled overland and subsurface flow: rainfall-runoff process.....	126
4.4.2 Surface water-groundwater interaction in a constructed wetland.....	129
4.4.3 Stream-aquifer interaction	133
4.5 Discussion and Conclusions	138
Acknowledgements.....	139
References.....	139
 Chapter 5 Integrated Modeling of Groundwater and Surface Water interactions in a constructed wetland	 143
Abstract.....	143

5.1 Introduction.....	144
5.2 Site Description	147
5.3 Model Tool: WASH123D.....	152
5.4 Input Data	152
5.5 Model Setup.....	153
5.6 Model Calibration and Validation	158
5.7 Model Simulation Results	159
5.7.1 Surface water flow.....	160
5.7.2 Subsurface Flow	165
5.7.3 Exchange Fluxes.....	173
5.8 Discussions	174
5.9 Summary and Conclusions	175
Acknowledgements.....	176
References.....	176
Chapter 6 Summary and Conclusions.....	181

LIST OF FIGURES

Figure 2-1: Water Depth Profiles for Test problem 1	31
Figure 2-2: Water Depth Profiles for Test Problem 2.....	33
Figure 2-3: Froude Number and bottom slope (%) profiles for Test Problem 2.....	34
Figure 2-4: Bottom slope (-) profiles for Test Problems 1 and 3.....	34
Figure 2-5: Water Depth Profile for Test Problem 3	36
Figure 2-6: Summary of error in the Diffusion wave solutions	37
Figure 2-7: Water depth profiles at time=5000s (numerical solutions by two-dimensional DYW, DIW and KIW)	39
Figure 2-8: Velocity magnitude profiles at time =5000s (numerical solutions by two-dimensional DYW, DIW and KIW).....	40
Figure 2-9: Finite element mesh and initial condition for the dam break problem.....	42
Figure 2-10: Water Depth profiles for Dam Break Problem.....	43
Figure 2-11: Comparison of Computed water depth hydrographs for Dam Break Problem.....	44
Figure 2-12: Finite Element mesh and Topography.....	46
Figure 2-13: Boundary Conditions and Vegetation, Observation point.....	47
Figure 2-14: Boundary Condition data applied in the wetland example	48
Figure 2-15: Comparison of Observed and Computed Stages.....	49
Figure 2-16: Velocity Magnitude and Vector plots (DIW and DYW solutions).....	50
Figure 2-17: Layout of the River bend example	51
Figure 2-18: Computed water depth and velocity magnitude (DYW).....	52
Figure 2-19: Difference in computed water depth (DIW – DYW).....	53
Figure 2-20: Difference in computed velocity magnitude (DIW – DYW).....	54
Figure 3-1: Bottom Slope for Example 1.....	78

Figure 3-3: Computed and Exact Water Depth along the Channel.....	79
Figure 3-4: Outflow Hydrograph (Analytical vs. numerical solutions)	81
Figure 3-5: Initial Water Depth of Circular Dam-break Problem.....	82
Figure 3-6: Water depth at time = 0.69 sec.....	83
Figure 3-7: Impact of Selected Characteristic Direction on Computed Water Depth.....	85
Figure 3-8: Computed and Observed Discharge Hydrograph for the three-plane cascade with rainfall duration of 30 s	87
Figure 3-9: Computed and Observed Discharge Hydrograph for the three-plane cascade with rainfall duration of 20 s	88
Figure 3-10: Computed and Observed Discharge Hydrograph for the three-plane cascade with rainfall duration of 10 s	89
Figure 3-11: Model Domain Layout	90
Figure 3-12: Variation of Land Surface Elevations (cm).....	91
Figure 3-13: Discharge Hydrograph at the Outlet.....	93
Figure 3-14: Water Depth Distribution at time =64,000 sec (m).....	94
Figure 3-15: Velocity Magnitude at time = 64,000 sec	95
Figure 3-16: Computed water depth at (250,200) obtained by using different wave directions.....	96
Figure 3-17: Computed velocity magnitude at (250,200) obtained by using different wave directions	97
Figure 4-1: Flow interactions between overland regime and subsurface media.	114
Figure 4-2: 2D overland and 3D subsurface finite element mesh for the coupling example.....	116
Figure 4-3: Iterative coupling loop between overland and subsurface flow	124
Figure 4-4: Flow coupling procedure of WASH123D.....	125
Figure 4-5: Layout of Example 1	127

Figure 4-6: Comparison of Outflow Hydrographs.....	128
Figure 4-7: Comparison of Total Exchange Fluxes.....	129
Figure 4-8: Schematic layout of the wetland example.....	131
Figure 4-9: Comparison of computed water levels.....	132
Figure 4-10: Three-dimensional finite element mesh.....	135
Figure 4-11: Pressure head distribution at x=500 m (time=14200 seconds).....	136
Figure 4-12: Pressure head distribution at y=430 m (time=14200 seconds).....	137
Figure 4-13: Computed Discharge hydrographs (coupled flow with different approaches).....	138
Figure 5-1: Location Map of ENR (SFWMD, 2000).....	149
Figure 5-2 Schematic Map of ENR (Modified after SFWMD, 2000).....	150
Figure 5-3: Vegetation types as simulated in the model.....	155
Figure 5-4: Finite Element Meshes for ENR Basin with Soil Types.....	158
Figure 5-5: Simulated and Observed Surface Water Levels at ENR101.....	162
Figure 5-6: Simulated and Observed Surface Water Levels at ENR301.....	163
Figure 5-7: Simulated and Observed Surface Water Levels at ENR203.....	164
Figure 5-8: Simulated and Observed Surface Water Levels at ENR401.....	165
Figure 5-9: Simulated and Observed Groundwater Levels at ENR102GW.....	167
Figure 5-10: Simulated and Observed Groundwater Levels at ENR303GW.....	168
Figure 5-11: Simulated and Observed Groundwater Levels at ENR203GW.....	169
Figure 5-12: Simulated and Observed Groundwater Levels at ENR401GW.....	170
Figure 5-13: Simulated Total Head Distribution (ft NGVD) on 2/4/1998.....	171
Figure 5-14: Location of Transects and Lithology of ENR (after Harvey et al., 2002).....	172

Figure 5-15: Total Head Distribution (2/4/1998) for two transects of ENR (ft
NGVD). 173

Figure 5-16: Distribution of Computed Vertical Flux (cm/day) (7/10/1998)..... 174

LIST OF TABLES

Table 1-1. Comparison of watershed models 8

Table 5-1. Hydraulic properties for Subsurface Flow158

Table 5-2. Summary of Simulation errors in Surface Water Levels163

Table 5-3. Summary of Simulation errors in Groundwater Levels168

ACKNOWLEDGEMENTS

I am very grateful for the support and encouragement of Dr. Gour-Tsyh Yeh throughout my graduate study.

I would also like to thank my other committee members, Dr. Arthur Miller, Dr. Christopher Duffy and Dr. Derek Elsworth for their time and effort on this thesis.

I am indebted to my family for their support and patience that have enabled me to successfully complete this work.

Last but not least, University of Central Florida (UCF) provided resources and facilities that were needed for my research in 2000 through 2002 when I conducted my research off the Penn State University (PSU) campus with my thesis Advisor, Dr. Gour-Tsyh Yeh who moved from Penn State to UCF in August 2000.

Chapter 1

Introduction

1.1 Overview of the Mathematical Modeling of Watersheds

A watershed model is an integrated representation of nearly any hydrological process of the hydrologic cycle; major processes within a watershed include precipitation, interception, evapotranspiration, infiltration, overland flow, channel/stream flow, and subsurface flow.

Watershed models are essential tools used to address various water resources and environmental protection problems (Singh and Frevert, 2006). The mathematical modeling of watersheds has been extensive since the creation of modern digital computers in the 1950s (Singh and Woolhiser, 2002). There is a plethora of all kinds of watershed models, ranging from purely empirical, black box type models to physics based, integrated models.

Many lumped or semi-distributed watershed models are similar in model structure and principle. The well-known conceptual Stanford watershed model (Crawford and Linsley, 1966) and its successor, HSPF (Donigian and Imhoff, 2006), are representative

of these watershed model types. The model structure is based on water balance in predefined conceptual storage zones, and model parameters are often without clear physical meaning. The limitation of lumped watershed models is well known - model parameters must be calibrated with historic data; estimated parameters are not transferable and distributed information on flow velocity and water depth cannot be provided for water quality modeling.

The development of watershed models is often guided by an intentional application and modeling objective. When information on the total quantity and timing of surface runoff at the watershed outlet (such as in flood control) is enough for the modeling objective, the traditional lumped watershed models can be used if historic data is available, in order to calibrate the model. But in other cases, such as non-point source pollution, soil erosion, land use effect, climate change, etc., users need information about the flow field (water velocity and depth distribution) or the timing of any extensive alterations to the watershed system from land use or deforestation; from here, a physics based, distributed hydrologic model is necessary. There are also great needs in real-world water management for such integrated models. For example, the importance of surface water and groundwater interaction has led to integrated models developed by local government agencies in South Florida (Lal et al., 2005) and California (LaBolle et al., 2003).

Since Freeze and Harlan published their blueprint for a three-dimensional model of watersheds (Freeze and Harlan, 1969) more than three decades ago, there has been much progress in this field. The SHE and its derivatives MIKE SHE are very popular in

Europe (Abbott et al., 1986). In the United States, the CASC2D and its newest version GSSHA (Downer, 2004) is a finite difference code that can do integrated modeling in a less rigorous approach. There are some model codes developed around the popular MODFLOW groundwater model [for example, MODBRANCH (Swain and Wexler (1996), MOD-HMS (Panday and Huyakorn (2004))].

There has been much debate and controversy on physics based, distributed watershed models (e.g., Grayson et al., 1992; Woolhiser, 1996; Beven, 2002 and Loague and VanderKwaak, 2004). Beven (2002) concluded that a radical change in paradigm is needed for watershed models. The Freeze and Harlan (1969) blueprint is however, flawed, and will eventually be abandoned. For instance, a major flaw is related to both scale (the point-scale mechanistic partial differential equations may not be valid at model grid scale) and equifinality (model over-parameterization).

Reggiani et al. (1998, 1999, 2000 and 2005) offer an alternative watershed model structure based on the discretization of a watershed into spatial units, termed 'representative elementary watersheds' (REWs). The point-scale conservation equations for mass, momentum, and energy is integrated over a sub-watershed. This flux-based formulation approach can be traced back to earlier research by Duffy (1996). The difficulties in determining hydrological fluxes are a major problem and, if the size of REWs is very small, it will run into the same scale problem as the point-scale, physics based models. On the other hand, if the size of REWs is large, the physical meaning of

state variables, such as flow velocity, pressure head, and water depth, are only nominal at best.

Young (2003) offers another alternative, termed the ‘data based mechanistic approach’; its use is intended for hydrologic models. It is said to be a stochastic model with a top-down approach that can incorporate physical reasoning into the statistical model. This approach is better suited for practical application (e.g., real-time flood forecasting) and not for what-if type explanation-oriented modeling.

In the proceeding chapters, the Freeze and Harlan (1969) blueprint of a physics based, three-dimensional watershed model (as a viable modeling approach for integrated watershed models) will be explored. The increasing availability of spatially distributed hydrological data through remote sensing, radar rainfall, GIS, and new measurement techniques also support such physics-based distributed models.

1.2 Physics-based, integrated watershed models

The mechanistic, process-oriented modeling of fluid flow in watersheds can be conveniently divided into flow component models and coupling mechanism. There have been extensive studies on component models (for example, overland flow models, channel network flow models, and subsurface flow models) and among them; the flow component coupling is another important issue.

Water flow components in a watershed are essentially comprised of surface water and subsurface flow, where ‘surface water flows’ include overland and channel flow. There are at least three distinct runoff generation mechanisms. The first one is the ‘Hortonian overland flow mechanism’, usually called ‘infiltration excess mechanism’. This has been the dominant concept in the current generation of surface hydrologic models. Under this paradigm, overland flow was extensively modeled, but the infiltration and subsurface flow components are treated empirically, as a water sink/loss. Field observation and further research have demonstrated that Hortonian overland flow is rare and of little impact in humid, forested regions, while the subsurface storm flow mechanism is the major contribution to runoff. In this case, most rainfall is to be absorbed by the soil, and subsurface flow becomes an important contribution to stream flow. Another runoff generation mechanism is called saturated excess, which represents the runoff process in place such as wetlands where the soil is saturated most of the time. Only a physics-based, integrated watershed models can simulate all these runoff generation mechanisms in a single model.

1.3 Motivation and Objectives

The watershed modeling in the past 30 years has been focused on individual flow components, e.g., overland flow, channel flow, groundwater flow, etc. Most overland flow modeling studies did not couple with subsurface flow and, in subsurface hydrology, the surface water processes were often only considered as a simple source/sink. When

coupling is considered, weak coupling or artificially created linkage terms are often used for flux-exchange calculations.

Freeze and Harlan (1969) were the first to develop a blueprint of the physically based watershed model. Smith and Woolhiser (1972) were one of the first to apply the one-dimensional Richards' equation for unsaturated flow in their overland model with a 1-D kinematic wave equation. Akan and Yen (1981) coupled a two-dimensional subsurface flow component with overland flow. One of the first attempts to build a comprehensive numerical model of a watershed based on the Freeze and Harlan blueprint is the SHE model in Europe (Abbott et al., 1986). In the SHE watershed model, the unsaturated zone is represented with one-dimensional Richards' equation. In USA, the focus has been toward a practical engineering application, so most of the watershed models are lumped. Among the few physically based models developed are CASC2D by Julien et al. (1995) and KINEROS by Woolhiser et al. (1990). CASC2D included the diffusion wave approximation of overland flow and channel flow; infiltration is based on the Green and Ampt model and the explicit finite difference method is used. KINEROS is based on the kinematic wave model for overland flow routing with empirical infiltration equations.

This thesis research concerns with the physics based, integrated mathematical modeling of watershed hydrology and hydraulics. The computational aspect of physics-based, integrated watershed models is investigated in term of proper selection of governing equations, coupling approaches, and numerical methods, etc. The hydrology

and hydraulics modules of the watershed model are particularly designed as the basis for modeling transport of sediments and pollutant at watershed scales.

Some recently developed physics-based, integrated watershed models are briefly compared in Table 1-1. All of these models apply Richards' equation for subsurface flow; however, the governing equations for surface flow, numerical methods and coupling approach are quite different. Therefore, several critical issues are still in need of further study, even though the Freeze and Harlan (1969) blueprint was proposed more than three decades ago.

Table 1-1: Comparison of watershed models

Code	Channel flow	Overland flow	Coupling between Surface and Subsurface Flows	Reference
GSSHA	DIW (FDM)	DIW (FDM)	Time-lagged	Downer and Orgden (2004)
INHM		DIW (CVFEM)	Discontinuous with linear Linkage-terms	VanderKwaak(1999)
MODHMS	DIW (FDM)	DIW (FDM)	Discontinuous with linear Linkage-terms	Panday and Huyakorn (2004)
Morita and Yen		DIW(FDM)	Continuous	Morita and Yen (2002)
WASH123D	DYW (MOC) DIW (FEM, ELM) KIW (ELM)	DYW (MOC) DIW (FEM, ELM) KIW (ELM)	Continuous or Discontinuous with general linkage terms (linear or nonlinear)	Yeh et al. (2006)

Note: DIW: diffusion wave; DYW: dynamic wave; KIW: kinematic wave; ELM: Eulerian-Lagrangian method; CVFEM: control volume finite element; FDM: finite difference method; MOC: method of characteristics.

1.4 Format

Chapter 1 is an introduction and review of state-of-the art physics based, integrated watershed modeling. The major findings from this thesis research are presented in the form of four journal articles, self titled as Chapters 2 through 5. Chapter 2 regards the accuracy and applicability of dynamic, diffusion, and kinematic wave models for surface runoff; it is based on a paper prepared for *Journal of Hydrologic Engineering, ASCE*. Chapter 3 regards dynamic wave modeling of overland flow, with a characteristics-based finite element method; it is based a paper prepared for the *International Journal of Numerical Methods in Fluids*. Chapter 4 is a comparative study of coupling approaches for surface water and groundwater interactions based on a paper

intended for submission to the *Journal of Hydrology*. Chapter 5 is an application on surface water and groundwater interactions in a constructed wetland, based on a paper prepared for possible publication on *Journal of Hydrologic Engineering, ASCE*. The last chapter, Chapter 6, is summary of work presented and a presentation of suggested research and future applications.

References

Abbot M.B., Bathurst J.C., Cunge J.A., O'Connell P.E., Rasmussen J. (1986), "An introduction to the European Hydrologic System-Systeme Hydrologique Europeen, SHE, 2: Structure of a physically-based, distributed modeling system." *Journal of Hydrology* **87**: 61–77.

Akan AO, Yen BC. (1981), Mathematical model of shallow water flow over porous media. *Journal of Hydraulics Division, American Society of Civil Engineers* 107: 479–494.

Beven K., (2002), Towards an alternative blueprint for a physically based digitally simulated hydrologic response modeling system, *Hydrological Processes*, 16, 189-202.

- Crawford NH, Linsley RS., (1966), *Digital Simulation in Hydrology: The Stanford Watershed Model IV*. Technical Report no. 39, Department of Civil Engineering, Stanford University, Palo Alto, CA.
- Donigian, A.S. and J. Imhoff. (2006), Chapter 2: History and evolution of watershed modeling derived from the Stanford Watershed model, in *Watershed Models*. Eds. By Singh VP and Frevert, CRC Press, Boca Raton, FL.
- Downer, C.W. and Ogden, F.L., (2004), GSSHA: Model to simulate diverse stream flow producing processes. *Journal of Hydrological Engineering*, 9 (3): 161-174.
- Duffy C.J. (1996), “A two-state integral-balance model for soil moisture and groundwater dynamics in complex terrain.” *Water Resources Research* **32**: 2421–2434.
- Freeze R.A. and Harlan R.L., (1969) “Blueprint for a physically-based digitally-simulated hydrologic response model.” *Journal of Hydrology*, 9, pp. 237–258.
- Grayson RB, Moore ID, McMahon TA. (1992), Physically-based hydrologic modelling. 2. Is the concept realistic? *Water Resources Research* 28: 2659.
- Julien, P. Y., Saghafian, B., and Ogden, F. L. (1995), “Raster-based hydrologic modeling of spatially varied surface runoff.” *Water Resour. Bull.*, 31(3), 523–536.

LaBolle EM, Ahmed AA, Fogg GE. (2003), Review of the Integrated Groundwater and Surface-Water Model (IGSM), *Ground Water*. 2003 Mar-Apr;41(2):238-46.

Lal W., Van Zee R. and Belnap M. (2005), Case Study: Model to Simulate Regional Flow in South Florida. *J. Hydr. Engrg.*, Volume 131, Issue 4, pp. 247-258 (April 2005).

Loague K, VanderKwaak JE. (2004), Physics-based hydrologic response simulation: platinum bridge, 1958 Edsel or useful tool. *Hydrological Processes* 18: 2949–2956.

Loague K, VanderKwaak JE.(2002), Simulating hydrologic response for the R-5 catchment: comparison of two models and the impact of the roads. *Hydrological Processes* 16: 1015–1032.

Panday S. and Huyakorn P.S. (2004), A fully coupled physically-based spatially-distributed model for evaluating surface/subsurface flow. *Advances in Water Resources*, 27 (2004) 361–382

Reggiani P., Sivapalan M., Hassanizadeh S.M. (1998), A unifying framework for watershed thermodynamics: balance equations for mass, momentum, energy and entropy and the second law of thermodynamics. *Advances in Water Resources* **23**(1): 15–40.

- Reggiani P, Hassanizadeh SM, Sivapalan M, Gray WG. (1999), A unifying framework for watershed thermodynamics: constitutive relationships. *Advances in Water Resources* **23**(1): 15–40.
- Reggiani, P., M. Sivapalan, and S. M. Hassanizadeh (2000), Conservation equations governing hillslope responses, *Water Resour. Res.*, 38(7), 1845– 1863.
- Reggiani, P., and T. H. M. Rientjes (2005), Flux parameterization in the representative elementary watershed approach: Application to a natural basin, *Water Resour. Res.*, 41, W04013, doi:10.1029/2004WR003693.
- Singh V.P. and Frevert D. K., editors. (2006), *Watershed Models*. CRC Press, Boca Raton, FL USA.
- Singh V. P. and Woolhiser D.A., (2002), Mathematical modeling of watershed hydrology, *Journal of Hydrologic Engineering*, Vol. 7, No.4, July 1, 2002.
- Swain ED, Wexler EJ, (1996), A coupled surface-water and groundwater flow model for simulation of stream–aquifer interaction. US Geological Survey Techniques of water-resources investigations, Book 6; 1996. 125 p [chapter A6].

- VanderKwaak, J. (1999), “Numerical simulation of flow and chemical transport in integrated surface-subsurface hydrologic systems.” Ph.D. Thesis, University of Waterloo, Waterloo, Canada. 217 pp.
- Woolhiser, D. A., Smith, R. E., and Goodrich, D. C. (1990), “KINEROS—A kinematic runoff and erosion model: Documentation and user manual.” Rep. No. ARS-77, USDA, Washington, D.C.
- Woolhiser, D.A. (1996), Search for physically based runoff model – a hydrologic El Dorado? *Journal of Hydrologic Engineering*, Vol. 122, 122-129.
- Yeh, G.T., G. B. Huang, H. P. Cheng, F. Zhang, H. C. Lin, E. Edris, and D. Richards. (2006), Chapter 9: A first principle, physics-based watershed model: WASH123D, in *Watershed Models*. Eds. By Singh VP and Frevert, CRC Press, Boca Raton, FL.
- Young, P. C. (2003), Top-down and data-based mechanistic modelling of rainfall-flow dynamics at the catchment scale, *Hydrol. Processes*, 17, 2195-2217.

Chapter 2

On simulating surface water flows with dynamic, diffusion and kinematic waves

Abstract

The complete Saint Venant equations/two-dimensional shallow water equations (dynamic wave equations) and the kinematic wave or diffusion wave approximations were implemented for one-dimensional channel network flow and two-dimensional overland flow in a watershed model, WASH123D. Careful choice of numerical methods is needed even for the simple kinematic wave model. Since the kinematic wave equation is of pure advection, the backward method of characteristics is used for the kinematic wave model. A characteristics based finite element method is chosen for the hyperbolic-type dynamic wave model. The Galerkin finite element method is used to solve the diffusion wave model. Diffusion wave and kinematic wave approximations are found in many surface runoff routing models. The error in these models has been characterized as overland/channel flow over simple geometry in some cases. However, the nature and propagation of these approximation errors under complex two-dimensional flow conditions are not well known. These issues are evaluated within WASH123D by comparison of simulation results for several example problems. The accuracy of the three wave models for one-dimensional channel flow was evaluated with several non-trivial (trans-critical flow; varied bottom slopes with frictions and non-prismatic cross-section)

benchmark problems, and for two-dimensional overland flow with dam-break problems and a wetland example. The applicability of dynamic-wave, diffusion-wave and kinematic-wave models to real watershed modeling is discussed with simulation results from these numerical experiments. It was concluded that kinematic wave model could lead to significant errors in most applications. On the other hand, the diffusion wave model is adequate for modeling overland flow in most natural watersheds. The complete dynamic wave equations are more accurate in low-terrain areas, such as flood plains, are more suitable for river flow at river bends and transient fast flow situations.

2.1 Introduction

Diffusion wave and kinematic wave approximations are found in many surface runoff flow routing models. The error in these models has been characterized for some cases of overland flow over simple, often one-dimensional geometry. Ponce et al. (1978) presented a criterion for the applicability of kinematic and diffusion waves models in surface flow derived from theoretical analysis on the linearized Saint Venant equations. Govindaraju et al. (1988, 1990) studied diffusion wave models for steady overland flow and approximate analytical solutions. Parlange et al. (1990) derived and estimated errors in kinematic and diffusion wave models for steady state overland flow on a single plane by comparing numerical simulations with numerical solutions of the full Saint Venant equations; they demonstrated that, in case where a kinematic wave is not accurate, use of a diffusion wave would not produce a noticeable difference. Through the analysis of relative magnitude of the acceleration terms in the governing equations, Richardson and

Julien (1994) concluded that diffusion wave approximation of overland flow is not suitable for supercritical flow condition. Singh and coworkers (e.g., Singh et al., 2005 Moramarco and Singh; 2002 and Singh and Aravamuthan, 1995) published a series of papers on the accuracy and error estimation of diffusion and kinematic waves overland flow on a plane by numerical experiments and concluded that diffusion wave approximation is fairly accurate for most overland flow conditions. Tayfur et al. (1993) compared numerical solutions of dynamic, diffusive and kinematic wave models for two-dimensional overland flow on rough surfaces with an average steep slope of 0.086; the results are essentially the same due to the steep slope. However, the nature and propagation of these approximation errors under more complex two-dimensional surface water flow conditions are not well known.

While diffusion wave approximation is a widely applied model in many current watershed models, kinematic wave approximation is prevailing in many current watershed models in research and practice (for example, HEC-HMS [Hydrologic Engineering Center(HEC), 2000], HSPF[Donigian and Imhoff, 2006], SWMM[Metcalf and Eddy et al. 1971] and some new GIS-based watershed models [e.g., Fortin and Turcotte et al., 2001; Olivera and Maidment, 1999]). This is attributed to its simplicity and ease of numerical solutions for kinematic wave models. However, significant error could be possible for kinematic wave models.

For one-dimensional channel flow, the fully dynamic wave approach has been implemented in many well-established stand-alone stream network flow models. These

dynamic wave channel network flow models are usually externally linked to traditional lumped watershed models for practical application of flow routing. Again, diffusion wave and kinematic wave approximations are popular in channel network flow module of most integrated watershed models.

The complete Saint Venant equations/two-dimensional shallow water equations (dynamic wave equations) and the kinematic wave or diffusion wave approximations were all implemented for one-dimensional channel network flow and two-dimensional overland flow in a watershed model, WASH123D. We will present some numerical experiments on these three options for overland flow and channel flow and demonstrate the potential errors in using one single wave model for all flow situations.

The research objectives include:

1. Apply accurate and stable numerical solutions of dynamic, kinematic and diffusion wave models;
2. Demonstrate applicability and limitations of kinematic and diffusion wave models by comparison with fully dynamic wave model through numerical experiments.

2.2 Governing Equations

The governing equations for surface water flows in a watershed can be derived from the conservation of water mass and momentum. The depth-averaged two-

dimensional shallow water equations and the cross-section-averaged one-dimensional Saint Venant equations are considered accurate representations of two-dimensional overland flow and one-dimensional channel network flow, respectively. Only equations for two-dimensional overland flow are described in detail, as follows.

2.2.1 Dynamic wave equations

The depth-averaged 2D shallow water equations for overland flow in matrix form are:

$$\frac{\partial U}{\partial t} + \frac{\partial F_x}{\partial x} + \frac{\partial F_y}{\partial y} = G \quad (1)$$

The conservative variables are $U=(h, uh, vh)$; h is water depth; u is the velocity component in the x -direction; v is the velocity component in the y -direction, respectively.

The flux vector F has two components F_x and F_y :

$$F_x = \begin{pmatrix} uh \\ u^2h + \frac{gh^2}{2} \\ uvh \end{pmatrix}, \quad F_y = \begin{pmatrix} vh \\ uvh \\ v^2h + \frac{gh^2}{2} \end{pmatrix}, \quad G = \begin{pmatrix} S \\ gh(S_{0x} - S_{fx}) \\ gh(S_{0y} - S_{fy}) \end{pmatrix} \quad (2)$$

where $S = R - E - I + SS$, is the source/Sink term as a result of rainfall (R), evapotranspiration (E) and infiltration (I), and human-induced source/sink (SS), etc. The eddy turbulent term, momentum exchange flux, surface shear stress (wind effect), etc. have been omitted from the momentum equations for the sake of simplicity of presentation.

The bed slopes are defined as:

$$S_{0x} = -\frac{\partial Z_0}{\partial x}, \quad S_{0y} = -\frac{\partial Z_0}{\partial y} \quad (3)$$

where g is gravitational acceleration and Z_0 is the bed elevation above a datum.

The friction slopes can be approximated by the Manning's equation as:

$$S_{fx} = \frac{n^2 u \sqrt{u^2 + v^2}}{h^{4/3}}, \quad S_{fy} = \frac{n^2 v \sqrt{u^2 + v^2}}{h^{4/3}} \quad (4)$$

where n is the Manning's roughness coefficient.

Boundary conditions for two-dimensional dynamic wave models (DYW) of overland flow are based on physical flow conditions at the boundary; there can be zero, one or two boundary conditions at the inflow and outflow boundaries based on supercritical, subcritical flow or critical flow conditions.

For one-dimensional channel network flow, Equations (1) through (4) can be applied with all variables in the y -direction being null for prismatic, rectangular cross-section channels. For channels with arbitrary shape cross-sections, the water depth (h) is replaced with the cross-sectional area (A) and some terms need to be adjusted.

2.2.2 Diffusion wave equation

The diffusion wave approximation (DIW) is based on simplified forms of the momentum equations that ignore the inertial terms but keep the pressure gradient term in Equation (1):

$$U = (h, 0, 0), \quad F_x = \begin{pmatrix} uh \\ \frac{gh^2}{2} \\ 0 \end{pmatrix}, \quad F_y = \begin{pmatrix} vh \\ 0 \\ \frac{gh^2}{2} \end{pmatrix}, \quad G = \begin{pmatrix} S \\ gh(S_{0x} - S_{fx}) \\ gh(S_{0y} - S_{fy}) \end{pmatrix} \quad (5)$$

It can be easily demonstrated that by combining the continuity equation with the simplified momentum equations, the diffusion wave equation is a partial differential equation of parabolic type with only one unknown variable (water stage, $H=h+Z_0$):

For two-dimensional overland flow:

$$\frac{\partial H}{\partial t} - \nabla \cdot (K \nabla H) = S \quad \text{where} \quad K = -\frac{a}{n} \frac{h^{5/3}}{\left[1 + (\nabla Z_0)^2\right]^{2/3} \sqrt{|\nabla H|}} \quad (6)$$

and for one-dimensional channel flow:

$$B \frac{\partial H}{\partial t} - \frac{\partial}{\partial x} \left(K \frac{\partial H}{\partial x} \right) = S \quad \text{where} \quad K = -\frac{a}{n} \frac{AR^{2/3}}{\left[1 + \left(\frac{\partial Z_0}{\partial x}\right)^2\right]^{2/3} \sqrt{\left|\frac{\partial H}{\partial x}\right|}} \quad (7)$$

where A is the cross-sectional area and R is the hydraulic radius, $B(x, h)$ is the top-width of the cross-section area. The variable a is a unit conversion factor ($a=1.0$ for SI unit and

a=1.486 for US Customary units). The term: $1 + \left(\frac{\partial Z_0}{\partial x}\right)^2$ can be considered as a factor that accounts for increased shear stress caused by a sloping land surface.

Both upstream (inflow) and downstream (outflow) boundary conditions are needed for the diffusion wave model. For two-dimensional overland flow, usually, no-flow condition is applied at the upstream watershed boundary and at the watershed outlet, a specified water stage or a stage-discharge rating curve (e.g., critical flow or zero-depth gradient condition) are imposed.

2.2.3 Kinematic wave equation

The pressure gradients are also dropped for the kinematic wave (KIW) and the momentum equations are further simplified as:

$$S_0 = S_f \quad (8)$$

Equation (8) combined with the continuity equation lead to the kinematic wave equation that represents the pure advection of water depth with source/sink terms.

The two-dimensional kinematic wave equation for overland flow can be written as:

$$\frac{\partial h}{\partial t} + u \frac{\partial h}{\partial x} + v \frac{\partial h}{\partial y} + h \frac{\partial u}{\partial x} + h \frac{\partial v}{\partial y} = S, \quad u = \frac{\sqrt{|S_{0x}|}}{n} h^{2/3}, \quad v = \frac{\sqrt{|S_{0y}|}}{n} h^{2/3} \quad (9)$$

By replacing the velocity (u,v) with the velocity formula, the kinematic wave equation is in a form of pure advection of water depth (h) with source term. Since kinematic wave contain only one characteristic in the downstream direction, no downstream boundary is needed. Therefore, backwater effect cannot be considered.

2.3 Numerical Methods

2.3.1 Dynamic wave model

The widespread application of diffusion and kinematic wave approximation of surface water flow routing in physics-based watershed models can be attributed to the fact that, numerical solutions of the full shallow water equations, under complex topography and transient, distributed forcing (e.g., rainfall and infiltration), are computationally intensive; furthermore, it suffers from numerical stability and convergence problems. Indeed, in rainfall-runoff/overland flow simulations, the full dynamic wave equations are rarely applied and, when applied, they are limited to small-scale geometry (experiment plots or single hillslopes) (for an example, see Chow and Ben-Zvi, 1973; Zhang and Cundy, 1989; Fielder and Ramirez, 2000). Therefore, making a careful and judicious choice regarding the numerical method for a dynamic wave model is critical. We consider the characteristics-based finite element method to be a natural choice based on flow physics of the full shallow water equations.

Comparing to the conservative form [Equation (1)], the primitive form is more revealing for the intrinsic physical property of the shallow water equations and amendable to advective schemes. The governing equations written in the primitive form:

$$\frac{\partial h}{\partial t} + u \frac{\partial h}{\partial x} + h \frac{\partial u}{\partial x} + v \frac{\partial h}{\partial y} + h \frac{\partial v}{\partial y} = S \quad (10)$$

$$\frac{\partial u}{\partial t} + g \frac{\partial h}{\partial x} + u \frac{\partial u}{\partial x} + v \frac{\partial u}{\partial y} = g(S_{0x} - S_{fx}) - \frac{uS}{h} \quad (11)$$

$$\frac{\partial v}{\partial t} + g \frac{\partial h}{\partial y} + u \frac{\partial v}{\partial x} + v \frac{\partial v}{\partial y} = g(S_{0y} - S_{fy}) - \frac{vS}{h} \quad (12)$$

Equations (10) through (12) can be written in matrix form as

$$\frac{\partial \mathbf{E}}{\partial t} + \mathbf{A}_x \frac{\partial \mathbf{E}}{\partial x} + \mathbf{A}_y \frac{\partial \mathbf{E}}{\partial y} = \mathbf{R};$$

$$\mathbf{E} = \{h \ u \ v\}^T, \quad \mathbf{A}_x = \begin{bmatrix} u & h & 0 \\ g & u & 0 \\ 0 & 0 & u \end{bmatrix}, \quad \mathbf{A}_y = \begin{bmatrix} v & 0 & h \\ 0 & v & 0 \\ g & 0 & v \end{bmatrix}, \quad \mathbf{R} = \begin{Bmatrix} S \\ g(S_{0x} - S_{fx}) - \frac{uS}{h} \\ g(S_{0y} - S_{fy}) - \frac{vS}{h} \end{Bmatrix} \quad (13)$$

For an arbitrary wave propagation direction $\mathbf{k} = (k_x, k_y) = (\cos \theta, \sin \theta)$; θ is the angle of the wave direction from x-direction, let the matrix \mathbf{B} be the linear combination of the matrices \mathbf{A}_x and \mathbf{A}_y as follows

$$\mathbf{B} = \mathbf{A} \cdot \mathbf{k} = \mathbf{A}_x \cos \theta + \mathbf{A}_y \sin \theta = \begin{bmatrix} u \cos \theta + v \sin \theta & h \cos \theta & h \sin \theta \\ g \sin \theta & u \cos \theta + v \sin \theta & 0 \\ g \sin \theta & 0 & u \cos \theta + v \sin \theta \end{bmatrix} \quad (14)$$

The three eigenvalues of matrix \mathbf{B} are

$$\lambda_1 = u \cos \theta + v \sin \theta, \quad \lambda_2 = u \cos \theta + v \sin \theta + c, \quad \text{and} \quad \lambda_3 = u \cos \theta + v \sin \theta - c \quad (15)$$

The wave celerity is defined as $c = \sqrt{gh}$. Accordingly, the primitive form can be recast in the characteristic form by using the eigenvectors associated with matrix \mathbf{B}

$$\frac{\partial \mathbf{W}}{\partial t} + \begin{bmatrix} u & 0 & 0 \\ 0 & u + c \cos \theta & 0 \\ 0 & 0 & u - c \cos \theta \end{bmatrix} \frac{\partial \mathbf{W}}{\partial x} + \begin{bmatrix} v & 0 & 0 \\ 0 & v + c \sin \theta & 0 \\ 0 & 0 & v - c \sin \theta \end{bmatrix} \frac{\partial \mathbf{W}}{\partial y} = - \begin{Bmatrix} S_1 \\ S_2 \\ S_3 \end{Bmatrix} + \mathbf{L}^{-1} \mathbf{R} \quad (16)$$

$$\begin{Bmatrix} S_1 \\ S_2 \\ S_3 \end{Bmatrix} = \begin{Bmatrix} g \left(\frac{\partial h}{\partial x} \sin \theta - \frac{\partial h}{\partial y} \cos \theta \right) \\ \frac{c}{g} \left[\frac{\partial u}{\partial x} \sin^2 \theta + \frac{\partial v}{\partial y} \cos^2 \theta - \left(\frac{\partial u}{\partial y} + \frac{\partial v}{\partial x} \right) \cos \theta \sin \theta \right] \\ -\frac{c}{g} \left[\frac{\partial u}{\partial x} \sin^2 \theta + \frac{\partial v}{\partial y} \cos^2 \theta - \left(\frac{\partial u}{\partial y} + \frac{\partial v}{\partial x} \right) \cos \theta \sin \theta \right] \end{Bmatrix} \quad (17)$$

The characteristic variable vector \mathbf{W} is defined as

$$\mathbf{W} = \begin{Bmatrix} W_1 \\ W_2 \\ W_3 \end{Bmatrix}^T = L^{-1} E = \begin{bmatrix} 0 & \sin \theta & -\cos \theta \\ \frac{1}{c} & \frac{\cos \theta}{g} & \frac{\sin \theta}{g} \\ -\frac{1}{c} & \frac{\cos \theta}{g} & \frac{\sin \theta}{g} \end{bmatrix} \begin{Bmatrix} h \\ u \\ v \end{Bmatrix} = \begin{Bmatrix} \frac{u \sin \theta - v \cos \theta}{g} \\ \frac{u \cos \theta + v \sin \theta + c}{g} \\ \frac{u \cos \theta + v \sin \theta - c}{g} \end{Bmatrix} \quad (18)$$

where W_1 is a characteristic variable associated with a shear wave, which has no equivalent in one-dimensional flow ($\theta=0$). W_2 and W_3 are characteristic variables associated with the positive and negative gravity waves, respectively.

This is the characteristic form of two-dimensional shallow water equations with an arbitrary wave direction $\mathbf{K} = (\cos\theta, \sin\theta)$. The left-hand terms represent water wave propagation in the characteristic wave directions and can be written with the total derivative along the characteristics:

$$\begin{pmatrix} \frac{D_{\bar{v}} W_1}{Dt} \\ \frac{D_{\bar{v}+c\bar{k}} W_2}{Dt} \\ \frac{D_{\bar{v}-c\bar{k}} W_3}{Dt} \end{pmatrix} = - \begin{pmatrix} S_1 \\ S_2 \\ S_3 \end{pmatrix} + \begin{bmatrix} 0 & \sin\theta & -\cos\theta \\ \frac{1}{c} & \frac{\cos\theta}{g} & \frac{\sin\theta}{g} \\ -\frac{1}{c} & \frac{\cos\theta}{g} & \frac{\sin\theta}{g} \end{bmatrix} R \quad (19)$$

The coupling terms (S_1, S_2, S_3) cannot be simultaneously eliminated and, as in the case of the Euler equations, this results in the non-unique selection of upwind directions for two-dimensional flows. It is noteworthy that the above characteristic equations in Lagrangian form (19) are identical to both the original conservative and primitive forms of the shallow water equations. No numerical approximations have been introduced.

The governing equations must be supplemented with initial condition and appropriate boundary conditions for a well-posed two-dimensional overland flow problem. Wave characteristic directions at the boundary determine the required boundary conditions.

Equation (19) is the basis of the characteristics-based finite element scheme. At the interior nodes, backward tracking along the three characteristics is performed by a

sub-element tracking scheme. The solution values at the foot of the characteristic curve are interpolated by a linear finite element method. At the boundary nodes, characteristic directions and flow directions are used to determine the needed boundary conditions (Yeh et al., 2006).

After the selection of two specific characteristic directions with the propagation angles, θ_1 and θ_2 , the new characteristic equations are defined as:

$$\frac{\partial \mathbf{W}}{\partial t} + \begin{bmatrix} u & 0 & 0 \\ 0 & u + c \cos \theta_2 & 0 \\ 0 & 0 & u - c \cos \theta_2 \end{bmatrix} \frac{\partial \mathbf{W}}{\partial x} + \begin{bmatrix} v & 0 & 0 \\ 0 & v + c \sin \theta_2 & 0 \\ 0 & 0 & v - c \sin \theta_2 \end{bmatrix} \frac{\partial \mathbf{W}}{\partial y} = - \begin{Bmatrix} S_1 \\ S_2 \\ S_3 \end{Bmatrix} + \mathbf{L}^* \mathbf{R} \quad (20)$$

$$\mathbf{L}^* = \begin{bmatrix} 0 & \frac{c}{2} & -\frac{c}{2} \\ \sin \theta_2 / \omega & \frac{g \cos \theta_2}{2\omega} & \frac{g \cos \theta_2}{2\omega} \\ -\cos \theta_2 & \frac{g \sin \theta_2}{2\omega} & \frac{g \sin \theta_2}{2\omega} \end{bmatrix}, \quad W = L^{*-1} E \quad (21)$$

where $\omega = \cos \theta_1 \cos \theta_2 + \sin \theta_1 \sin \theta_2$. Since ω should not be zero, the two wave directions cannot be orthogonal.

Choosing the two wave characteristic directions (θ_1 and θ_2) is the most critical part of the characteristics-based finite element method for two-dimensional dynamic wave models. It can be seen that the first characteristic speed (u, v) is along the streamlines and only the two characteristic directions associated with the gravity waves need to be chosen. Detail on implementation of the characteristics-based finite element method for dynamic wave models can be found in (Yeh et al. 2006).

2.3.2 Diffusion wave model

The Galerkin finite element method is used to solve the diffusion wave model. Alternatively, the semi-Lagrangian method can be applied for the same results.

Galerkin Finite Element Method.

Applying the Galerkin finite element method to Equation (6), we obtain the following matrix equation.

$$[M] \frac{d\{H\}}{dt} + [S]\{H\} = \{Q_S\} + \{Q_B\} \quad (22)$$

in which

$$\begin{aligned} M_{ij} &= \int_M N_i N_j dR, & S_{ij} &= \int_M \nabla N_i \cdot K \cdot \nabla N_j dR, \\ Q_{Si} &= \int_M N_i S dR, & Q_{Bi} &= \int_B N_i \mathbf{n} \cdot K \nabla H dB \end{aligned} \quad (23)$$

where N_i and N_j are the base functions of nodes at i and j , respectively; \mathbf{n} is the outward normal unit vector; $[M]$ is the mass matrix, $[S]$ is the stiff matrix, $\{H\}$ is the solution vector of H , $\{Q_B\}$ is the flow rate through the boundary nodes, $\{Q_S\}$ is the flow rate from source/sink terms.

From our experience in solving various example problems, mass lumping is necessary for numerical stability and wetting/drying treatment (upstream weighting of the K value for dry nodes) is needed to avoid the occurrence of unphysical negative water depth in the numerical solution obtained with the Galerkin finite element method.

Semi-Lagrangian Method.

The Semi-Lagrangian method for diffusion wave model takes the advective form of the continuity equation and applies a backward particle-tracking scheme to solve for the unknown variable (water depth). This is described in the following kinematic wave model section.

For the Semi-Lagrangian approach, wetting/drying can be naturally treated while mass error control is a major concern.

2.3.3 Kinematic wave model

Since a kinematic wave is purely advective, there is no physical diffusion in the model. As a result, in the numerical solution of kinematic waves, the numerical diffusion is a major concern (Ponce, 1989). We apply the semi-Lagrangian method, which is a natural choice based on the form of the kinematic governing equation. In the hydrologic modeling literature, the Galerkin finite element methods are used for some kinematic wave models (for example, Jaber and Mohtar, 2003; Garg and Sen, 2001), although some stability control was proposed, it is inherently numerically unstable and oscillatory.

For the semi-Lagrangian method, a backward tracking scheme is applied to solving the kinematic wave equation:

$$\frac{Dh}{D\tau} = S - h \frac{\partial u}{\partial x} - h \frac{\partial v}{\partial y} \quad (24)$$

Integrating Equation (24) along its characteristic line (u,v) from a new time level to the foot of characteristics at the previous time level or reaching on the boundary.

2.4 Comparative examples

We will focus on how the incorporation of all three waves - optional dynamic wave (DYW), diffusion wave (DIW) and kinematic wave (KIW) models can be used to investigate the applicability and potential errors of simplified DIW and KIW approaches.

From previous studies, it is well known that the accuracy of diffusion and kinematic wave approximation does not solely depend on bottom slopes, but also rainfall intensity and duration, boundary conditions, etc. Generalized formal theoretical analyses are not tractable for two-dimensional flow; numerical experiments are the only way to investigate the different results obtained by different wave models.

Several numerical tests were conducted to demonstrate the applicability and accuracy of diffusion or kinematic wave approximation in comparison to the full dynamic wave solutions. The test examples encompass one-dimensional channel flows with exact solutions, dam break-type flow, rainfall-induced overland flow and structure flow driven wetland flow, and two-dimensional river bend flow.

2.4.1 Verification and comparison of steady flow in one-dimensional channels

Three channel flow benchmark problems provided by (MacDonald et al., 1997) were used to verify the numerical schemes implemented for the DYW, DIW, and KIW and the error of DIW and KIW solutions were discussed.

The one-dimensional channel flow is pure subcritical, subcritical at inflow/supercritical at outflow, and mixed flow with hydraulic jump, respectively for Test Problem 1, 2 and 3. The bed slope is given by an analytical function of the pre-selected water depths. Details on these test problem set-up and the derived exact analytical solutions can be found in the aforementioned reference.

Test Problem 1: pure subcritical flow

The channel is rectangular with a width of 10 m. The total length is 1,000 m. A constant flow of 20 m³/s is applied at the upstream end. The flow is pure subcritical. A water depth of 0.748409 m is specified at the downstream outlet. The Manning's n value is 0.03. The bottom slope is given by:

$$S_o(x) = \left[1 - \frac{4}{gh(x)^3} \right] \frac{dh}{dx} + 0.36 \frac{[2h(x) + 10]^{4/3}}{[10h(x)]^{10/3}} \quad (25)$$

which is depicted in Figure 2-4. For this test problem, the analytical solution of the fully dynamic wave model at steady state is given by MacDonald et al. (1997) as

$$h(x) = \left(\frac{4}{g} \right)^{1/3} \left\{ 1 + 0.5 \exp \left[-16 \left(\frac{x}{1000} - \frac{1}{2} \right)^2 \right] \right\} \quad (26)$$

This problem was simulated numerically with one-dimensional DYW, DIW and KIW. The computed steady state water depth profiles (Figure 2-1) were compared to the exact solution, Eq. (26). The numerical solution obtained by the characteristics-based finite element method was accurate. On the other hand, the DIW solution still contains an absolute relative error of less than 4%. And even though the kinematic wave (KIW) solution can be obtained analytically for this simple problem, the computed water depth is underestimated by up to 12%. Also, the downstream boundary cannot be applied for KIW and the water depth is computed by KIW at the outlet. The large error of KIW can be attributed to the boundary conditions, since the bottom slopes are not very small.

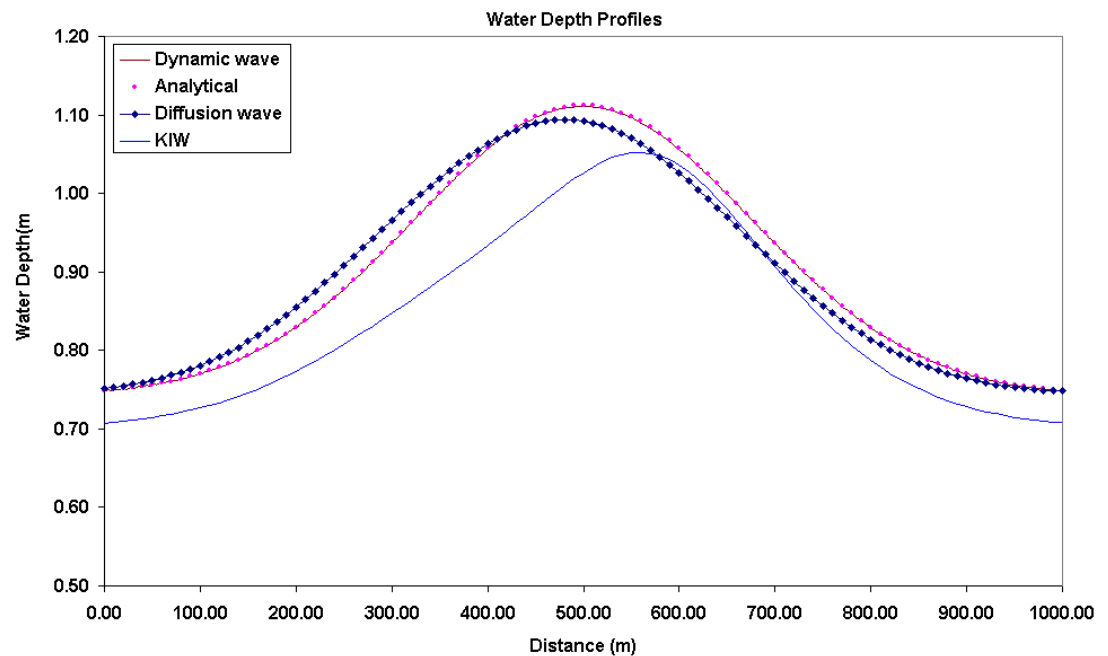


Figure 2-1: Water Depth Profiles for Test problem 1

Test problem 2: Mixed Subcritical/Supercritical Flow:

A rectangular channel of 1,000 m, with a width of 10 m, is given a constant flow rate of $20 \text{ m}^3/\text{s}$ (for the entire channel). The bottom slope is variable and is given as function of x as

$$S_o(x) = \left[1 - \frac{4}{gh(x)^3} \right] \frac{dh}{dx} + 0.16 \frac{[2h(x) + 10]^{4/3}}{[10h(x)]^{10/3}} \quad (27)$$

The bottom slope given in Eq. (27) would render the flow conditions subcritical at the inflow boundary and supercritical at the outlet (Figure 2-3). The Manning's n value is 0.02. This test problem has an exact solution (MacDonald et al. 1997)

$$h(x) = \begin{cases} \left(\frac{4}{g} \right)^{1/3} \left\{ 1 - \frac{1}{3} \tanh \left[3 \left(\frac{x}{1000} - \frac{1}{2} \right) \right] \right\} & 0 \leq x \leq 500 \\ \left(\frac{4}{g} \right)^{1/3} \left\{ 1 - \frac{1}{6} \tanh \left[6 \left(\frac{x}{1000} - \frac{1}{2} \right) \right] \right\} & 500 \leq x \leq 1000 \end{cases} \quad (28)$$

For numerical simulations, there is one inflow boundary condition and no downstream boundary for the dynamic wave model. For diffusive wave model, two boundary conditions must be given. In this case, the known water depth at outlet was specified as downstream boundary based on the exact water depth solution given in Eq. (28).

The dynamic wave model was able to solve this mixed flow problem with good accuracy. No numerical instabilities have been encountered. The diffusive wave model also provides satisfactory results (4% error in water depth). The kinematic wave solution underestimated the water depth by 4% to 6% (Figure 2-2). The Froude number profile

plot in Figure 2-3 confirms the mixed flow condition. The bottom slopes range from 0.2% to 0.8%.

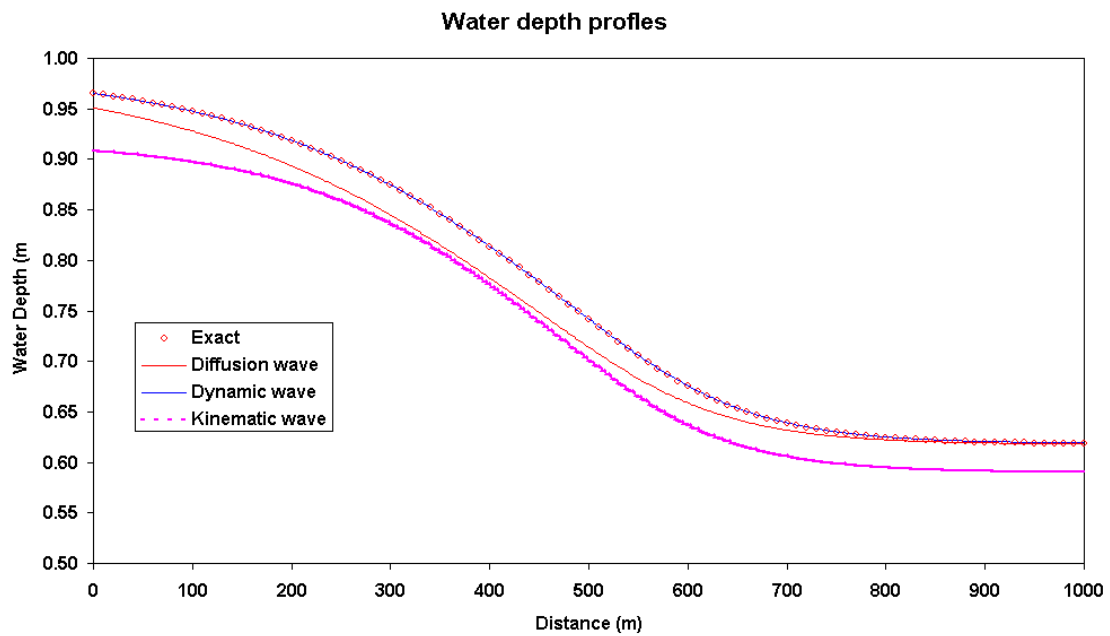


Figure 2-2: Water Depth Profiles for Test Problem 2

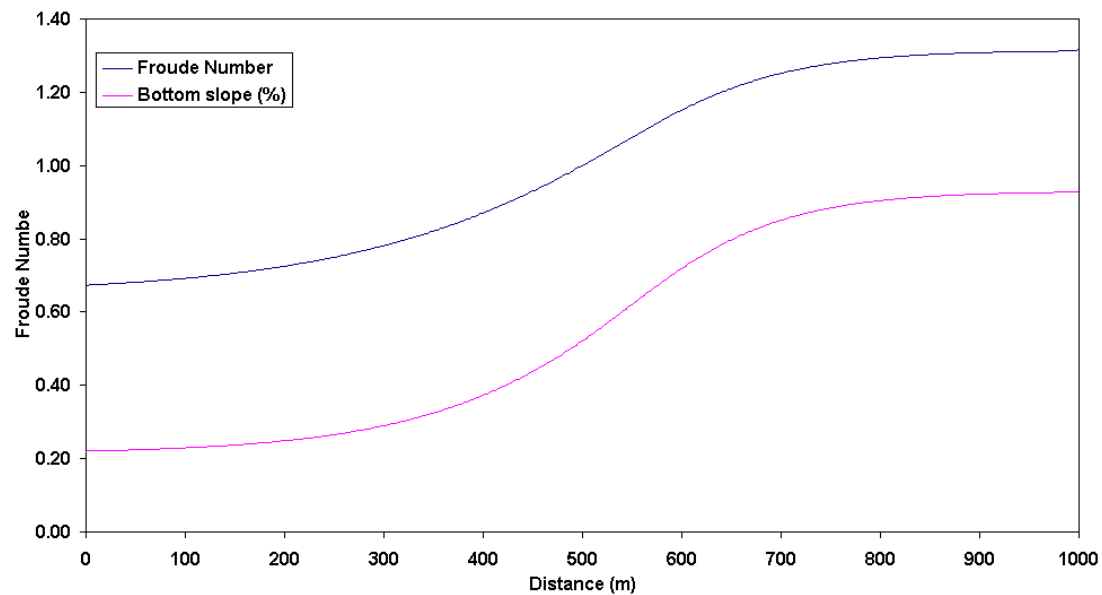


Figure 2-3: Froude Number and bottom slope (%) profiles for Test Problem 2

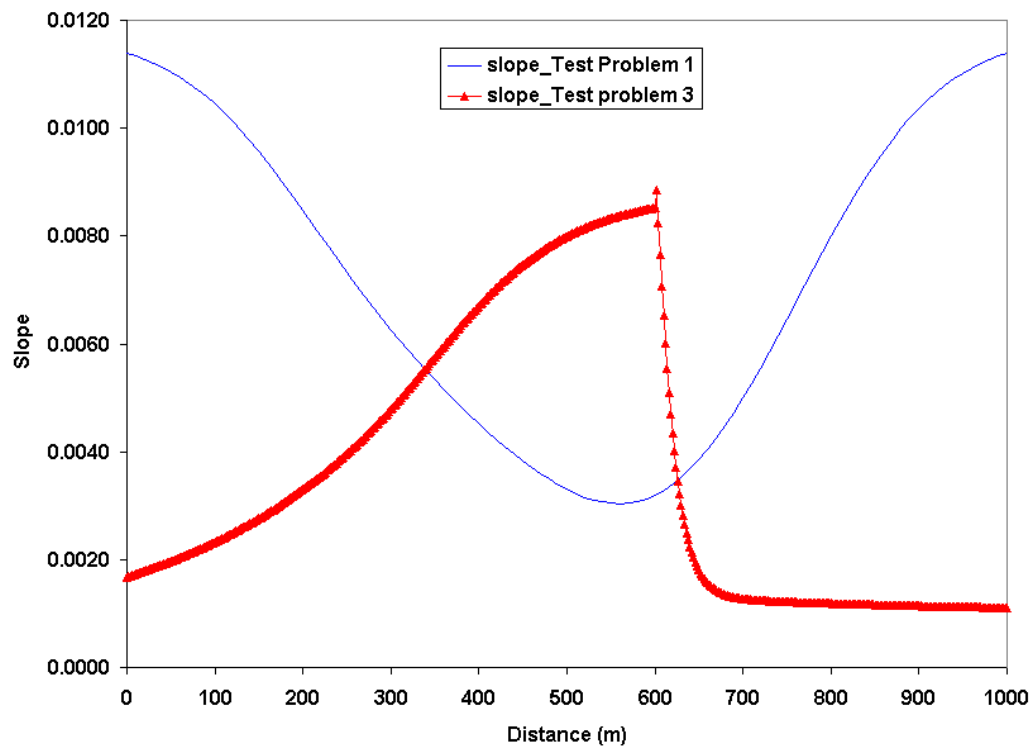


Figure 2-4: Bottom slope (-) profiles for Test Problems 1 and 3

It is interesting to note that even though the dynamic wave model requires less input data than the diffusive wave model (one boundary condition versus two), it yields more accurate simulations.

Test problem 3: Mixed Subcritical/Supercritical Flow with Hydraulic Jump

This test problem is described in MacDonald et al. (1997). The channel is trapezoidal, with a total length of 1,000 m. The upstream inflow is a constant discharge of 20 m³/s. At the downstream outlet, a specified water depth of 1.349963 m was applied. The side slope of the trapezoidal cross-section is 1:1. The Manning's n value is 0.02. The bottom slope is given as function of x as:

$$S_o(x) = \left[1 - \frac{400[10 + 2h(x)]}{g[10 + h(x)]^3 h(x)^3} \right] \frac{dh}{dx} + 0.16 \frac{[2\sqrt{2}h(x) + 10]^{4/3}}{[[10 + h(x)]^{10/3} h(x)^{10/3}]} \quad (29)$$

which is depicted in Figure 2-4. The exact solution for this problem is (MacDonald et al. 1997)

$$h(x) = \begin{cases} 0.723449 \left\{ 1 - \tanh \left[\left(\frac{x}{1000} - \frac{3}{10} \right) \right] \right\} & 0 \leq x \leq 300 \\ 0.723449 \left\{ 1 - \frac{1}{6} \tanh \left[6 \left(\frac{x}{1000} - \frac{3}{10} \right) \right] \right\} & 300 \leq x \leq 600 \\ \frac{3}{4} + \sum_{k=1}^3 a_k \exp \left[-20k \left(\frac{x}{1000} - \frac{3}{5} \right) \right] + \frac{3}{5} \exp \left(\frac{x}{1000} - 1 \right) & 600 < x \leq 1000 \end{cases} \quad (30)$$

The abrupt change in bed slope (Figure 2-4) causes a hydraulic jump. Both inflow and outflow boundaries are subcritical.

The bed slope of the channel has an abrupt change at $x = 500$ m (cf. Eq. (29)) and this causes the occurrence of a hydraulic jump. The dynamic and diffusion wave solutions were computed and compared (Figure 2-5). As expected, the accuracy of diffusive wave approximation for this mixed flow case is not satisfactory. At the zone of supercritical flow, the error induced by diffusive wave approximation is high at the supercritical zone.

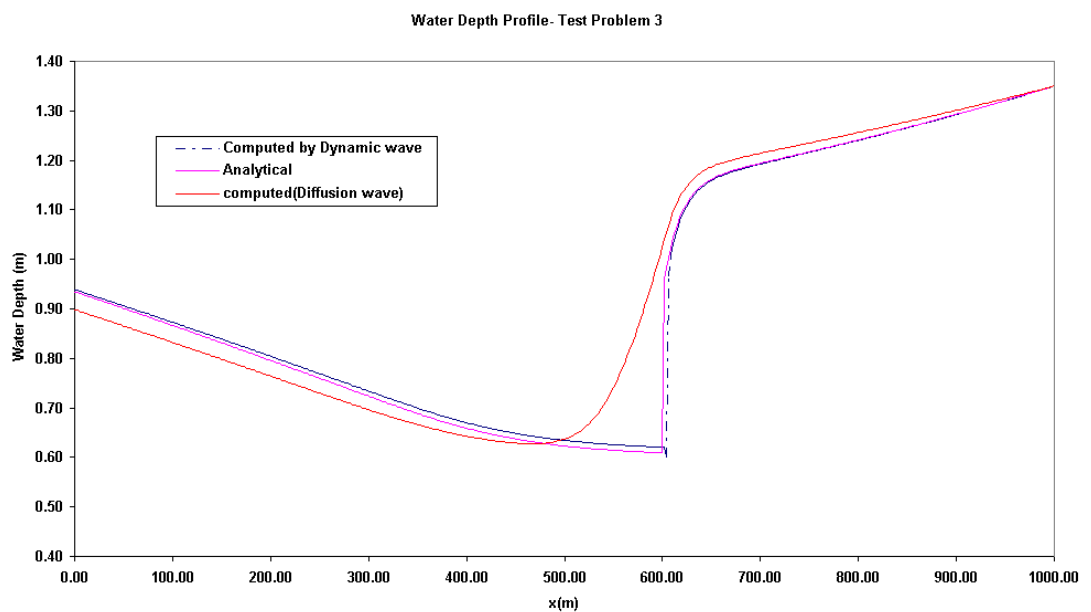


Figure 2-5: Water Depth Profile for Test Problem 3

The dynamic wave solutions obtained with the characteristics-based finite element method are very accurate and the hydraulic jump in Test Problem 3 was captured. On the other hand, the diffusion wave approximation generated significant errors for the hydraulic jump and an absolute error of less than 5% still exists for the two simpler problems (Figure 2-6).

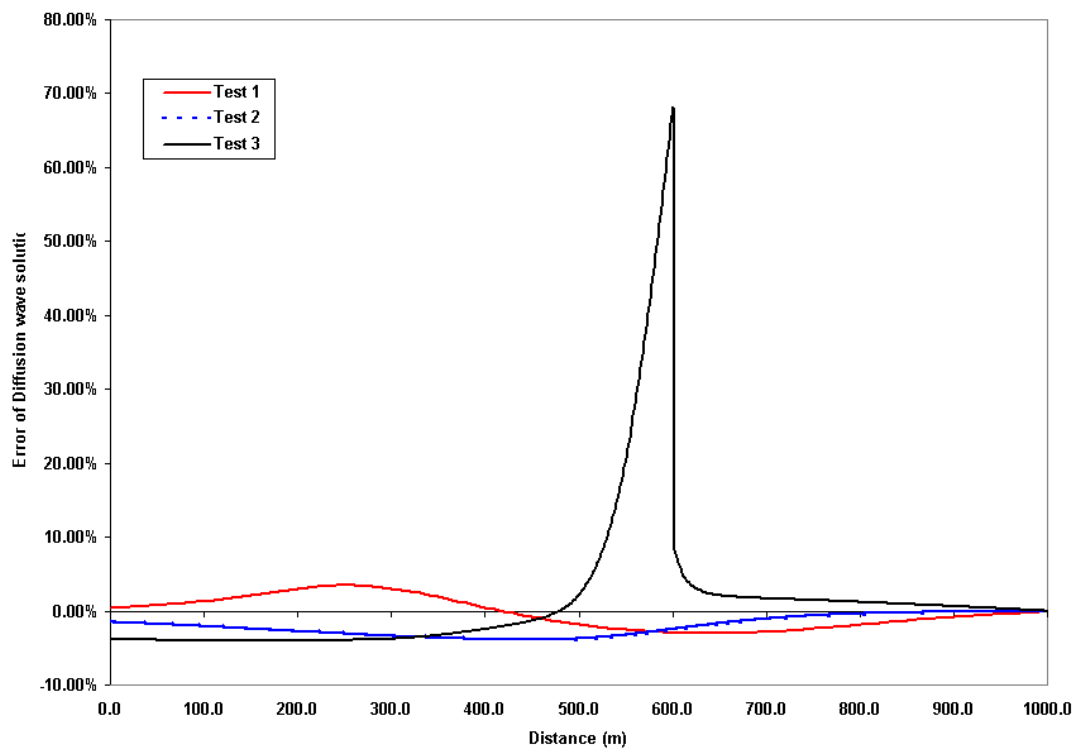


Figure 2-6: Summary of error in the Diffusion wave solutions

2.4.2 Rainfall-runoff over a plane

This simple example is used to test and verify that the implementation of the numerical schemes for two-dimensional DYW, DIW and KIW for rainfall-driven overland flow. The relatively steep slope in this example is expected to produce close results for all wave models.

Overland flow on a sloping plane was simulated. The impervious plane is 800 m x 1000 m. The bottom slope is 0.5% and the Manning's roughness coefficient value is 0.015. A constant rainfall intensity of 10.8 mm/hour and duration of 1.5 hours was applied uniformly on the surface.

The flow domain was discretized into 100 rectangular elements of 80 m x 100 m. At the downstream outlet, a zero depth gradient boundary was applied. A time step of 120 s was applied during the simulation run of 170 minutes.

Since the slope is relatively steep (0.5%), both the diffusion and kinematic wave approximations are relatively accurate. The computed water depth and velocity magnitude profiles at peak steady state level (time =5,000 seconds) were compared for solutions of the three DYW, DIW, and KIW wave models in Figures 2-7 and 2-8. As expected, the numerical solutions for both water depth and velocity are very close.

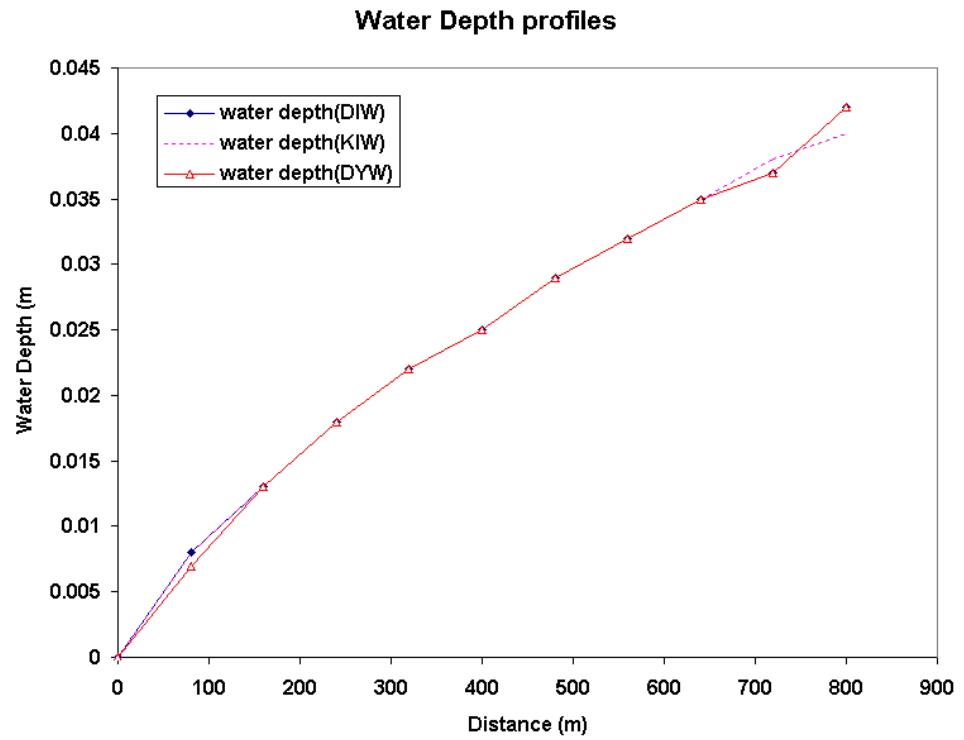


Figure 2-7: Water depth profiles at time=5000s (numerical solutions by two-dimensional DYW, DIW and KIW)

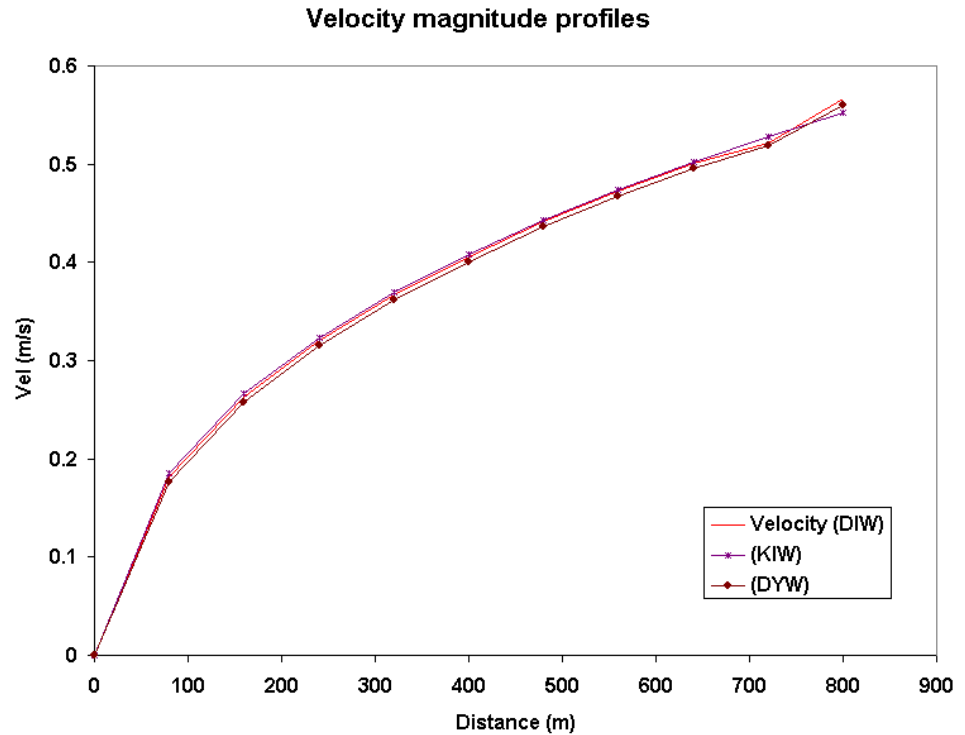


Figure 2-8: Velocity magnitude profiles at time =5000s (numerical solutions by two-dimensional DYW, DIW and KIW)

2.4.3 Two-dimensional partial dam break with friction

This example demonstrates the effect of strong inertial terms on significantly different results by diffusion wave and dynamic wave.

This a two-dimensional partial dam break problem similar to the example in (Fennema and Chaudhry, 1990). But the downstream water depth was set to 0.05 m, so this is a dry bed simulation, very difficult to be solved numerically by conventional finite difference or finite element methods. The rectangular channel is horizontal with a

dimension of 200 x 200 m in length and width, respectively. The initial water depth is 10 m in the reservoir, and 0.05 m in the downstream. A Manning's n value of 0.02 was applied. The breach or opening of sluice gates is 75 m, between $x = 95$ and 170 m. The domain was divided into 40 x 40 rectangular elements and the elements at the location of the dam are excluded.

At the beginning of the simulation, the dam has partially collapsed instantaneously. At time $t = 0$, the water depth in the dam is 10.0 m, and a water depth of 0.05 m is presented elsewhere (Figure 2-9). Since the bottom slope is zero, KIW cannot be used. DIW and DYW were applied to simulate the dam break flow process. The simulation results were compared for water depth distribution in the domain and computed depth hydrographs for the point inside the reservoir (B) and downstream of the dam location (A) (Figures 2-10 and 2-11). It can be seen that without consideration of inertial terms, the diffusion wave (DIW) results are incorrect and highly distorted. DIW solution spreads water quickly within the domain while dynamic wave solution predicts the correct advance of the wave front.

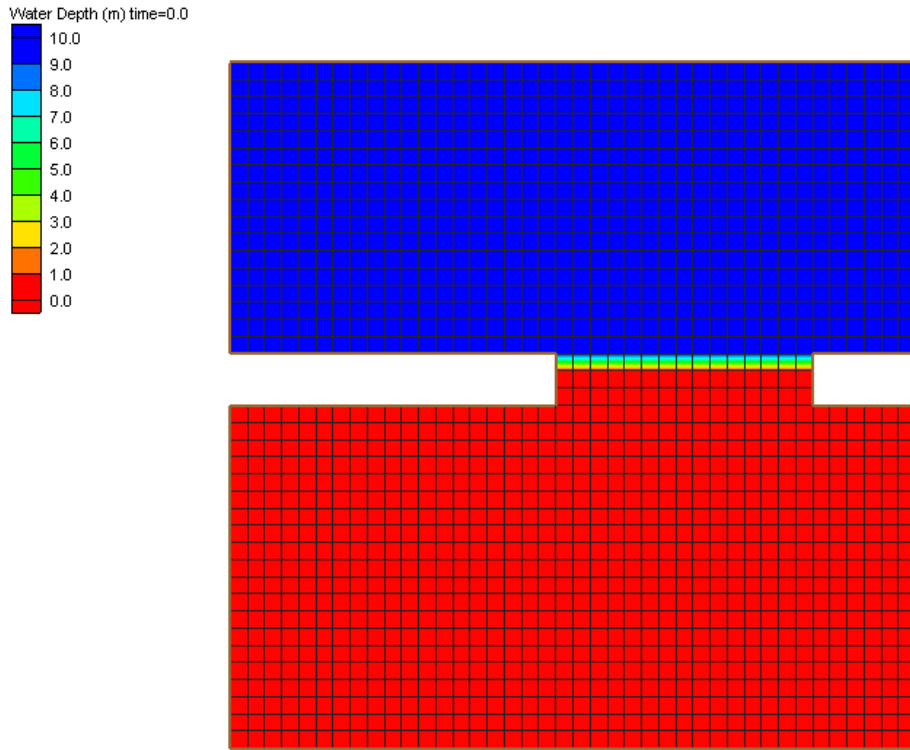
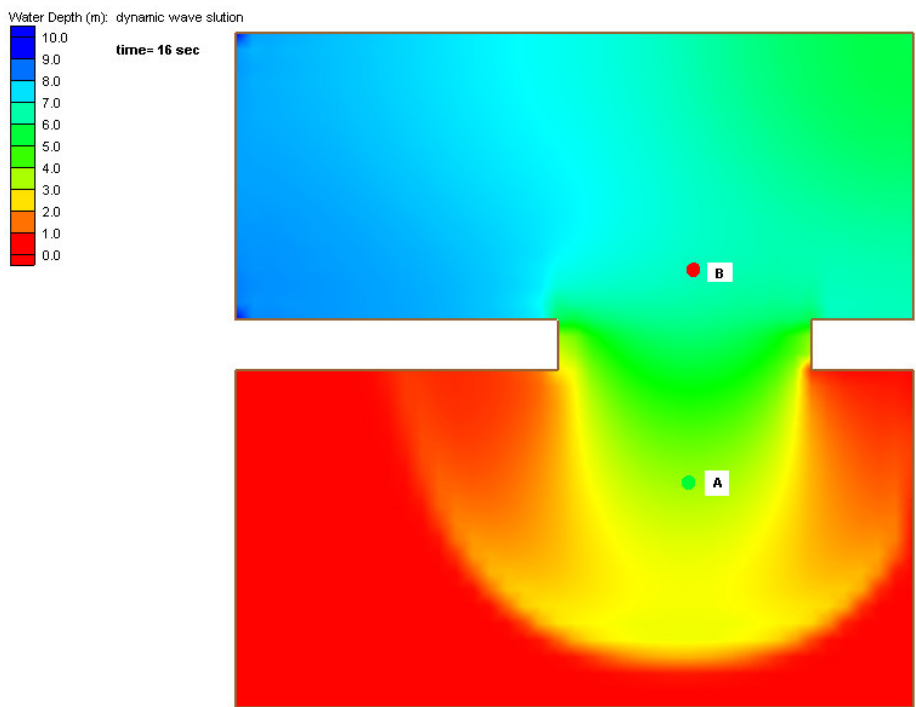
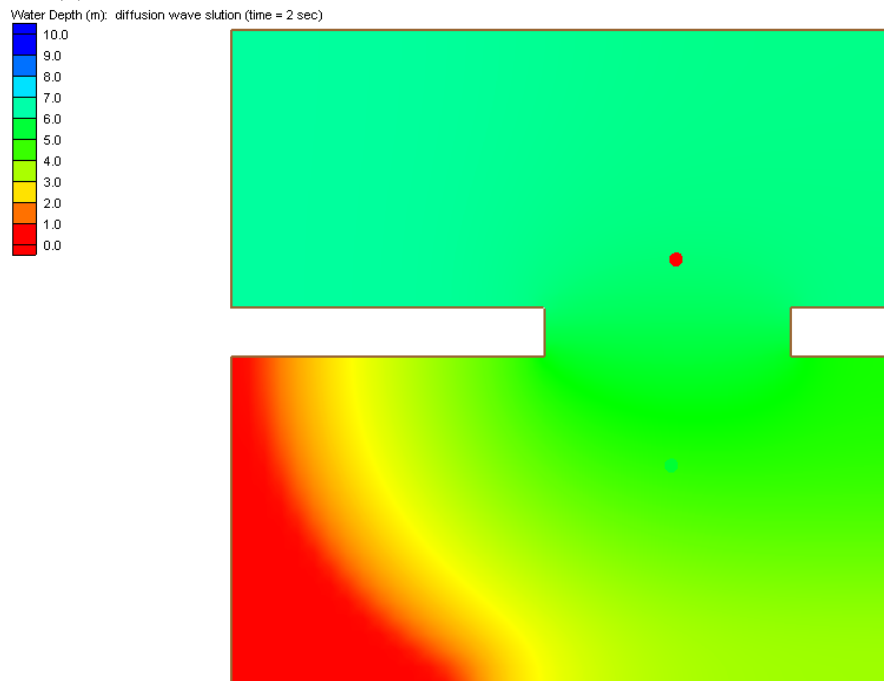


Figure 2-9: Finite element mesh and initial condition for the dam break problem



(a) DYW Solution at Time =16.0 sec and Location of Point A and B



(b) DIW Solution at Time = 2.0 sec

Figure 2-10: Water Depth profiles for Dam Break Problem

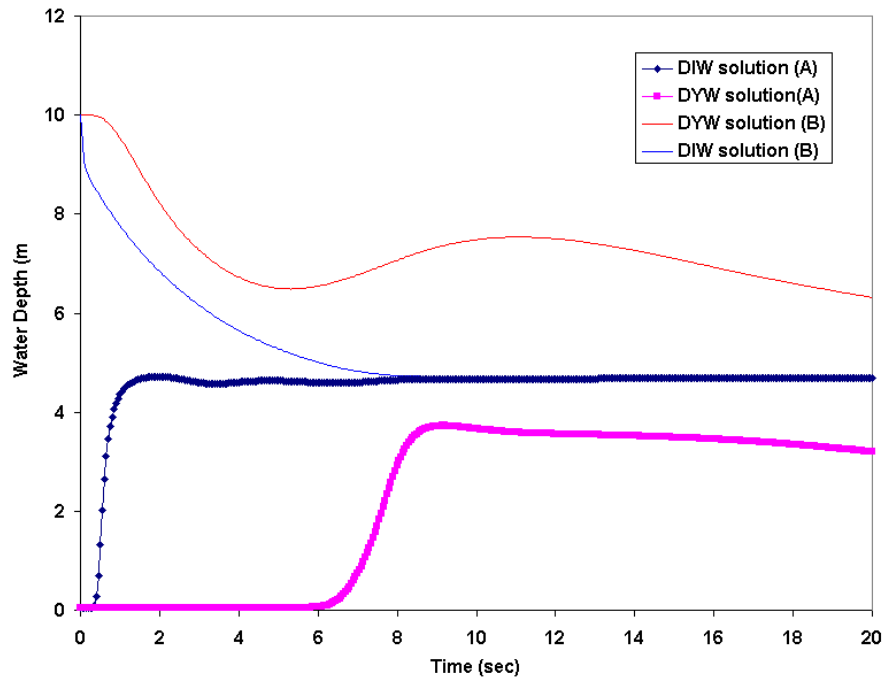


Figure 2-11: Comparison of Computed water depth hydrographs for Dam Break Problem

2.4.4 Two-dimensional unsteady flow in a treatment wetland

One important application of the full two-dimensional shallow water equations is water movement in low terrain areas (e.g., flood plains, wetlands, irrigated farmlands and tidal flats) where simplified diffusion wave approximation may not be appropriate. The numerical simulation of overland flow in a treatment cell in a constructed wetland was made to test model performance of diffusion wave approximation under such a mild slope condition.

The flow domain is about 4.18 km^2 . The slope of land surface elevations ranges from 0.0003 to 0.007. The boundary is closed by a perimeter levee, except flow through

the inflow and outflow culverts in the levee (Figures 2-12 and 2-13). There are observed flow and stage data for this treatment cell and a stage monitoring station is located at the center of the cell.

Flow during a time period of 240 hours (10 days) was simulated with time-varied historic flow and stage data (Figure 2-14) and the simulation results of DYW and DIW were compared. Identical finite element mesh, model parameters and boundary conditions were used. Both the DYW and DIW solutions were plotted for the water levels at the observed point with the observed data. Close match (less 0.01 m with water levels range between 3.80 m to 3.95 m) among the observed, DYW and DIW values were obtained (Figure 2-15). This example demonstrates that DIW can be applicable to slow flow on a very mild slope.

For sediment and contaminant transport, accurate velocity calculation is also very important. There are concerns that flow dynamics cannot be adequately captured by diffusion wave or kinematic wave approximations. The velocity magnitude and vector plots also show similar pattern (Figure 2- 16).

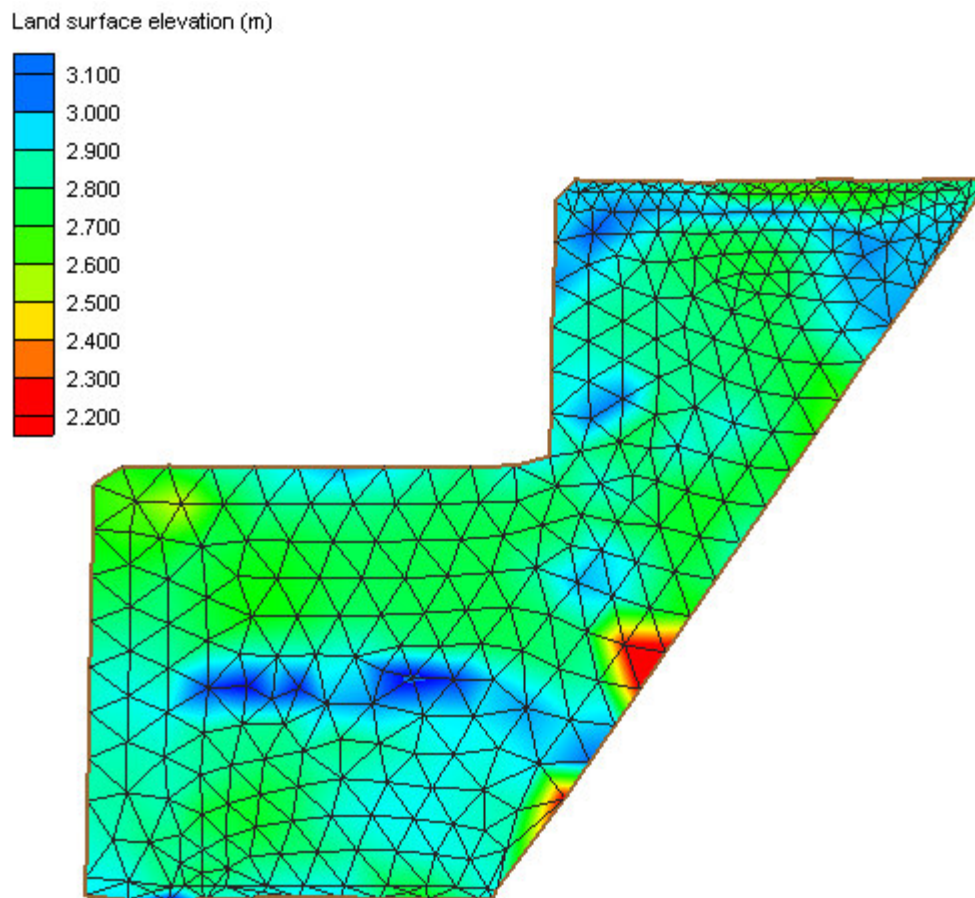


Figure 2-12: Finite Element mesh and Topography

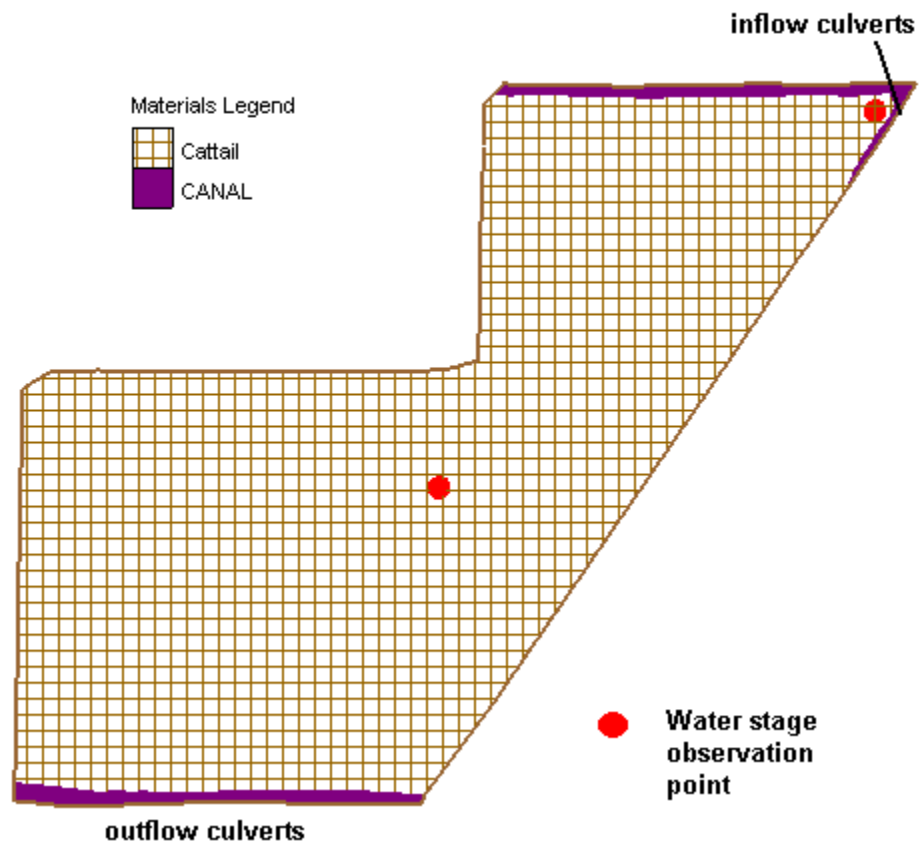


Figure 2-13: Boundary Conditions and Vegetation, Observation point.

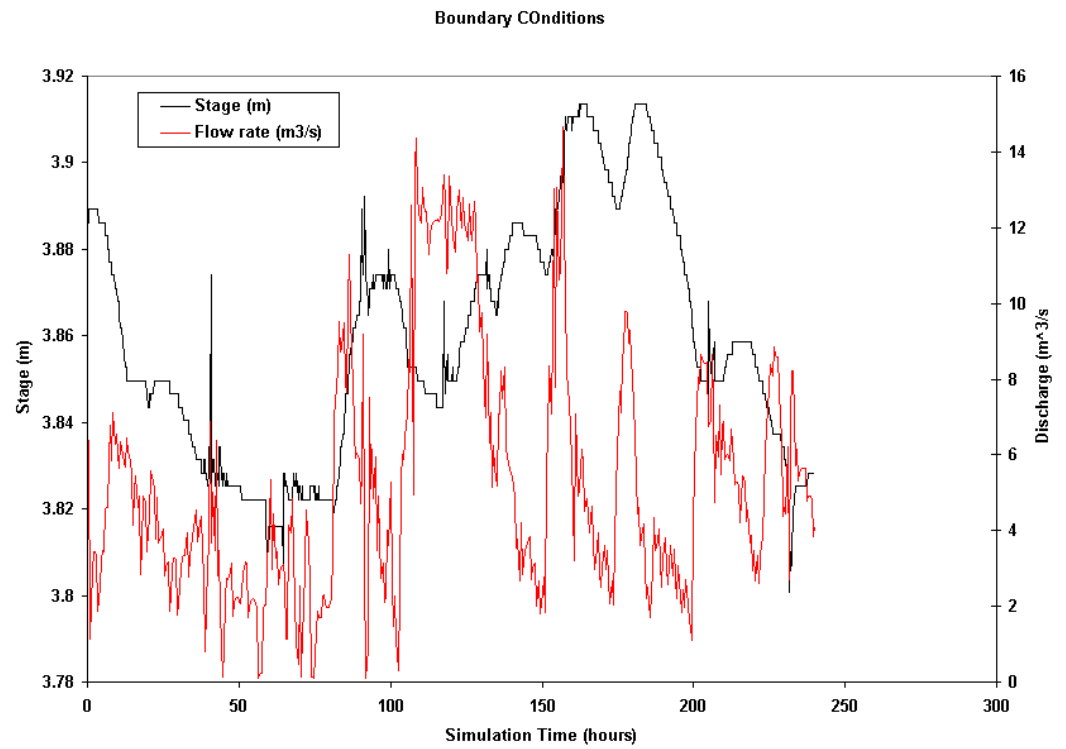


Figure 2-14: Boundary Condition data applied in the wetland example

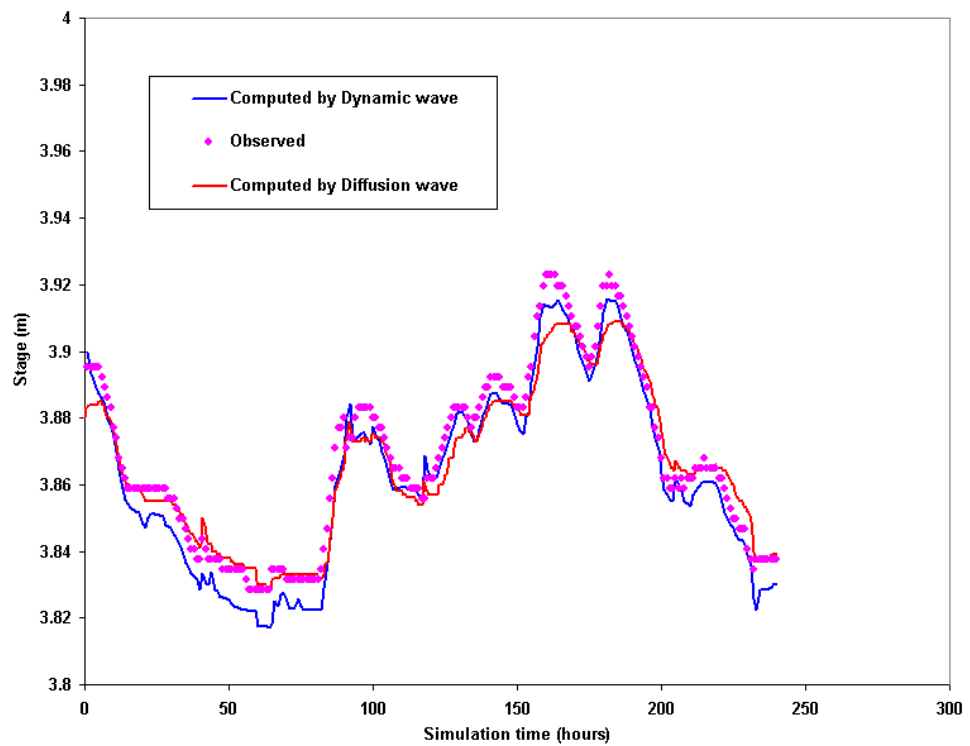


Figure 2-15: Comparison of Observed and Computed Stages.

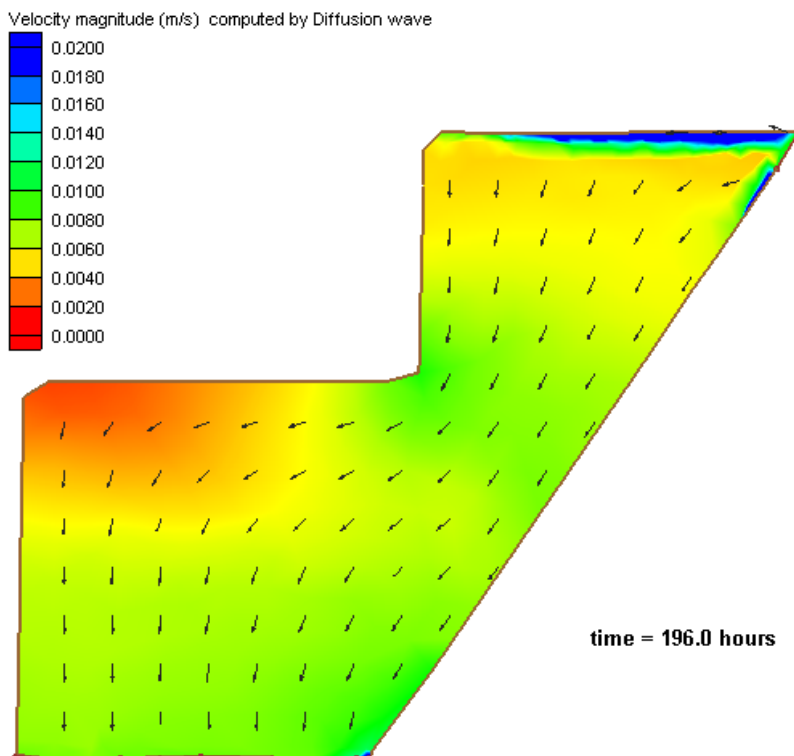
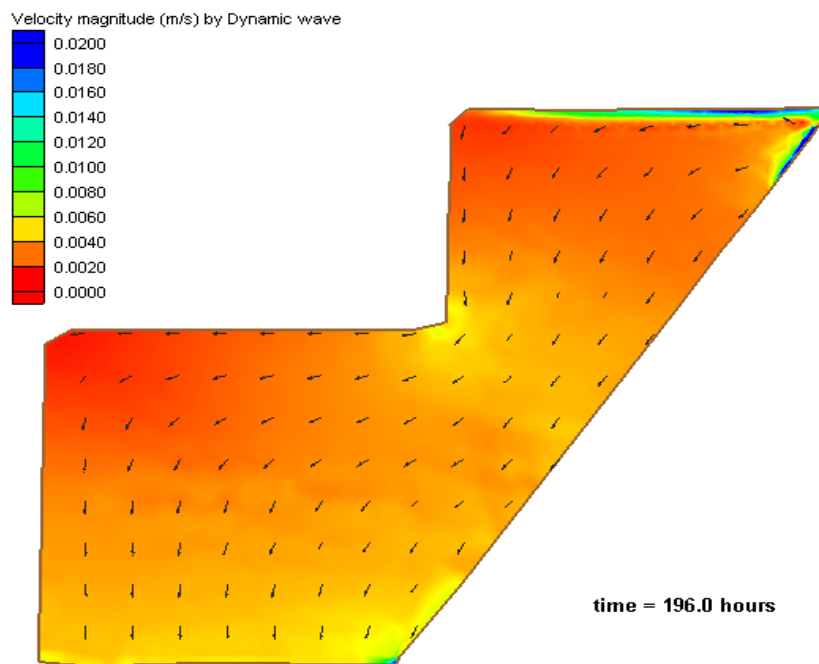


Figure 2-16: Velocity Magnitude and Vector plots (DIW and DYW solutions)

2.4.5 Two-dimensional river flow at a river bend

This example is designed to estimate the error of diffusion wave approximation when flow vorticity and eddies may play an important role. The steady flow at a segment of a river bend was simulated (Figure 2-17). The river reach is about 800 m long and 50 m wide. The bottom is horizontal. A constant inflow of $500 \text{ m}^3/\text{s}$ is applied at one end and a specified river stage of 3.0 m is applied as the downstream boundary. The Manning's n value is 0.025.

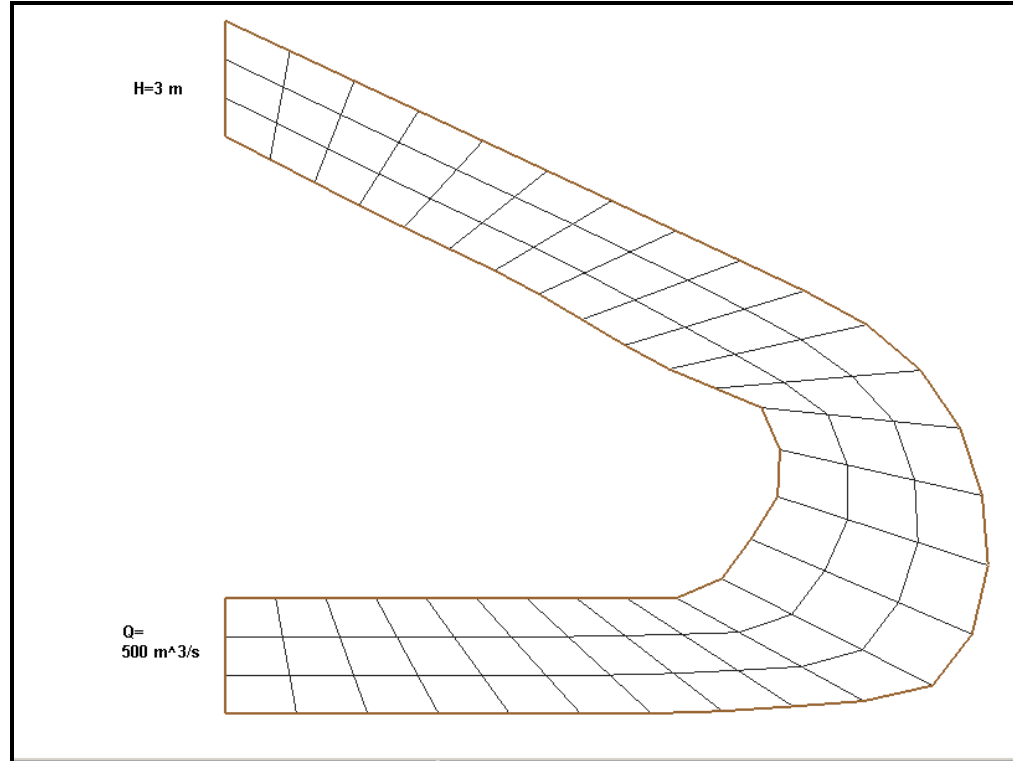


Figure 2-17: Layout of the River bend example

The dynamic wave and diffusion wave models were applied to solve this example problem. The DYW solution is shown in Figure 2-18.

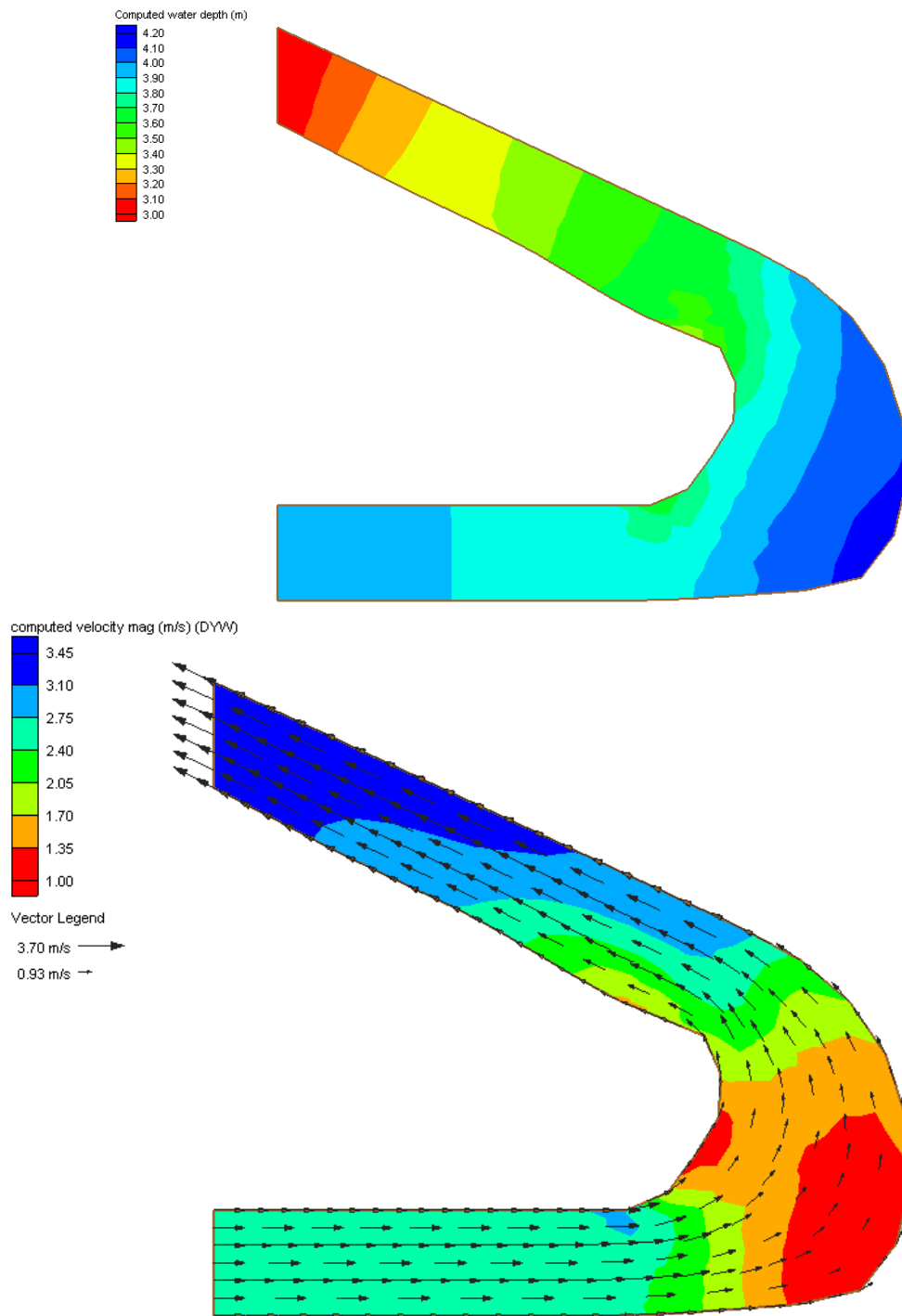


Figure 2-18: Computed water depth and velocity magnitude (DYW)

The computed water depth and velocity magnitude obtained with DIW are compared to the DYW solution and the differences are plotted in Figures 2-19 and 2-20. It can be seen that the errors in water depth and velocity magnitude computed with the diffusion wave approximation are significant at the bending segment, even though eddies do not occur. Under this flow condition and geometry, the diffusion wave approximation is not appropriate.

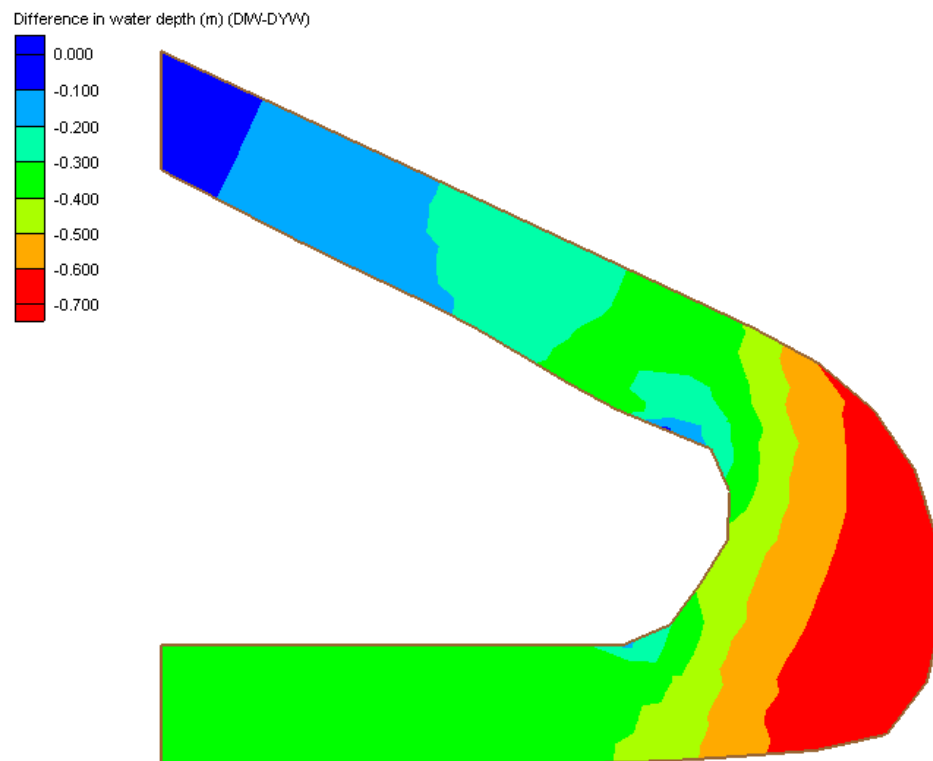


Figure 2-19: Difference in computed water depth (DIW – DYW)

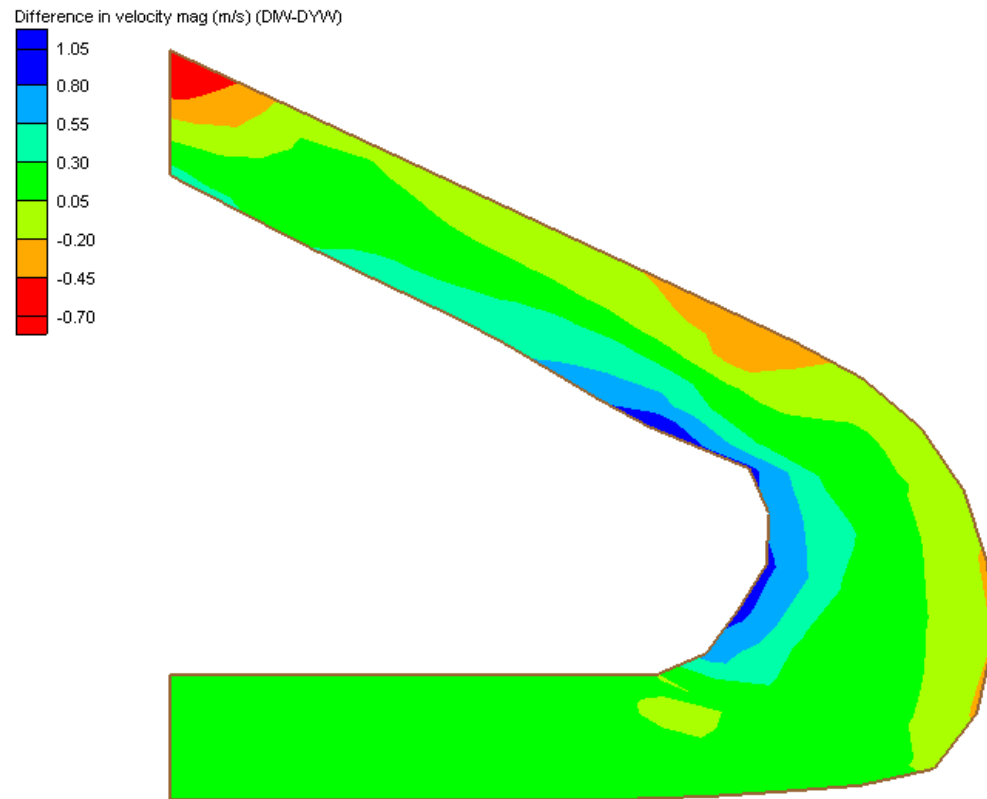


Figure 2-20: Difference in computed velocity magnitude (DIW – DYW)

2.5 Discussions

The dynamic wave model should be mandated for strong dynamic flow cases (e.g., dam break type flow), or momentum fluxes are important compared to gravity force (e.g., when the slope is very small, cf. Section 2.4.5). The diffusion wave model is usually adequate for overland flow on hill-slopes. The accuracy of diffusion wave under very mild slope is not guaranteed as flow dynamics and downstream boundary may play a key role.

The kinematic wave model is still popular in many watershed models. It should be limited though, specifically to steep-slope mountainous watersheds and where downstream conditions are not important. Instead of this method, an adaptive scheme for applying DYW, DIW, or KIW in different sub-domains of a watershed may prove to be more efficient and therefore advantageous.

2.6 Summary and Conclusions

The implementation of dynamic wave, diffusion wave, and kinematic wave models in a single watershed model is an advantage in order to strongly validate the derived approximations. This is illustrated by some numerical examples that demonstrate the potential errors in diffusion wave and kinematic wave models for overland flow.

Acknowledgements

This research is supported by the U.S. EPA - Science To Achieve Results (STAR) Program under Grant # R-82795602 with the University of Central Florida.

References

- Donigian, A.S. and J. Imhoff. (2006). Chapter 2: History and evolution of watershed modeling derived from the Stanford Watershed model, in *Watershed Models*. Eds. By Singh VP and Frevert, CRC Press, Boca Raton, FL.
- Fennema R.J. and M.H. Chaudhry (1990). Explicit methods for 2-D transient free-surface flows, *Journal of Hydraulic Engineering*, Vol. 116, No.8, pp.1012-1033, 1990.
- Fortin, J. P., Turcotte, R., Massicotte, S., Moussa, R., Fitzback, J., and Villeneuve, J. P. (2001). “A distributed watershed model compatible with remote sensing and GIS data. I: Description of model.” *J. Hydrologic Eng.*, 6(2), 91–99.
- Govindaraju, R. S., Jones, S. E., and Kavvas, M. L. (1988). ‘On the diffusion wave model for overland flow: 2. Steady state analysis’, *Water Resources Research*, 24, 745-754.
- Govindaraju, R.S., Kavvas, M.L. and Jones, S.E. (1990). 'Approximate analytical solutions for overland flows.' *Water Resources Research*, 26(12), pp. 2903-2912.

- Hydrologic Engineering Center(HEC). (2000). “Hydrologic modeling system HEC-HMS user’s manual, version 2.” Engineering, U.S. Army Corps of Engineers, Davis, Calif.
- Maconald I., Baines, M.J., Nichols N.K. and Samuels P.G. (1997). Analytic Benchmark Solutions for Open Channel Flows, *Journal of Hydraulic Engineering*, Vol. 123, No. 11, November, 1997.
- Metcalf and Eddy, Inc., Univ. of Florida, and Water Resources Engineers, Inc. (1971). “Storm water management model, Vol. 1—Final report.” EPA Rep. No. 11024DOC07/71 (NITS PB-203289), EPA, Washington, D.C.
- Moramarc01 T. and Singh V.P., (2002). Accuracy of kinematic wave and diffusion wave for spatial-varying rainfall excess over a plane. *Hydrol. Process.* 16, 3419–3435.
- Jaber F.H. and Mohtar R.H., (2003). Stability and accuracy of two-dimensional kinematic wave overland flow modeling, *Advances in Water Resources* 26 (2003) 1189–1198.
- Olivera, F., and Maidment, D. (1999). “Geographical information system ~GIS!-based spatially distributed model for runoff routing.” *Water Resour. Res.*, 35(4), 1155–1164.

- Parlange, J. Y., Hogarth, W., Sander, G., Rose, C., Haverkamp, R., Surin, A., and Brutsaert, W. (1990). 'Asymptotic expansion for steady state overland flow', *Water Resources Research*, 26, 579-583.
- Ponce, V.M., R.M. Li, and D.B. Simons, (1978). Applicability of kinematic and diffusion wave models. *Journal of the Hydraulics Division, ASCE*, 104: 353-360.
- Richardson, J.R. and P.Y. Julien (1994). 'Suitability of simplified overland flow equations.' *Water Resources Research*, 30 (3), pp. 665-671.
- Singh VP, Aravamuthan V. (1995). Accuracy of kinematic wave and diffusion wave approximations for time-independent flows. *Hydrological Processes* 9: 755–782.
- Singh, V.P., S. K. Jain and M. M. Sherif, (2005). Errors of kinematic wave and diffusion wave approximations for time-independent flows with infiltration and momentum exchange included, *Hydrol. Process.* 19, 1771–1790.
- Tayfur, G., Kavvas, M. L., Govindaraju, R. S., and Storm, D. E., (1993), "Applicability of St. Venant equations for two dimensional overland flows over rough infiltrating surfaces." *J. Hydraul. Eng.*, 119(1), 51–63.
- Yeh, G.T., G. B. Huang, H. P. Cheng, F. Zhang, H. C. Lin, E. Edris, and D. Richards. (2006). A first principle, physics-based watershed model: WASH123D, in *Watershed*

Models. Eds. By Singh VP and Frevert D.K., CRC Press, Boca Raton, FL, September 2005.

Chapter 3

Dynamic Wave Modeling of Two-dimensional Overland Flow using Characteristics-based Finite Element Method

Abstract

The Method of Characteristics (MOC), within the context of the finite element method, was applied to the complete two-dimensional shallow water equations for two-dimensional overland flow. For two-dimensional overland flow, finite element or finite volume methods are more flexible in dealing with complex boundary. Recently, finite volume methods have been very popular in numerical solution of the shallow water equations. Some (e.g., Hirsch et al, 1987; Garcia-Navarro et al., 1995 and Guinot, 2004) have pointed out that finite volume methods for two-dimensional flow are fundamentally one-dimensional (normal to the cell interface). The results may rely on the grid orientation. The search for genuinely multidimensional numerical schemes for two-dimensional flow is an active topic. We consider the Method of Characteristics (MOC) in the context of finite element method as a good alternative. Many researchers (e.g., Zhang and Cundy, 1989; Chow and Ben-Zvi, 1973 and Katopodes and Strelkoff, 1979) have pointed out the advantage of MOC in solving two-dimensional shallow water hyperbolic equations having wave-like solutions. At the same time, they considered MOC for two-dimensional overland flow being non-tractable on complex topography. The intrinsic difficulty in implementing MOC for two-dimensional overland flow is that there are infinite numbers of wave characteristics in the two-dimensional context,

although only three independent wave directions are needed for a well-posed solution to the characteristic equations. We have implemented a numerical scheme that attempts to diagonalize the characteristic equations based on a pressure and velocity-gradient relationship. This new scheme was evaluated by comparison with other choices of wave characteristic directions, given in the literature. Example problems of mixed sub-critical flow/super-critical flow in a channel, with approximate analytical solutions, were used to verify the numerical algorithm. Then experiments of overland flow on a cascade of three planes (Iwagaki, 1955) were solved with the new method. The circular dam break problem was solved with different selections of wave characteristic directions, and the performance of each selection was evaluated based on accuracy and numerical stability. Finally, two-dimensional overland flow over complex topography in a wetland setting, with very mild slope, was solved with the new numerical method to demonstrate its applicability.

3.1 Introduction

The simplified form of the two-dimensional shallow water equations (e.g. the diffusion wave or kinematic wave approximation) has been frequently used in modeling the two-dimensional shallow overland flow originated from the rainfall/runoff process, surface flow in irrigation and wetlands, and flooding in floodplains. On the other hand, the full two-dimensional shallow water equations have been extensively studied for fast transient flow processes (dam break type flood propagation and hydraulic jumps) or deep surface water flows in estuary and ocean.

The characteristics of overland flow in comparison to deep surface water flow can be summarized as (e.g. Zhang and Cundy, 1989): (1) very small water depth; (2) large bed shear stress; (3) impact of grid scale micro-topography; (4) stiff source term induced by rainfall and infiltration; and, (5) dynamically wetting and drying boundary. The full two-dimensional shallow water equations are the most appropriate for capturing all these complex overland flow features.

Chow and Ben-Zvi (1973) reported the first two-dimensional hydrodynamic model for overland flow using the Lax-Wendroff scheme. Zhang and Cundy (1989) applied the explicit MaCormack finite difference scheme for two-dimensional overland flow. Fielder and Ramirez (2000) also applied the explicit MaCormack scheme with some special treatment of the advection and source terms for two-dimensional overland shallow water equations. Simulation of overland flow at plot size at the scale of $1 \sim 10 \text{ m}^2$ was reported in these studies. These classical methods and some other central difference schemes are prone to numerical instabilities and special treatments are required to achieve a stable and convergent numerical solution. Zhao et al. (1994) developed a finite volume model for two-dimensional surface water flow. Finite volume methods combined with shock capturing scheme have been very popular and seem successful for the homogeneous shallow water equations. However, finite volume methods are intrinsically one-dimensional (normal to the cell interfaces) and the manipulation of source terms is difficult and complicated for higher order schemes. In the finite

difference context, the classical method of characteristics has been considered to be advantageous in solving the two-dimensional shallow water equations for overland flow, but it is also thought to be extremely difficult and not tractable for the general overland flow case of complex topography and variability (Chow and Ben-Zvi, 1973; Zhang and Cundy, 1989). Katopodes and Strelkoff (1978; 1979) developed a numerical scheme based on the method of characteristics in the framework of finite difference method for two-dimensional dam break simulations.

In the finite element framework, it is well known that Galerkin finite element methods perform very poorly for advection-dominant shallow water flows. The streamline upwind finite element methods (SUPG) apply selective dissipation to dampen numerical oscillation (Katopodes, 1984). Lately, the discontinuous Galerkin finite element method has also been applied for trans-critical shallow water flows (Schwanenberg and harms, 2004).

All above-mentioned methods are Eulerian with some stabilization schemes. Since the shallow water equations are partial differential equations of hyperbolic type, characteristics-based or Eulerian-Lagrangian methods are more appropriate. The characteristic Galerkin method (Zienkiewicz et al., 1999) was developed for the scalar advection equation, but is not directly applicable to the shallow water equations because more than one characteristic speeds are involved. The characteristic-based split (CBS) scheme was proposed to resolve this difficulty. Paillere et al. (1998), Brufau and Garcia-

Navarro (2003) and Garcia-Navarro et al. (1995) studied genuinely multidimensional upwinding schemes for the 2D shallow water equations based on a residual distribution scheme with wave models. Guinot (2005) studied approximate two-dimensional Riemann solver for hyperbolic systems of conservation laws in the framework of finite volume methods. They applied the new scheme for dam break problems and demonstrated the improvement in the numerical solutions by a two-dimensional approach for computing the numerical flux in finite volume methods.

In this paper, we present the classical Method of Characteristics (MOC) in the context of finite element methods in the Eulerian-Lagrangian framework; the intrinsic difficulty in two-dimensional MOC methods for two-dimensional shallow water equations is that there are infinite characteristic wave directions to choose from, although there are only three independent wave directions. Hirsch et al. (1987) proposed a diagonalization approach for the multidimensional Euler equations. It is well known that the shallow water equations are analogous to the Euler equations for gas dynamics. Thus, a similar diagonalization was implemented for the shallow water equations in the framework of finite element in the current study. The characteristic decomposition model used by Paillere et al. (1998) was also tested for better stability for sub-critical flow. Numerical schemes based on different combinations of characteristic wave directions were evaluated using typical overland flow examples. The numerical experiments on frictionless circular dam break problem, rainfall-runoff over complex surface, wetland

hydraulics and mixed sub-critical/super-critical flow regime were presented to demonstrate the advantage and limitation of the new method.

3.2 Governing Equations

The governing equations for two-dimensional overland flow are the shallow water equations based on the conservation law of mass and momentum. The two-dimensional shallow water equations in the conservative form are written as follows (Zhao et al., 1994).

$$\frac{\partial U}{\partial t} + \frac{\partial F_x}{\partial x} + \frac{\partial F_y}{\partial y} = G \quad (1)$$

The conservative variables are

$$U = (h, uh, vh)^T \quad (2)$$

where h is water depth; u is the velocity component in the x -direction; v is the velocity component in the y -velocity, respectively. The flux vector F has two components F_x and F_y :

$$F_x = \begin{pmatrix} uh \\ u^2h + \frac{gh^2}{2} \\ uvh \end{pmatrix}, \quad F_y = \begin{pmatrix} vh \\ uvh \\ v^2h + \frac{gh^2}{2} \end{pmatrix} \quad (3)$$

The source term is:

$$G = \begin{pmatrix} R \\ gh(S_{0x} - S_{fx}) \\ gh(S_{0y} - S_{fy}) \end{pmatrix} \quad (4)$$

where R is the source/Sink term as a result of rainfall, evapotranspiration and infiltration, etc. Without losing generality, the eddy turbulent term, momentum exchange flux, surface shear stress (wind effect), etc. have been omitted. When these terms are included, the readers are referred to Yeh, et al. (2006).

The bed slopes are defined as:

$$S_{0x} = -\frac{\partial Z_0}{\partial x}, \quad S_{0y} = -\frac{\partial Z_0}{\partial y} \quad (5)$$

where g is the gravitational acceleration and Z_0 is the bed elevation above a datum. The friction slopes can be approximated by the Manning's equation as

$$S_{fx} = \frac{n^2 u \sqrt{u^2 + v^2}}{h^{4/3}}, \quad S_{fy} = \frac{n^2 v \sqrt{u^2 + v^2}}{h^{4/3}} \quad (6)$$

where n is the Manning's roughness coefficient.

The conservative form is preferred for some conservative schemes such as finite volume methods, and is considered advantageous in dealing with discontinuities in solutions.

On the other hand, the primitive form is more revealing for the intrinsic physical property of the shallow water equations and amendable to advective schemes. With

mathematical manipulations, Equations (1) can be written in the primitive form using (h, u, v) as dependent variables:

$$\frac{\partial h}{\partial t} + u \frac{\partial h}{\partial x} + h \frac{\partial u}{\partial x} + v \frac{\partial h}{\partial y} + h \frac{\partial v}{\partial y} = R \quad (7)$$

$$\frac{\partial u}{\partial t} + g \frac{\partial h}{\partial x} + u \frac{\partial u}{\partial x} + v \frac{\partial u}{\partial y} = g(S_{0x} - S_{fx}) - \frac{uR}{h} \quad (8)$$

$$\frac{\partial v}{\partial t} + g \frac{\partial h}{\partial y} + u \frac{\partial v}{\partial x} + v \frac{\partial v}{\partial y} = g(S_{0y} - S_{fy}) - \frac{vR}{h} \quad (9)$$

which can be written in matrix form as

$$\frac{\partial \mathbf{E}}{\partial t} + \mathbf{A}_x \frac{\partial \mathbf{E}}{\partial x} + \mathbf{A}_y \frac{\partial \mathbf{E}}{\partial y} = \mathbf{R} \quad (10)$$

in which

$$\mathbf{E} = \{h \ u \ v\}^T; \quad \mathbf{A}_x = \begin{bmatrix} u & h & 0 \\ g & u & 0 \\ 0 & 0 & u \end{bmatrix}; \quad \mathbf{A}_y = \begin{bmatrix} v & 0 & h \\ 0 & v & 0 \\ g & 0 & v \end{bmatrix} \quad \text{and} \quad \mathbf{R} = \begin{Bmatrix} R \\ g(S_{0x} - S_{fx}) - \frac{uR}{h} \\ g(S_{0y} - S_{fy}) - \frac{vR}{h} \end{Bmatrix} \quad (11)$$

For an arbitrary wave propagation direction $\mathbf{k} = (k_x, k_y) = (\cos \theta, \sin \theta)$; θ is the angle of the wave direction from x-direction, let the matrix \mathbf{B} be the linear combination of the matrices \mathbf{A}_x and \mathbf{A}_y as follows

$$\mathbf{B} = \mathbf{A} \cdot \mathbf{k} = \mathbf{A}_x \cos \theta + \mathbf{A}_y \sin \theta = \begin{bmatrix} u \cos \theta + v \sin \theta & h \cos \theta & h \sin \theta \\ g \sin \theta & u \cos \theta + v \sin \theta & 0 \\ g \sin \theta & 0 & u \cos \theta + v \sin \theta \end{bmatrix} \quad (12)$$

The three eigenvalues of matrix \mathbf{B} are

$$\lambda_1 = u \cos \theta + v \sin \theta, \quad \lambda_2 = u \cos \theta + v \sin \theta + c, \quad \text{and} \quad \lambda_3 = u \cos \theta + v \sin \theta - c \quad (13)$$

where c is the wave celerity, defined as:

$$c = \sqrt{gh} \quad (14)$$

The right eigenvector of \mathbf{B} is

$$\mathbf{L} = \begin{bmatrix} 0 & \frac{c}{2} & -\frac{c}{2} \\ \sin \theta & \frac{g \cos \theta}{2} & \frac{g \cos \theta}{2} \\ -\cos \theta & \frac{g \sin \theta}{2} & \frac{g \sin \theta}{2} \end{bmatrix} \quad (15)$$

and the inverse matrix of \mathbf{L} :

$$\mathbf{L}^{-1} = \begin{bmatrix} 0 & \sin \theta & -\cos \theta \\ \frac{1}{c} & \frac{\cos \theta}{g} & \frac{\sin \theta}{g} \\ -\frac{1}{c} & \frac{\cos \theta}{g} & \frac{\sin \theta}{g} \end{bmatrix} \quad (16)$$

By definition,

$$\Lambda = \begin{pmatrix} \lambda_1 & 0 & 0 \\ 0 & \lambda_2 & 0 \\ 0 & 0 & \lambda_3 \end{pmatrix} \text{ and } A_x \cos \theta + A_y \sin \theta = L\Lambda L^{-1} \quad (17)$$

The diagonal matrix Λ is the matrix of the eigenvalues of $(\mathbf{A}_x \cos \theta + \mathbf{A}_y \sin \theta)$. It is noteworthy that these eigenvalues are unique for both the Jacobian matrices of the conservative variables and the primitive variables. Let us define a characteristic variable vector \mathbf{W} as

$$\begin{aligned}
\mathbf{W} = \begin{Bmatrix} W_1 \\ W_2 \\ W_3 \end{Bmatrix}^T &= \mathbf{L}^{-1} \mathbf{E} = \begin{bmatrix} 0 & \sin \theta & -\cos \theta \\ \frac{1}{c} & \frac{\cos \theta}{g} & \frac{\sin \theta}{g} \\ -\frac{1}{c} & \frac{\cos \theta}{g} & \frac{\sin \theta}{g} \end{bmatrix} \begin{Bmatrix} h \\ u \\ v \end{Bmatrix} \\
&= \begin{Bmatrix} \frac{u \sin \theta - v \cos \theta}{h + \frac{u \cos \theta}{c} + \frac{v \sin \theta}{c}} \\ \frac{g}{c} \\ -\frac{h}{c} + \frac{u \cos \theta}{g} + \frac{v \sin \theta}{g} \end{Bmatrix} = \begin{Bmatrix} \frac{u \sin \theta - v \cos \theta}{u \cos \theta + v \sin \theta + c} \\ \frac{g}{u \cos \theta + v \sin \theta - c} \\ \frac{g}{g} \end{Bmatrix}
\end{aligned} \tag{18}$$

where W_1 is a characteristic variable associated with a shear wave, which has no equivalent in one-dimensional flow ($\theta = 0$). W_2 and W_3 are characteristic variables associated with the positive and negative gravity waves, respectively.

$$\frac{\partial \mathbf{W}}{\partial t} + \mathbf{L}^{-1} \mathbf{A}_x \mathbf{L} \frac{\partial \mathbf{W}}{\partial x} + \mathbf{L}^{-1} \mathbf{A}_y \mathbf{L} \frac{\partial \mathbf{W}}{\partial y} = \mathbf{L}^{-1} \mathbf{R} \tag{19}$$

i.e.,

$$\frac{\partial \mathbf{W}}{\partial t} + \begin{bmatrix} u & \frac{gc \sin \theta}{2} & -\frac{gc \sin \theta}{2} \\ \frac{c \sin \theta}{g} & u + c \cos \theta & 0 \\ -\frac{c \sin \theta}{g} & 0 & u - c \cos \theta \end{bmatrix} \frac{\partial \mathbf{W}}{\partial x} + \begin{bmatrix} v & -\frac{gc \cos \theta}{2} & \frac{gc \cos \theta}{2} \\ -\frac{c \cos \theta}{g} & v + c \sin \theta & 0 \\ \frac{c \cos \theta}{g} & 0 & v - c \sin \theta \end{bmatrix} \frac{\partial \mathbf{W}}{\partial y} = \mathbf{L}^{-1} \mathbf{R} \tag{20}$$

It is noted that the coefficient matrices $\mathbf{L}^{-1} \mathbf{A}_x \mathbf{L}$ and $\mathbf{L}^{-1} \mathbf{A}_y \mathbf{L}$ of $(\partial \mathbf{W} / \partial x)$ and $(\partial \mathbf{W} / \partial y)$, respectively, cannot be simultaneously diagonalized by the same matrix \mathbf{L} .

Rearranging Equation (20), we obtain

$$\frac{\partial \mathbf{W}}{\partial t} + \begin{bmatrix} u & 0 & 0 \\ 0 & u + c \cos \theta & 0 \\ 0 & 0 & u - c \cos \theta \end{bmatrix} \frac{\partial \mathbf{W}}{\partial x} + \begin{bmatrix} v & 0 & 0 \\ 0 & v + c \sin \theta & 0 \\ 0 & 0 & v - c \sin \theta \end{bmatrix} \frac{\partial \mathbf{W}}{\partial y} = - \begin{Bmatrix} S_1 \\ S_2 \\ S_3 \end{Bmatrix} + \mathbf{L}^{-1} \mathbf{R} \quad (21)$$

in which

$$\begin{Bmatrix} S_1 \\ S_2 \\ S_3 \end{Bmatrix} = \begin{Bmatrix} g \left(\frac{\partial h}{\partial x} \sin \theta - \frac{\partial h}{\partial y} \cos \theta \right) \\ \frac{c}{g} \left[\frac{\partial u}{\partial x} \sin^2 \theta + \frac{\partial v}{\partial y} \cos^2 \theta - \left(\frac{\partial u}{\partial y} + \frac{\partial v}{\partial x} \right) \cos \theta \sin \theta \right] \\ \frac{-c}{g} \left[\frac{\partial u}{\partial x} \sin^2 \theta + \frac{\partial v}{\partial y} \cos^2 \theta - \left(\frac{\partial u}{\partial y} + \frac{\partial v}{\partial x} \right) \cos \theta \sin \theta \right] \end{Bmatrix} \quad (22)$$

This is the characteristic form of two-dimensional shallow water equations with an arbitrary wave direction $\mathbf{K} = (\cos \theta, \sin \theta)$. The left hand side terms represent water wave propagation in the characteristic wave directions and can be written with the total derivative along the characteristics:

$$\begin{Bmatrix} \frac{D_{\vec{v}} W_1}{Dt} \\ \frac{D_{\vec{v}+c\vec{k}} W_2}{Dt} \\ \frac{D_{\vec{v}-c\vec{k}} W_3}{Dt} \end{Bmatrix} = - \begin{Bmatrix} S_1 \\ S_2 \\ S_3 \end{Bmatrix} + L^{-1} R \quad (23)$$

The coupling terms (S_1, S_2, S_3) cannot be simultaneously eliminated and, as in the case of the Euler equations (Hirsh et al., 1987), this results in the non-unique selection of upwind directions for two-dimensional flows.

It is noteworthy that the above characteristic equations in Lagrangian form, Equation (23), are identical to both the original conservative and primitive forms of the shallow water equations. No numerical approximations have been introduced.

The governing equations must be supplemented with initial condition and appropriate boundary conditions for a well-posed two-dimensional overland flow problem. Wave characteristic directions at the boundary determine the required boundary conditions. For example, at an inflow boundary, if flow is subcritical, both shear wave traveling along the streamline and the positive gravity wave along the normal into the flow domain, so two boundary conditions have to be imposed.

3.3 Numerical Methods

The Eulerian-Lagrangian method (ELM) is a popular framework for the numerical solution of the scalar advection-diffusion transport equation. This can be extended to the solution of advection dominant flow equations. In the case of two-dimensional shallow water equations, the advection of shear wave and gravity wave properties in the space-time domain can be decoupled into three convective equations with source terms, as shown in Equation (23).

After the selection of two specific characteristic directions with the propagation angles, θ_1 and θ_2 , new characteristic variables are defined as

$$\mathbf{W} = \begin{Bmatrix} W_1 \\ W_2 \\ W_3 \end{Bmatrix}^T = L^{*-1} E = \begin{bmatrix} 0 & \sin \theta_1 & -\cos \theta_1 \\ \frac{1}{c} & \frac{\cos \theta_2}{g} & \frac{\sin \theta_2}{g} \\ -\frac{1}{c} & \frac{\cos \theta_2}{g} & \frac{\sin \theta_2}{g} \end{bmatrix} \begin{Bmatrix} h \\ u \\ v \end{Bmatrix} \quad (24)$$

$$\mathbf{L}^* = \begin{bmatrix} 0 & \frac{c}{2} & -\frac{c}{2} \\ \sin \theta_2 / \omega & \frac{g \cos \theta_2}{2\omega} & \frac{g \cos \theta_2}{2\omega} \\ -\cos \theta_2 & \frac{g \sin \theta_2}{2\omega} & \frac{g \sin \theta_2}{2\omega} \end{bmatrix} \quad (25)$$

where $\omega = \cos \theta_1 \cos \theta_2 + \sin \theta_1 \sin \theta_2$. Since ω should not be zero, the two wave directions cannot be orthogonal. By replacing the new characteristic variables and matrix \mathbf{L}^* into Equation (19), we obtain the following equations:

$$\frac{\partial \mathbf{W}}{\partial t} + \begin{bmatrix} u & 0 & 0 \\ 0 & u + c \cos \theta_2 & 0 \\ 0 & 0 & u - c \cos \theta_2 \end{bmatrix} \frac{\partial \mathbf{W}}{\partial x} + \begin{bmatrix} v & 0 & 0 \\ 0 & v + c \sin \theta_2 & 0 \\ 0 & 0 & v - c \sin \theta_2 \end{bmatrix} \frac{\partial \mathbf{W}}{\partial y} = - \begin{Bmatrix} S_1 \\ S_2 \\ S_3 \end{Bmatrix} + \mathbf{L}^{*-1} \mathbf{R} \quad (26)$$

$$\begin{Bmatrix} S_1 \\ S_2 \\ S_3 \end{Bmatrix} = \begin{Bmatrix} g \left(\frac{\partial h}{\partial x} \sin \theta_1 - \frac{\partial h}{\partial y} \cos \theta_1 \right) \\ \frac{c}{g} \left[\frac{\partial u}{\partial x} \sin^2 \theta_2 + \frac{\partial v}{\partial y} \cos^2 \theta_2 - \left(\frac{\partial u}{\partial y} + \frac{\partial v}{\partial x} \right) \cos \theta_2 \sin \theta_2 \right] \\ -\frac{c}{g} \left[\frac{\partial u}{\partial x} \sin^2 \theta_2 + \frac{\partial v}{\partial y} \cos^2 \theta_2 - \left(\frac{\partial u}{\partial y} + \frac{\partial v}{\partial x} \right) \cos \theta_2 \sin \theta_2 \right] \end{Bmatrix} \quad (27)$$

A numerical scheme is designed to solve Equation (26):

- (1) From a new time step, the intermediate values of the unknowns (h, u, v) at a global node (h*, u*, v*) are obtained by backward tracking

along the characteristics until the foot of the characteristics at the old time step is reached or a boundary is hit.

- (2) The final numerical solutions are obtained by integrating the RHS terms along the characteristic lines with a simple trapezoidal integration rule.

3.3.1 Backward Tracking approach

In the finite element context, the backward tracking scheme is a sub-element-tracking scheme developed by Cheng et al. (1996) and improved by Suk (2003). The solution values at the foot of the characteristic curve are interpolated by linear finite elements.

3.3.2 Characteristic wave directions

Choosing the two wave characteristic directions (θ_1 and θ_2) is the most critical part of the characteristics-based finite element method. It can be seen that the first characteristic speed (u, v) is along the streamlines and only the two characteristic directions associated with the gravity waves need to be chosen.

The first approach is the wave directions based on maximum diagonalization: The first choice is based on the minimization of the coupling term (Equation (27)). This follows the diagonalization approach for the Euler equations suggested by Hirsh et al. (1987). By setting the coupling terms to zero, we have the following relationships.

$$\begin{aligned}
g \left(\frac{\partial h}{\partial x} \sin \theta_1 - \frac{\partial h}{\partial y} \cos \theta_1 \right) &= 0, \\
\frac{c}{g} \left[\frac{\partial u}{\partial x} \sin^2 \theta_2 + \frac{\partial v}{\partial y} \cos^2 \theta_2 - \left(\frac{\partial u}{\partial y} + \frac{\partial v}{\partial x} \right) \cos \theta_2 \sin \theta_2 \right] &= 0, \\
\frac{-c}{g} \left[\frac{\partial u}{\partial x} \sin^2 \theta_2 + \frac{\partial v}{\partial y} \cos^2 \theta_2 - \left(\frac{\partial u}{\partial y} + \frac{\partial v}{\partial x} \right) \cos \theta_2 \sin \theta_2 \right] &= 0
\end{aligned} \tag{28}$$

From the above algebraic equations, we observe that the first characteristic direction is related to the shear wave and the two gravity waves share the same second characteristic direction.

The first characteristic direction is determined by

$$\tan \theta_1 = \frac{\partial h / \partial y}{\partial h / \partial x} \tag{29}$$

which is in the pressure gradient direction.

The second characteristic direction, if one exists, is based on the solution of the following equation:

$$\frac{\partial u}{\partial x} \sin^2 \theta_2 + \frac{\partial v}{\partial y} \cos^2 \theta_2 - \left(\frac{\partial u}{\partial y} + \frac{\partial v}{\partial x} \right) \cos \theta_2 \sin \theta_2 = 0 \tag{30}$$

Equation (30) can have two, one, or no solutions. If no solutions can be found, the following particular characteristic direction as suggested in Roe (1986) for the treatment of the Euler equations will be used

$$\tan \theta_2 = \frac{\partial u / \partial y + \partial v / \partial x}{\partial u / \partial x - \partial v / \partial y} \tag{31}$$

If one solution can be found, it is used in computing θ_2 . If two real solution can be found, the one that maximizes $\omega = \cos\theta_1 \cos\theta_2 + \sin \theta_1 \sin \theta_2$ will be used.

It is noteworthy that by choosing wave decomposition following the flow gradients (depth and velocity), it may be possible to minimize the coupling terms and obtain diagonalization of the shallow water equations. However, numerical experiments show that this approach often suffer from convergence problem (e.g., Paillere et al., 1998). The characteristic directions are dependent on the numerical solution and sensitive to the accurate evaluation of the gradients of water depth and velocity components. Numerical stability and convergence are the major concern.

The second approach is the characteristic decomposition: Proposed by Paillere et al., 1998, when the flow is supercritical, the angle θ_2 is taken to be along the Froude line as

$$\sin \theta_2 = \frac{1}{Fr} \quad (32)$$

where Fr is the Froude number defined as ($Fr^2 = (u^2+v^2)/c^2$). If the flow is subcritical, the propagation angle is taken as

$$\tan \theta_2 = \frac{1}{\sqrt{1-Fr^2}} \quad (33)$$

The first characteristic direction θ_1 is chosen to be equal to the angle θ_2 in order to maximize the determinant of the transformation ($\omega = 1.0$).

The coupling terms will not be zero with this selection of characteristic directions. On the other hand, numerical experiments show that this approach is more stable.

The last approach is the ad-hoc wave directions based on some geometric parameters:

The first characteristic direction can always be selected in the depth gradient direction. The second characteristic directions can be chosen arbitrary, for example, along the x-direction, the y-direction or the steepest elevation gradients. This approach is less accurate and grid orientation of the numerical solutions may occur.

3.4 Verification and Validation Examples

3.4.1 Example 1: non-uniform steady flow in a straight channel

This is a nontrivial channel flow benchmark problem reported by (MacDonald et al., 1997) to verify and test the performance of numerical methods for open channel flows.

A steady flow of $20 \text{ m}^3/\text{s}$ is maintained in a 1000 m of rectangular channel with a constant width of 10 m. the Manning's roughness coefficient for the channel is 0.02 and the bottom slope is given as a function of desired water depth profile. The flow is subcritical at the upstream boundary and supercritical at the downstream boundary and critical flow at 500 m from upstream end. The exact analytical solution was provided by (MacDonald et al., 1997).

The bottom slope is variable and is given as function of x as

$$S_o(x) = \left[1 - \frac{4}{gh(x)^3} \right] \frac{dh}{dx} + 0.16 \frac{[2h(x) + 10]^{4/3}}{[10h(x)]^{10/3}} \quad (34)$$

The bottom slope given in Eq. (34) would render the flow conditions subcritical at the inflow boundary and supercritical at the outlet. The Manning's n value is 0.02. This test problem has an exact solution (MacDonald et al. 1997)

$$h(x) = \begin{cases} \left(\frac{4}{g} \right)^{1/3} \left\{ 1 - \frac{1}{3} \tanh \left[3 \left(\frac{x}{1000} - \frac{1}{2} \right) \right] \right\} & 0 \leq x \leq 500 \\ \left(\frac{4}{g} \right)^{1/3} \left\{ 1 - \frac{1}{6} \tanh \left[6 \left(\frac{x}{1000} - \frac{1}{2} \right) \right] \right\} & 500 \leq x \leq 1000 \end{cases} \quad (35)$$

The bed slope is plotted in Figure 3-1. For simulation, 500 rectangular element size of 2 m x 10 m is used and specified inflow of 20 m³/s is applied at the upstream end and since the flow is supercritical at the outflow end, no boundary conditions were used at that location. A transient simulation was conducted with the constant boundary conditions until the solution approached steady state.

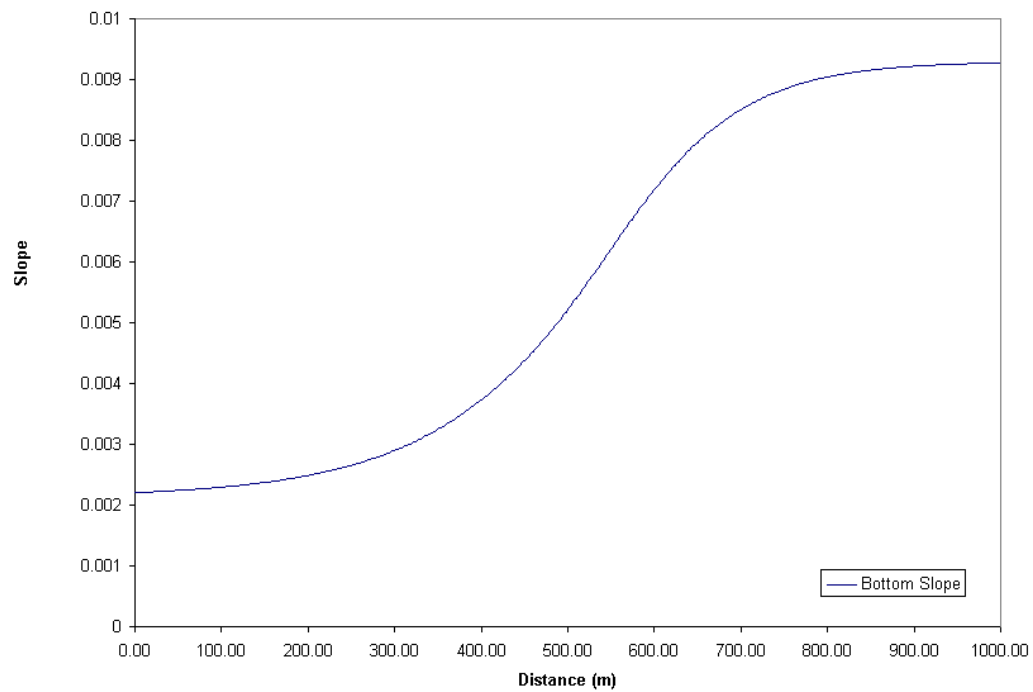


Figure 3-1: Bottom Slope for Example 1

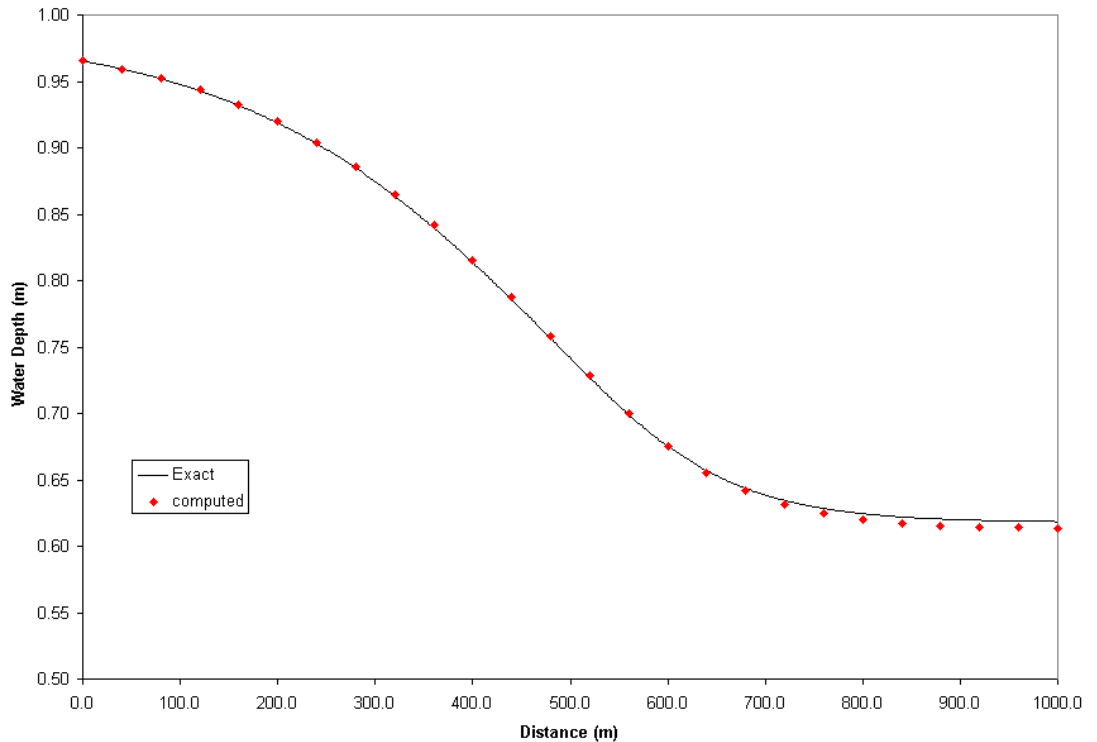


Figure 3-2: Computed and Exact Water Depth along the Channel

As shown in Figure 3-2, the good match between computed and exact solutions demonstrates that the characteristics based finite element method is correctly implemented and can solve mixed subcritical and supercritical flow regimes with adequate accuracy and numerical stability.

3.4.2 Example 2: Rainfall-runoff on a sloping plane

This simple example is used to test and verify that the implementation of the characteristics-based numerical scheme is correct and accurate for overland flow.

Overland flow on a sloping plane was simulated and compared with the analytical solution. The impervious plane is 800 m x 1,000 m, the bottom slope is 0.05, and the Manning's roughness coefficient value is 0.015. A constant rainfall intensity of 10.8 mm/hour over the duration of 1.5 hours was applied uniformly on the surface.

The flow domain was discretized into 100 rectangular elements of 80 m x 100 m. At the downstream outlet, a zero depth gradient boundary was applied. A time step of 20 s was applied during the simulation run of 170 minutes. Since the slope is steep (5%), the kinematic wave approximation is relatively accurate and there is a kinematic analytical solution for the outlet discharge (Singh, 1996).

The computed outlet discharge hydrograph was compared with the kinematic analytical solution in Figure 3-3. The numerical solution is very close to the analytical solution and the mass error is very small.

The characteristics-based method is stable and no numerical oscillation occurred. For this example, the flow is one-dimensional, so the down slope direction was selected as the wave characteristic direction.

Since the characteristics-based method is not inherently conservative, significant mass error may occur when coarse meshes and large time steps are used.

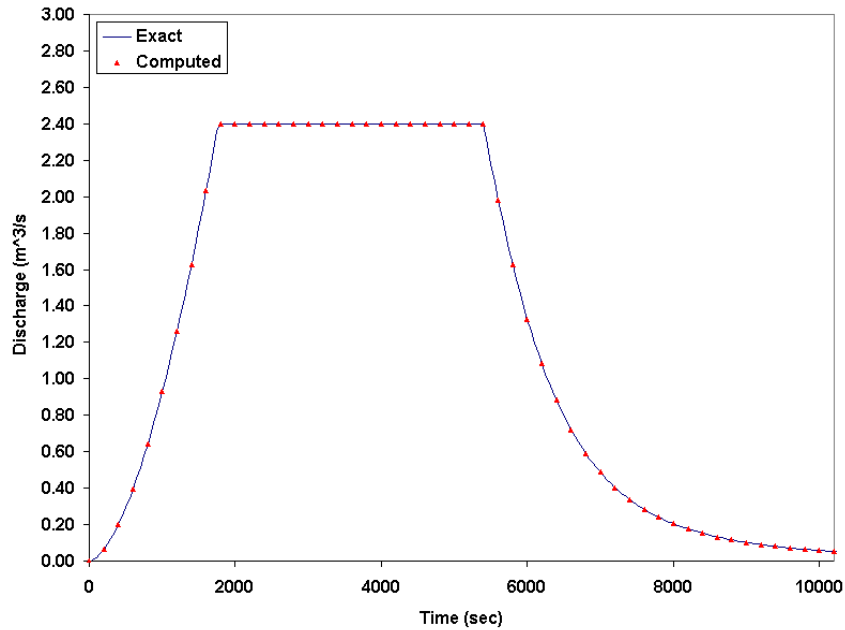


Figure 3-3: Outflow Hydrograph (Analytical vs. numerical solutions)

3.4.3 Example 3: Two-dimensional Circular dam break problem

This is an academic test problem. A circular dam with a radius of 11 m is located in the center of a 50 m x 50 m computational domain. The bed is horizontal and frictionless. The initial water depth in the dam is 10 m and 1 m outside the dam (Figure 3-4). The dam is instantaneously removed at time = 0.

It has been widely used in hydraulics literature to test performance of different numerical methods (e.g., Schwanenberg and harms, 2004; Tseng and Chu, 2000 and Alcrudo and Garcia-Navarro, 1993, among others).

The dominant wave propagation direction is known *a priori*. It is along the radial directions. So it is a good example to test impact of chosen wave directions on numerical solutions.

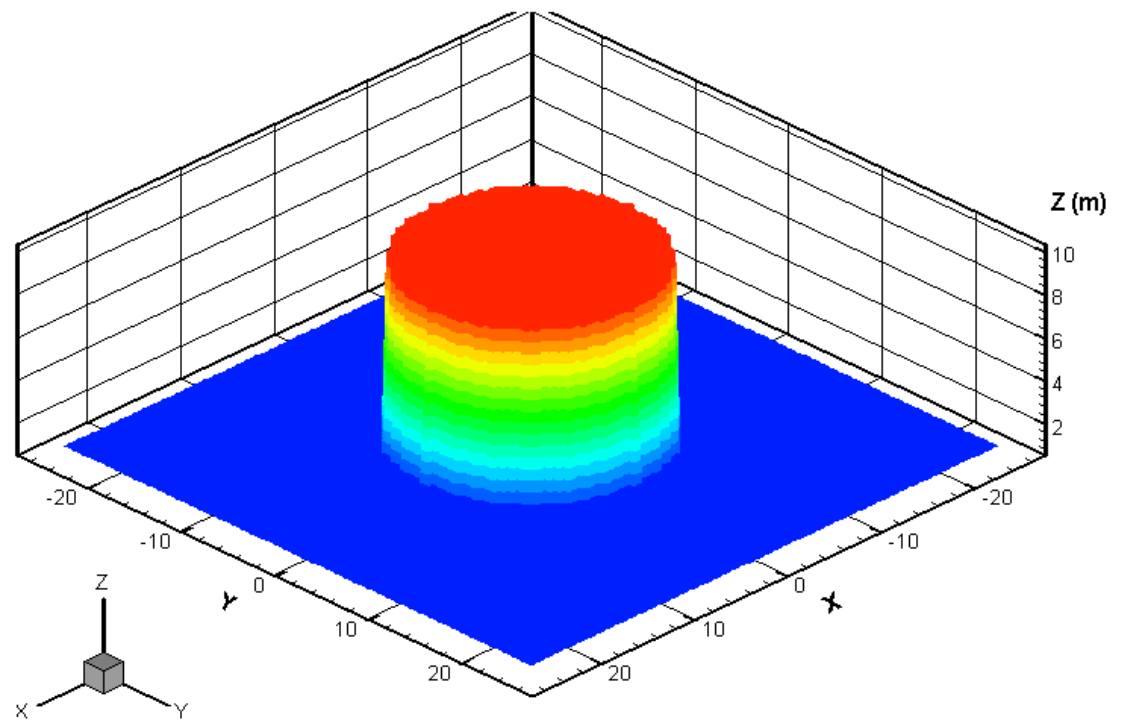


Figure 3-4: Initial Water Depth of Circular Dam-break Problem

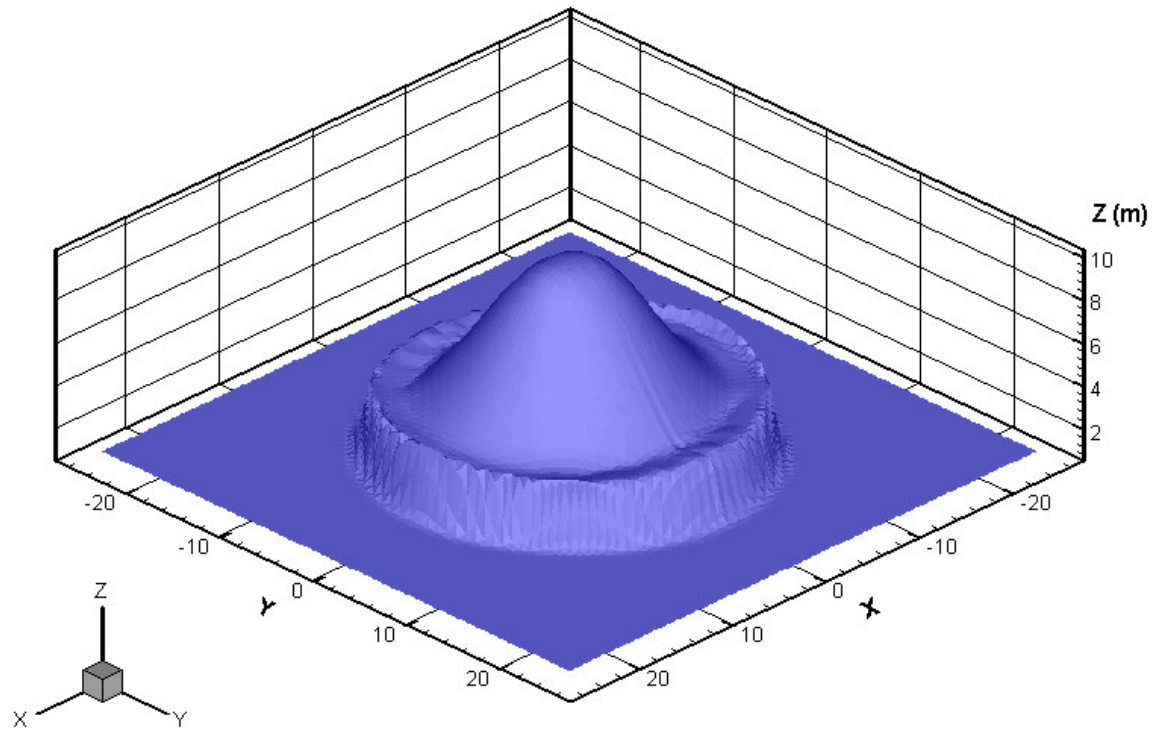


Figure 3-5: Water depth at time = 0.69 sec

As pointed out by Schwanenberg and harms (2004), the solution between the shock wave and the rarefaction wave is not flat as in the corresponding one-dimensional dam break. This difference arises from the two-dimensional nature of the flow and is a good test for the correctness of a numerical solution. As shown in Figure 3-5, the solution solved by the characteristics based finite element method was able to capture this aspect of the solution quite well. The radial symmetry of water depth is also preserved well considering the use of triangular elements and a perfect symmetry could not be set at the beginning of the simulation. The solution shown in Figure 3-5 was obtained by the wave directions based on maximum diagonalization.

The grid orientation effect of selected arbitrary wave directions was demonstrated in a solution that used the x-direction ($\theta_2 = 0$) as the second characteristic direction. As can be seen in Figure 3-6, a pre-specified characteristic direction cannot capture the two-dimensional nature as well as by a dynamically computed wave direction, significant spatial bias in the y-direction is revealed.

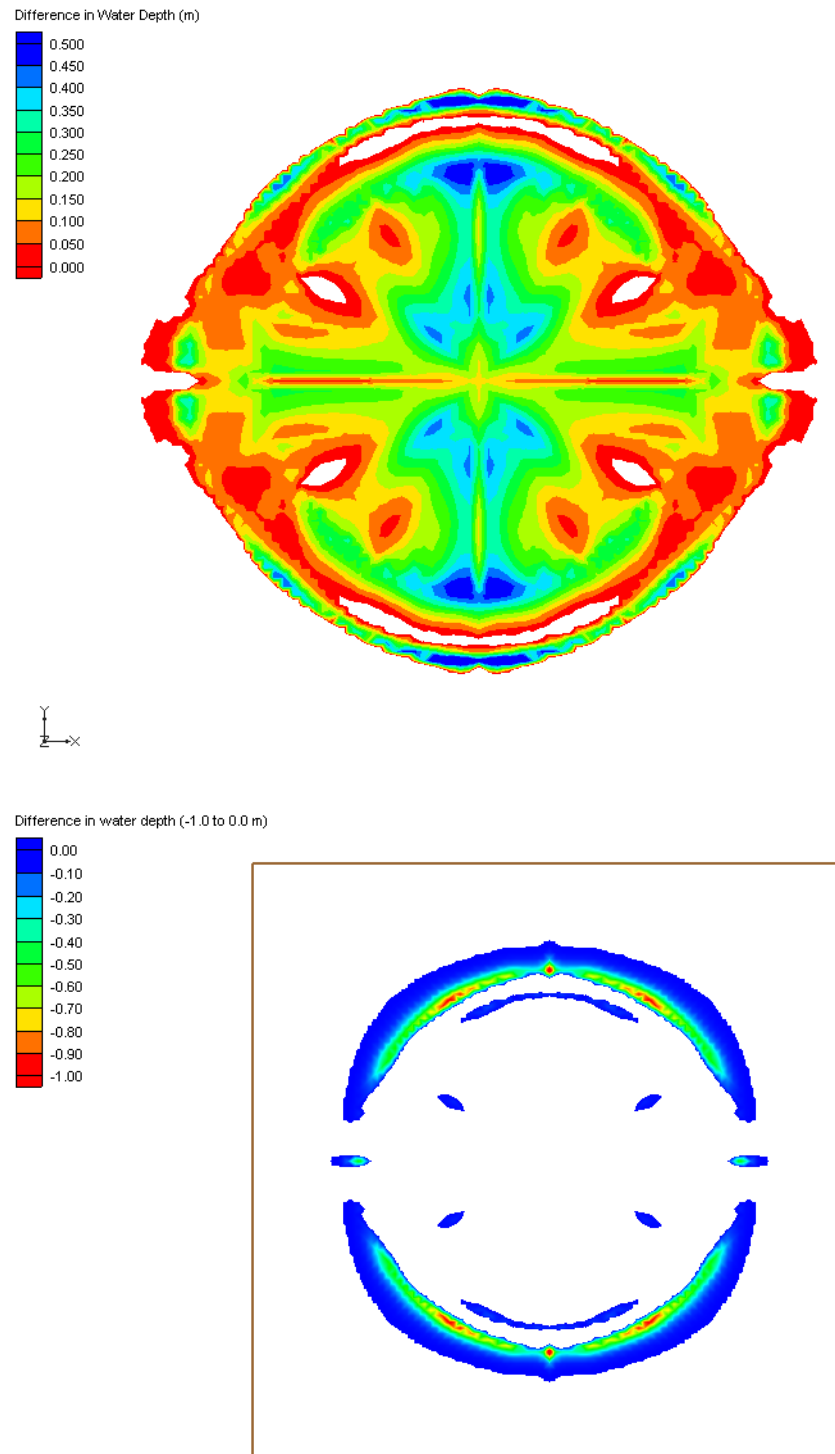


Figure 3-6: Impact of Selected Characteristic Direction on Computed Water Depth

3.4.4 Example 4: rainfall-runoff process over a three-plane cascade surface

This example is simulated to partially validate the appropriateness of the governing equations for modeling the physical phenomena of overland flow by comparison with experimental data. Furthermore, kinematic shock waves were generated by the changes in bed slopes for the case of short rainfall duration (10 s) and it is a good test of the capability of the numerical scheme in dealing with this.

Overland flow on a three-plane cascade surface was experimented by Iwagaki (1955). A series of artificial rainfall was applied on a smooth aluminum laboratory flume surface. The flume is 24 m in length and is divided into three planes with constant slopes of 0.020, 0.015, and 0.010, respectively from upstream to downstream. The constant rainfall intensities of 389, 230, and 288 cm/hour were applied to upper, middle and lower plane, respectively, for the durations of 10 s, 20 s, and 30 s in three experiments.

The model simulations of the three-plane cascade example were made with a uniform finite element mesh size of 0.25 m by 0.25 m. The whole plane surface consisted of 768 elements and 873 nodes. A Manning's roughness coefficient of 0.007 was used. No-flow boundary condition was applied except a critical flow condition was used at the outlet. This is a one-dimensional flow problem, so the wave directions are known *a priori*, and they are along the direction of the plane slopes.

The computed outflow hydrograph compares Iwagaki's 1955 experimental data for the three cases are shown in Figures 3-7 through 3-9. The difficult case with shock wave (rainfall duration of 10 s) was simulated successfully as well. This example has been simulated with a kinematic shock-fitting model (Borah et al., 1980) and the shallow water equations with the MacCormack finite difference scheme (Zhang and Cundy, 1989) or upwind finite element method (Tisdale et al., 1998). Numerical instabilities and oscillations were reported in most of these previous studies. On the other hand, the numerical solutions by the characteristics-based finite element method did not encounter similar difficulties.

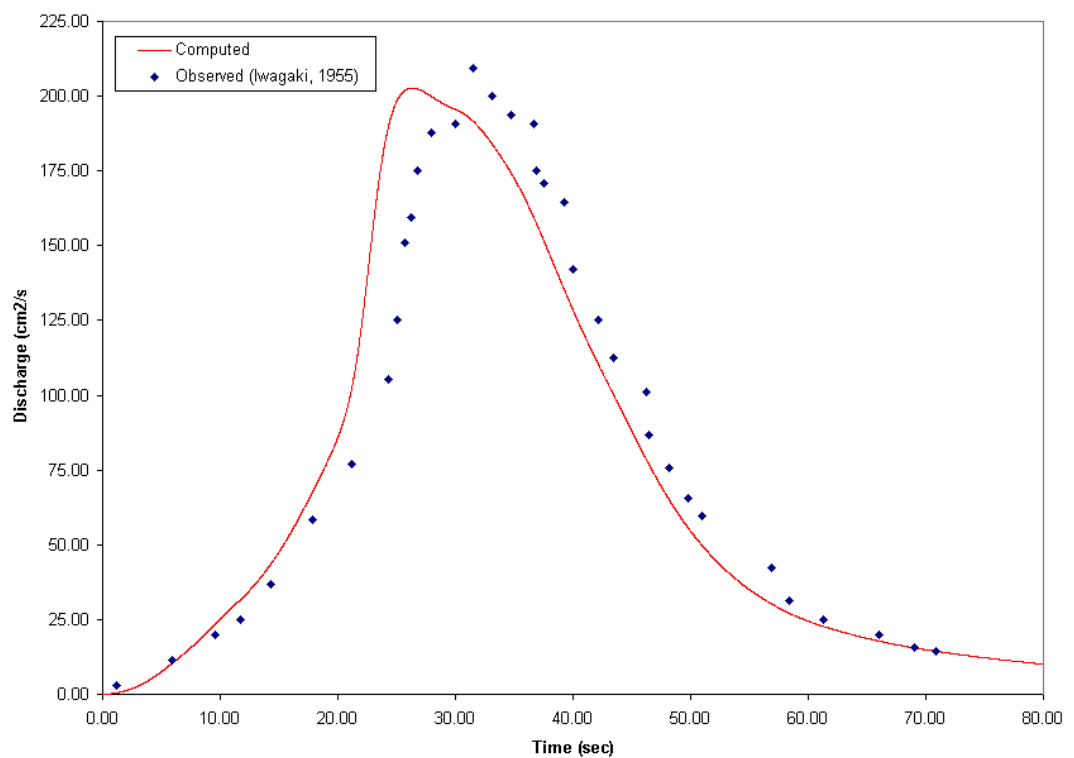


Figure 3-7: Computed and Observed Discharge Hydrograph for the three-plane cascade with rainfall duration of 30 s

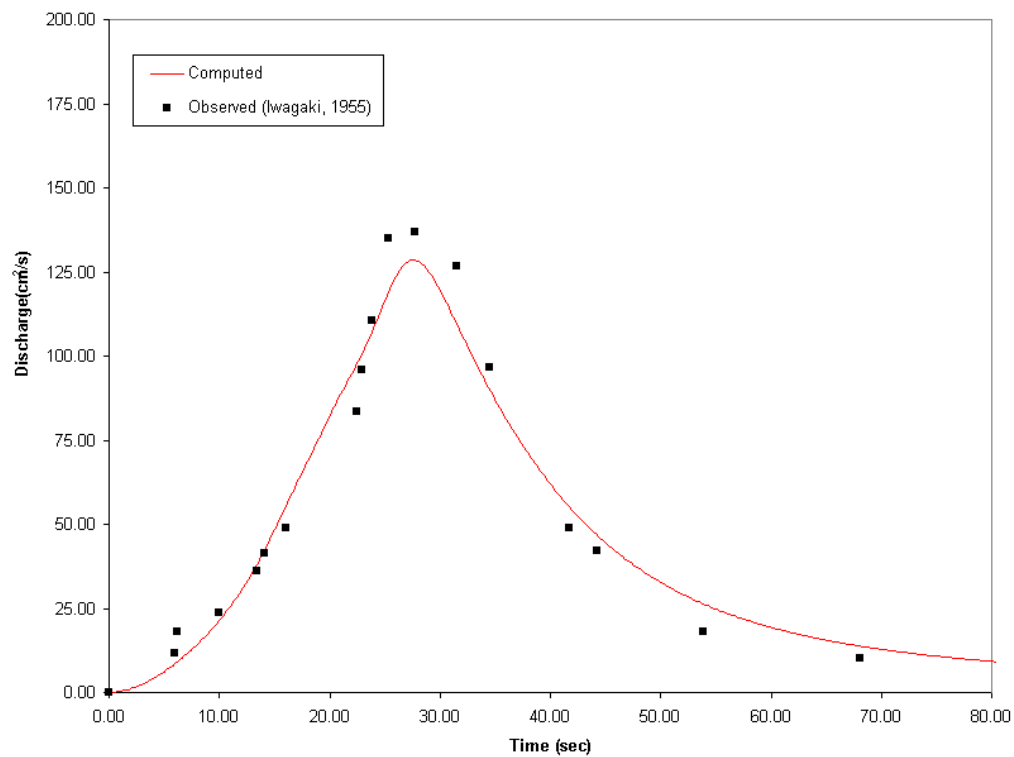


Figure 3-8: Computed and Observed Discharge Hydrograph for the three-plane cascade with rainfall duration of 20 s

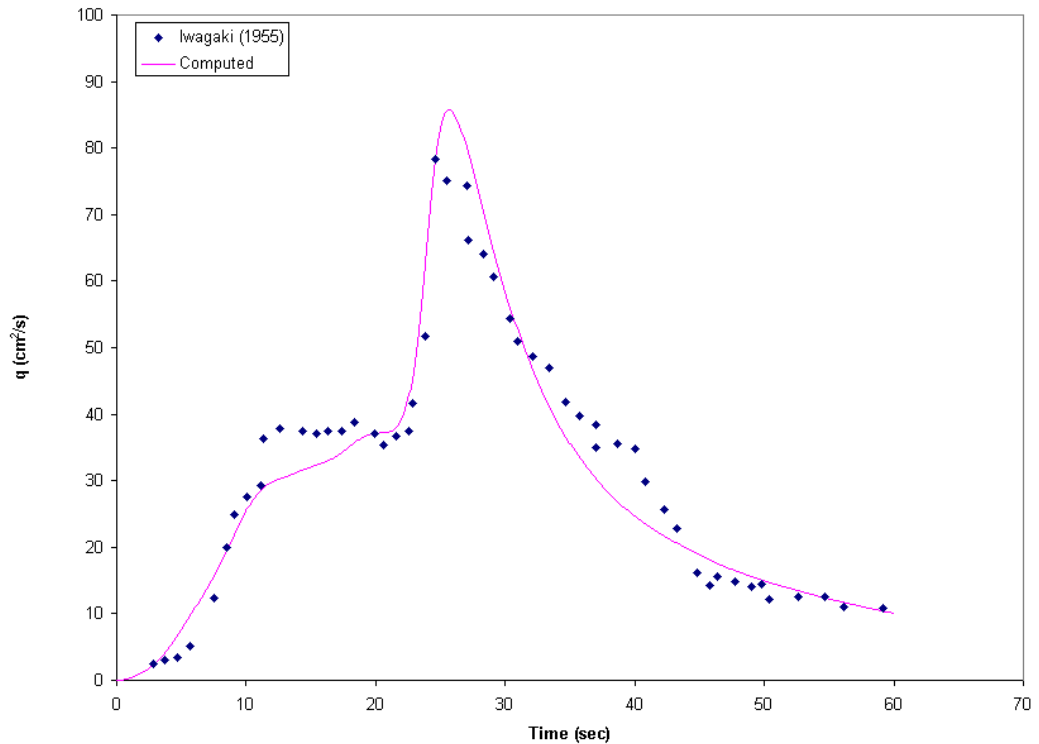


Figure 3-9: Computed and Observed Discharge Hydrograph for the three-plane cascade with rainfall duration of 10 s

3.4.5 Example 5: Overland flow in a hypothetical wetland

One important application of the full two-dimensional shallow water equations is water movement in low terrain areas (e.g., flood plains, wetlands irrigated farmlands and tidal flats) where simplified diffusion wave approximation is not appropriate. A numerical experiment was designed to test model performance under such conditions.

The overland domain is a rectangular area of 500 m x 400 m. No-flow boundary was applied except there was an opening of 100 m at the center of the downstream boundary (Figure 3-10). This partial outlet and the micro-topography produced the two-

dimensional nature of overland flow. Micro-topography was added to the horizontal land surface elevations (200.0 m). The land surface elevations range from 199.98 m to 200.02 m (Figure 3-11).

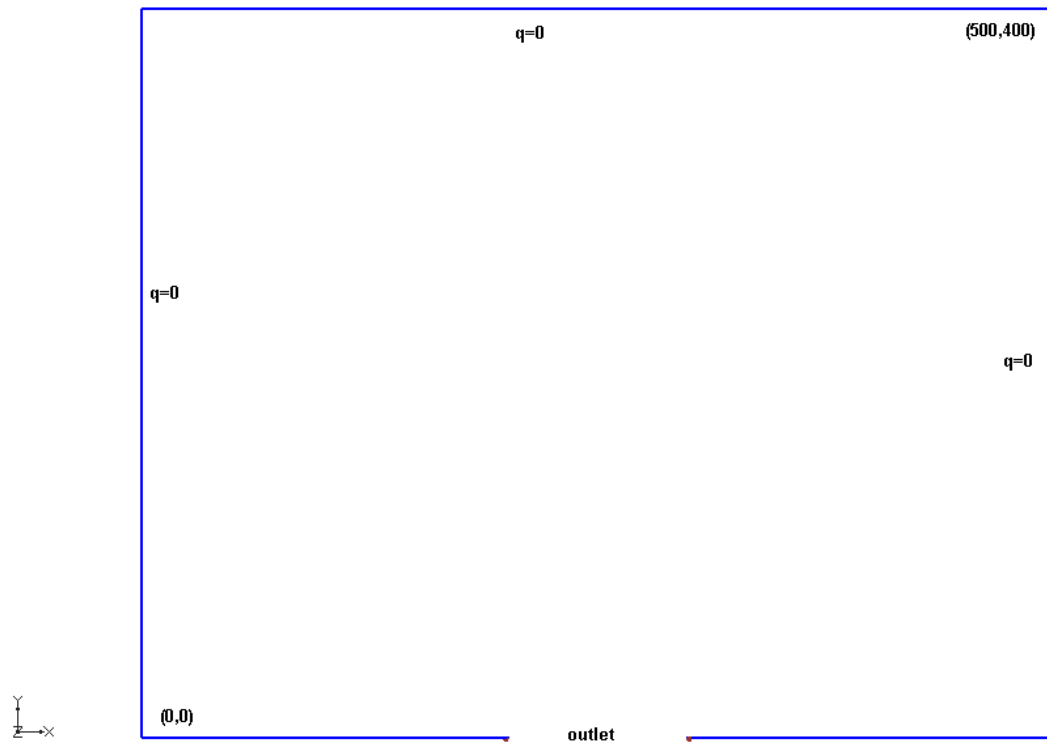


Figure 3-10: Model Domain Layout

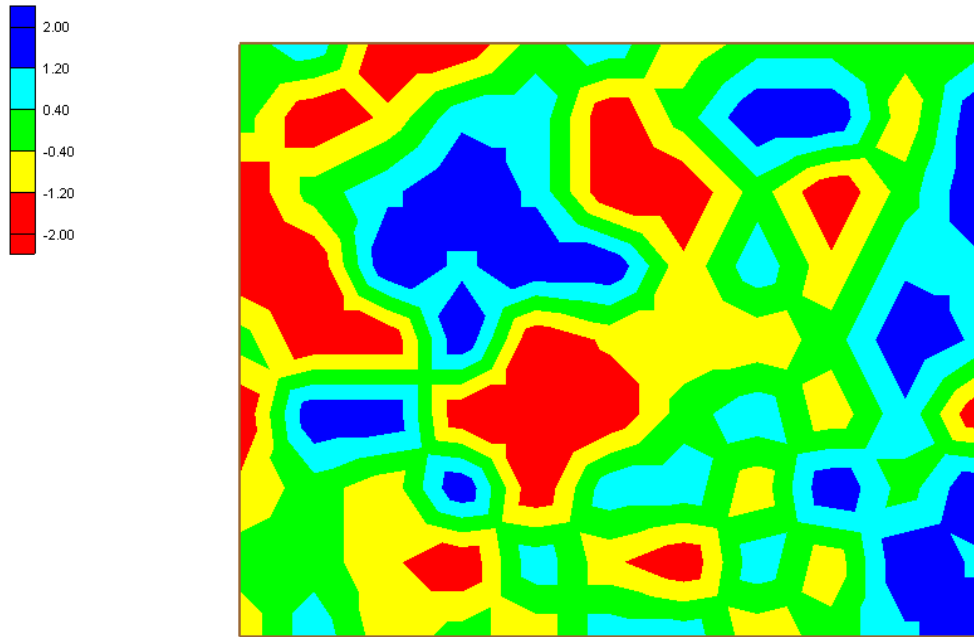


Figure 3-11: Variation of Land Surface Elevations (cm)

A constant rainfall intensity of 4.0×10^{-6} m/s was applied to the whole surface area for 64,000 seconds and critical flow boundary condition was used at the outlet. The model domain was discretized into 640 identical triangular elements. A Manning's roughness coefficient of 0.20 was used. Model simulations were conducted with a time step of 10 seconds.

The computed discharge hydrograph at the outlet and water depth and velocity magnitude distribution at the end of rainfall were plotted in Figures 3-12 through 3-14, respectively. These results demonstrate that the model can be applied to real field problem with complex topography.

The aforementioned simulation results were obtained by applying the diagonalized wave characteristic directions (the first approach in Section 3.3.2). Several other wave characteristic directions were also tested for this example problem. These other wave characteristic directions include: (1) the Froude line directions (the second approach); (2) in the computed velocity direction; (3) fixed in the y-directions.

The computed water depth and velocity magnitude at the center of the domain $(x,y) = (250, 200)$ are compared in Figures 3-15 and 3-16. From the simulation results, the use of the diagonalized wave directions and computed velocity directions produce very close water depth and velocity. On the other hand, the Froude line approach obtained lowest computed water depth and highest velocity magnitude. The use of fixed y-direction as wave characteristic directions results in computed water depth and velocity between the ranges of results obtained with the other two approaches. This means that selected wave directions have impact on simulation results.

Since the approaches using the diagonalization wave direction and computed velocity direction yield very close simulations, we surmise that these simulations are the correct solutions. On the other hand, we suspect that the simulations with the Froude line approach or the fixed y-direction approach may have produced inaccurate solutions.

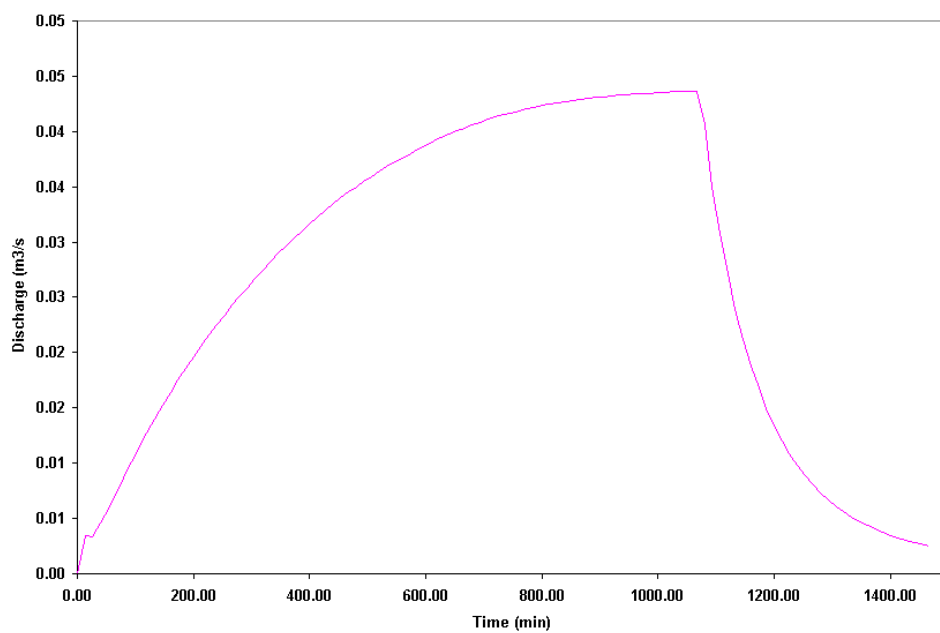


Figure 3-12: Discharge Hydrograph at the Outlet

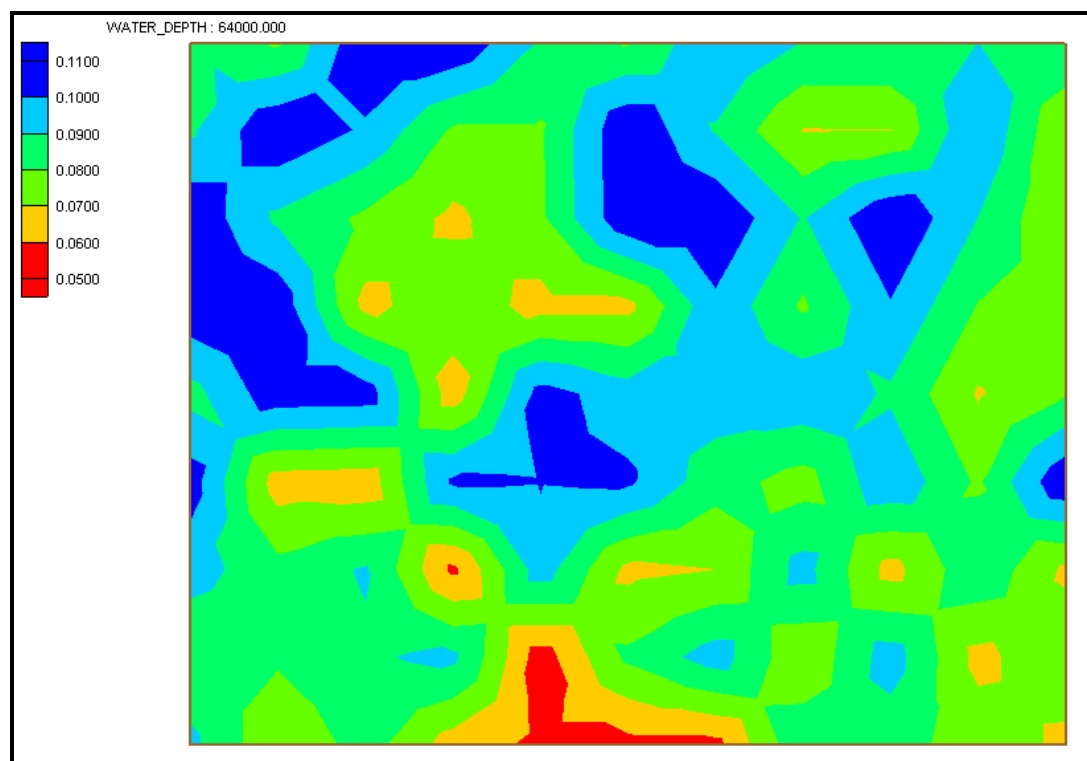


Figure 3-13: Water Depth Distribution at time =64,000 sec (m)

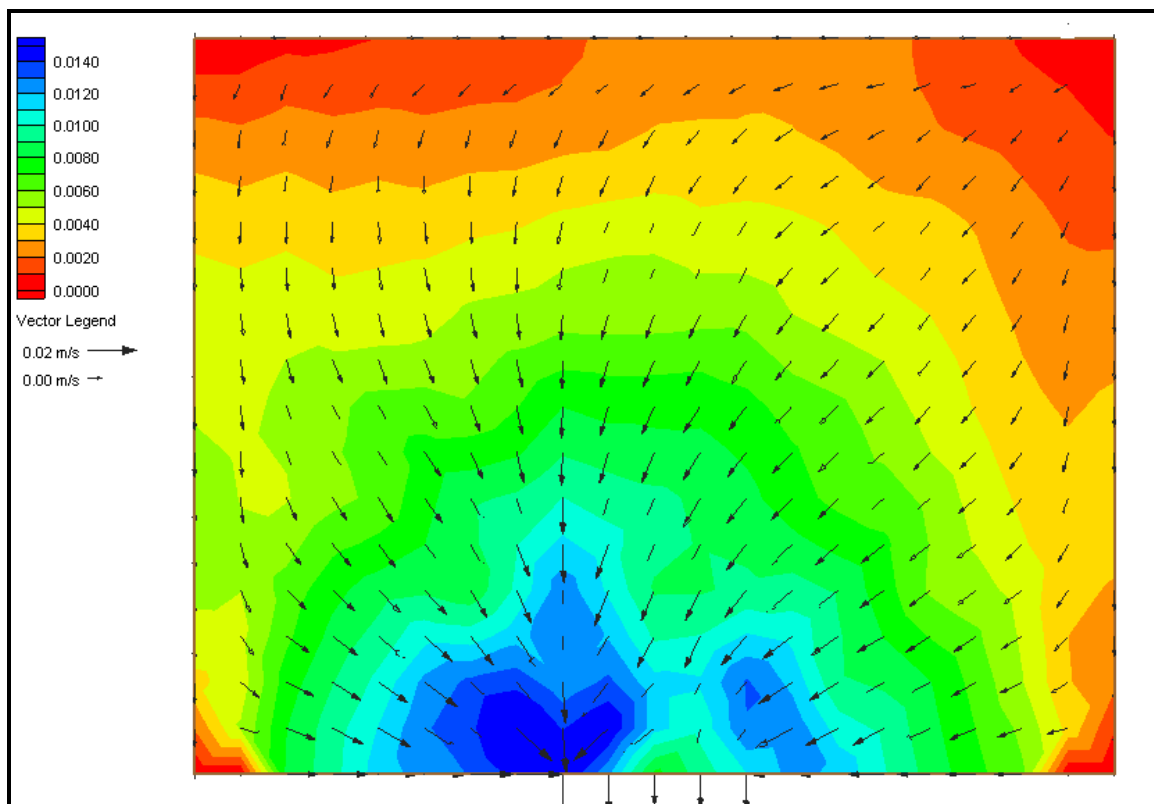


Figure 3-14: Velocity Magnitude at time = 64,000 sec

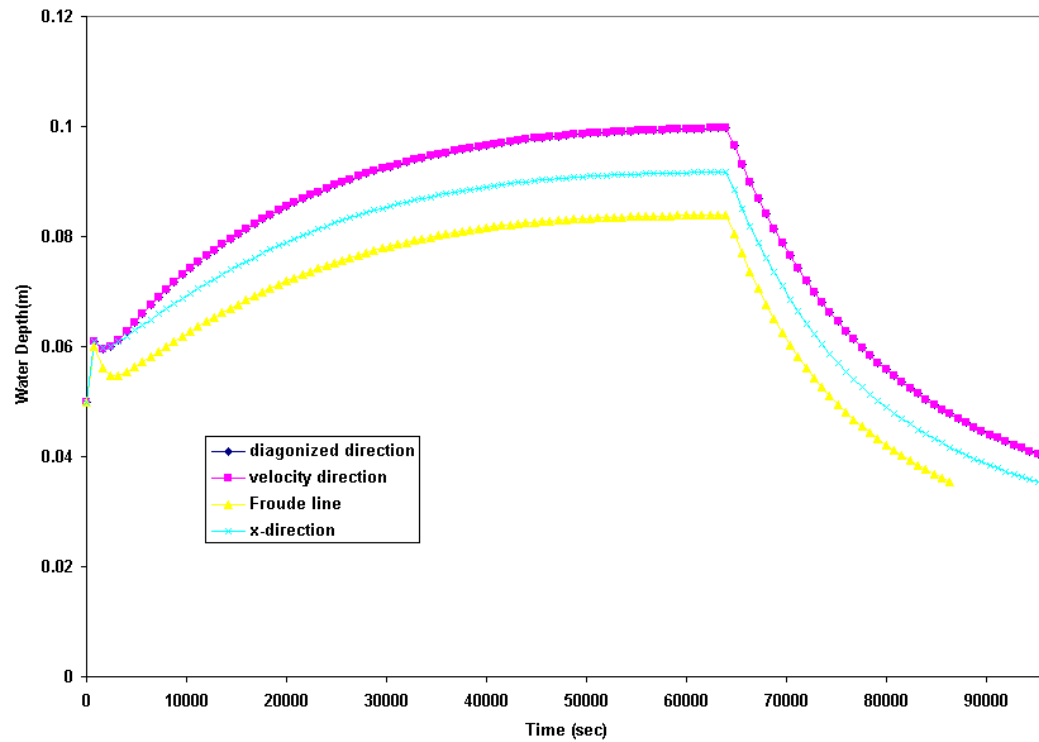


Figure 3-15: Computed water depth at (250,200) obtained by using different wave directions

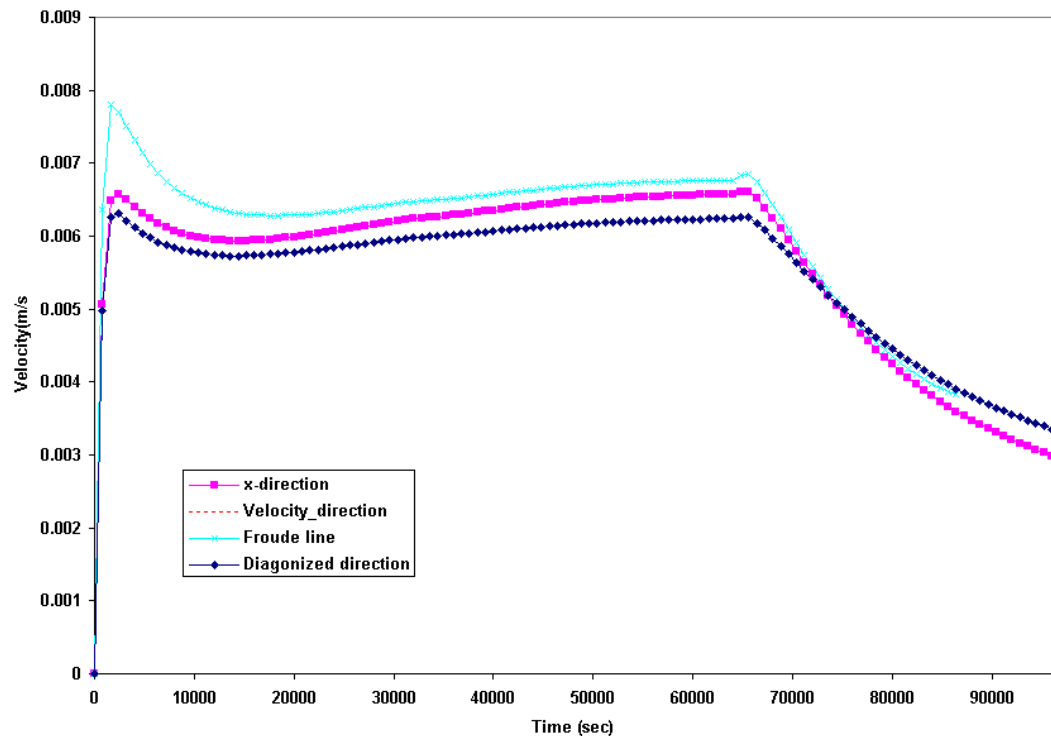


Figure 3-16: Computed velocity magnitude at (250,200) obtained by using different wave directions

3.5 Discussions

We have demonstrated that it is feasible to apply the finite element method for two-dimensional shallow water equations used to measure overland flow. The advantages in such a numerical scheme include: (a) straightforward and physics-based treatment of boundary conditions; (b) source terms are easily handled; and (c) numerical instabilities and oscillation in Galerkin or simple upwind finite element methods are avoided.

By implementing the numerical schemes with linear finite elements, the accuracy is first-order in space and time. Numerical diffusion is a major concern, however, the maximum and minimum water depth were preserved satisfactory in the circular dam break problem. A further work is to compare the performance of the current scheme with the characteristic-based split (CBS) scheme (Zienkiewicz et al., 1999).

3.6 Summary and Conclusions

A characteristics based finite element method was applied to solve the two-dimensional shallow water equations for overland flow. Implementation details, especially the selection of characteristic wave directions, were discussed. In the selection of wave characteristic directions, numerical simulations of the circular dam break and overland flow in a hypothetical wetland, computed water depth, and velocity are affected. Arbitrarily selected wave directions (e.g., x or y directions) result in less accurate results in the circular dam break example. Further examination of this issue, with more test examples having observed or exact solutions, is warranted.

It is concluded that this numerical method is very suitable for numerical solutions of two-dimensional overland flow with thoughtful selection of wave characteristic directions. One of this method's advantages is that the treatment of the source term and boundary conditions; they are straightforward and physically based. Further study is needed to make it more stable for real watersheds with complex topography. Since the

Lagrangian approach is not inherently mass conservative, careful checking of mass error is a must for the model's successful application.

Acknowledgements

This research is supported by the U.S. EPA - Science To Achieve Results (STAR) Program under Grant # R-82795602 with the University of Central Florida.

References

- Alcrudo, F. and Garcia-Navarro, P. (1993). "A high-resolution Godunov-type scheme in finite volumes for the 2D shallow water equations.", *International Journal of Numerical Methods in Fluids*, 16, 489-505.
- Borah, DK; Prasad, SN; Alonso, CV. (1980). Kinematic Wave Routing Incorporating Shock Fitting. *Water Resources Research* Vol 16, No 3, p 529-541, June 1980.
- Brufau P., P. Garc_1a-Navarro. (2003). Unsteady free surface flow simulation over complex topography with a multidimensional upwind technique. *Journal of Computational Physics* 186 (2003) 503–526.

Cheng H-P., Cheng J-R, Yeh GT. (1996). “ A particle tracking technique for the Lagrangian-Eulerian finite element method in multi-dimensions.” *International Journal of Numerical Methods in Engineering*. 39: 1115-1136.

Chow and Ben-Zvi. (1973). Hydrodynamic modeling of two-dimensional watershed flow, *Journal of Hydraulic Division ASCE*, 99(HY1), P.2023--2024, 1973.

Fiedler F.R. and Ramirez J.A.. (2000). A numerical method for simulating discontinuous shallow flow over an infiltrating surface. *Int. J. Numer. Meth. Fluids* 2000; 32: 219–240

Garcia-Navarro P., Hubbard M. and Priestley A. (1995). “ Genuinely multidimensional upwinding for the 2D shallow water equations”, *Journal of Computational Physics*, Vol. 121, 79-93, 1995.

Guinot V. (2005). An approximate two-dimensional Riemann solver for hyperbolic systems of conservation laws. *Journal of Computational Physics*, Volume 205, Issue 1, p. 292-314.

Hirsch C., Lacon C. and Deconinck H. (1987). “Convection algorithms based on a diagonalization procedure for the multidimensional Euler equations”, *AIAA paper* 87-1163.

- Iwagaki, Y. (1955). “ Fundamental studies on runoff analysis by characteristics.” Bull. 10, Disaster Prev. Res. Inst., Kyoto Univ., Kyoto, Japan, 1-25.
- Katopodes N., T. Strelkoff. (1979) Two-dimensional shallow-water wave models, J. Eng. Mech. Div., ASCE 105 (1979) 317–334.
- Katopodes N., T. Strelkoff. (1978) Computing two-dimensional dam-break flood waves, J. Hydraulics Div., ASCE Vol. 104, No. HY9 (1978) 1269–1288.
- Katopodes, N.D. (1984). Dissipative Galerkin Scheme for Open-Channel Flow, Journal of Hydraulic Engineering. Vol. 110, no. 4, pp. 450-466. Apr. 1984.
- MacDonald I., Baines M., Nichols N. and Samuels P. (1997). “Analytical benchmark solutions for open-channel flows”, Journal of Hydraulic Engineering, ASCE, Vol. 123, No.11, November, 1997.
- Paillère H., G. Degrez, H. Deconinck (1998). Multidimensional upwind schemes for the shallow water equations, International Journal for Numerical Methods in Fluids, Volume 26, Issue 8 , Pages 987 – 1000.
- Singh, V.P. (1996). Kinematic wave modeling in water resources: surface water hydrology, Wiley, New York.

Suk H-J. (2003). “ Development of 2-D and 3-D simulator for three-phase flow with general initial and boundary conditions.” Ph.D. Dissertation, the Pennsylvania State University, University Park, PA.

Schwanenberg D. and M. Harms M., (2004). Discontinuous Galerkin Finite-Element Method for Transcritical Two-Dimensional Shallow Water Flows. *J. Hydr. Engrg.* ASCE, Volume 130, Issue 5, pp. 412-421.

Tayfur G., Kavvas M., Govindaraju R. and Storm D. (1993). “Applicability of St. Venant equations for two-dimensional overland flows over rough infiltrating surfaces”, *Journal of Hydraulic Engineering*, ASCE, Vol. 119, No.1, January, 1993.

Tisdale T.S., Scarlatos, P.D., Hamrick, J.M. (1998). Streamline Upwind Finite-Element Method for Overland Flow. *Journal of Hydraulic Engineering*, ASCE. Vol. 124, no. 4, pp. 350-357. April 1998.

Tseng, M.H. and Chu, C. H. (2000). “Two-dimensional shallow water flows simulation using TVD-MacCormack scheme.” *Journal of Hydraulic Research*, 38(2), 123-131.

Zhang W. and Cundy W. (1989). “Modeling of two-dimensional overland flow”, *Water Resources Research*, Vol. 25, No. 9, Pages 2019 –2035, September, 1989.

Zhao, D. H., Shen, H. W., Tabios, G. Q., III, Lai, J. S., and Tan, W. Y. (1994). “Finite-volume two-dimensional unsteady-flow model for river basins.” *J. Hydr. Engrg.*, ASCE, 120(7), 863–883.

Zienkiewicz P. , Nithiarasu P., Codina R., Vazquez M. and Ortiz P. (1999). The characteristic-based split procedure: an efficient and accurate algorithm for fluid problems. *Int. J. Numer. Meth. Fluids* **31**: 359–392.

Chapter 4

A Comparative Study of coupling Approaches for Surface water and groundwater interactions

Abstract

In the core of an integrated watershed model exists the coupling among surface water and subsurface water flows. Recently, interest displayed in hydrology literature, regarding fully coupled approach for surface water and groundwater interactions, has increased. For example, the assumption of a gradient-type flux equation, based on Darcy's law (linkage term) and the numerical solution of all governing equations in a single global matrix (VanderKwaak, 1999; Panday and Huyakorn, 2004 and Gunduz and Aral, 2005) has been reported. However, this trend is unfounded. This paper argues that this "fully coupled approach" is only a special case of all possible coupling combinations and, if not applied with caution, the non-physics interface parameter becomes a calibration tool. Generally, there are two cases of surface/subsurface coupling based on the physical nature of the interface: continuous or discontinuous assumption; when a sediment layer exists at the interface, the discontinuous assumption may be justified. As for numerical schemes, there are three cases: time-lagged, iterative, and simultaneous solutions. Since modelers often resort to the simplest, fastest schemes in practical applications, it is desirable to quantify potential errors and the performance specific to each coupling scheme. This paper evaluates these coupling schemes in a watershed model, WASH123D. Numerical experiments are used to compare the performance of

each coupling approach for different types of surface water and groundwater interactions. These experiments are done in terms of surface water and subsurface water solutions, along with exchange flux (e.g. infiltration/seepage rate). It is concluded that different coupling approaches are justified for flow problems of different spatial and temporal scales and the physical setting of interfaces; however, the time-lagged approach should be avoided since it is the least accurate approach.

4.1 Introduction

In the core of an integrated, physics-based watershed model is a study of coupling among surface water and subsurface water flows. In this study, we focus on physics-based coupling approaches that utilize partial differential equations both in surface water flow (Saint Venant equations) and variably saturated subsurface flow models (Richards equation). For simpler watershed models, the infiltration term is treated by an empirical algebraic equation; accordingly, the surface water/groundwater interaction computation is straightforward and independent of water flow solutions. Although the numerical solution of the Richards equation is computationally intensive and difficult at watershed scales, it is essential for a complete, physics-based representation of the subsurface flow.

The consideration of surface water/subsurface water interactions consists of two parts: stream-aquifer interaction and overland-subsurface interaction. The stream-aquifer interaction has been extensively studied by coupling saturated groundwater flow with one-dimensional channel flow (for example, Pinder and Sauer, 1971; Swain and Wexler,

1996, and Hunt, 1990, among others). The role of unsaturated zone on stream-aquifer interaction is rarely considered. The overland-subsurface interaction is usually studied in the context of runoff generation at the watershed scales (for example, Freeze, 1972; Smith and Woolhiser, 1971; Akan and Yen, 1981 and Abbott et al., 1986).

Recently, the physics-based coupling of surface and subsurface flows has been an active research topic. Panday and Huyakorn (2004) discussed the utility of different coupling schemes in a new watershed model and seemed to favor the conductance-type, linkage term approach. Morita and Yen (2002) classified coupling approaches as fully coupled (simultaneous solution), alternating iterative coupling and externally coupling (decoupled). In their model, the concept of infiltrability was introduced. This term refers to the variable boundary conditions in numerical solution of Richards equation; however, a leakage term was used in the coupling process.

With the assumption of a linkage term at the interface, the full implicit coupling approach has been tested in some recent models: InHM (VanderKwaak, 1999), MODHMS (Panday and Huyakorn, 2004), and Gunduz and Aral (2005). Enhanced numerical stability and accuracy were reported on some test examples as a result of solving the coupled governing equations in a single global matrix. However, this approach also has intrinsic limitations: an assumption has to be made that there exists a discontinuous layer at the interface, and usually, identical time steps have to be used for both surface water and subsurface flow.

Kollet and Maxwell (2005) pointed out the limitation of the linkage-term approach, based on the interface conductance concept, and considered overland flow as part of a subsurface flow boundary condition in their coupled model. The continuity of pressure head at the interface was imposed. However, in their coupled model, the same time step must be used for both overland and subsurface flow.

The time-lagged, decoupled approach is still very popular in some loosely coupled models that consist of an existing surface water model and a subsurface flow counterpart. Earlier studies make use of this approach to reduce computation effort. Smith and Woolhiser (1971) coupled a one-dimensional Richards equation with one-dimensional kinematic wave overland flow to simulate rainfall-runoff on a plane. Singh and Bhallamudi (1998) developed a coupled overland flow model with one-dimensional dynamic wave equations and two-dimensional Richards equation. The time-lagged, decoupled approach was used for surface water/groundwater interaction. Langevin et al. (2005) simulated the integrated surface water/groundwater interaction in coastal wetlands in south Florida by coupling the two-dimensional hydrodynamic model (SWIFT2D) with the SEWAT density-dependent groundwater model in a time-lagged, decoupled manner.

Although all the coupling approaches are conceptually simple, there seems to be no consensus regarding the best approach in hydrology literature. The so-called 'fully coupled approach' has a different definition and meaning for different people in current

hydrologic modeling research and practice; some refer to the inclusion of hydrological processes while others refer to the coupling schemes.

It is also interesting to see how different coupling approaches can reach similar results for the example problem of Smith and Woolhiser (1971). In their original paper, a kinematic wave approximation was applied for overland flow and a time-lagged, decoupled approach was used. Singh and Bhallamudi (1998) applied the full St. Venant equations for overland flow with a decoupled scheme. Morita and Yen (2002) applied the iterative coupling approach and VanderKwaak (1999) applied a linkage-term based simultaneous coupling approach to the same problem. All models reported a close match with the experiment data. A possible explanation is that the example is a typical Hortonian runoff problem and subsurface flow contribution to surface runoff is not important, so the surface/subsurface interaction is weak.

In this paper, the pros and cons of several combinations of coupling schemes, including continuous or discontinuous interfaces, time-lagged, iterative, and simultaneous solutions, will be discussed. The implementation of coupling schemes in a physics-based, integrated watershed model (WASH123D), will be described; in addition, results of numerical experiments will be compared in term of exchange flux (infiltration rate), outlet discharge hydrograph, groundwater table, and soil moisture and computation time, etc. The major motivation for such an analysis is that, in watershed and regional scale practical applications, many simplifications and assumptions may have to be made on surface water and groundwater interactions. The widely used weakly coupled, or

decoupled approaches were taken for the sole purpose of alleviating the computation burden regardless if these approaches were adequate or not. In fact, examples shall demonstrate that the decoupled approaches generally yield inadequate simulations. We should fully understand the implication on the choice of coupling approaches on simulation results.

4.2 Governing equations and Interface Conditions

Without losing generality, we will present the diffusion wave approximation to the Saint Venant equations for surface water flows. And the three-dimensional Richards equation is applied for subsurface flow. The interface conditions in connection to source/sink terms and boundary conditions of the governing equations will be discussed.

4.2.1 Channel Network Flow

The governing equations of water flow in one-dimensional river/stream/canal can be derived based on the conservation law of water mass and linear momentum. The diffusion wave approximation is based on the continuity equation and a simplified form of the momentum equation.

The continuity equation is:

$$\frac{\partial A}{\partial t} + \frac{\partial Q}{\partial x} = S_S + S_R - S_E - S_I + S_O \quad (1)$$

where t is time [T]; x is the axis along the channel direction [L]; A is cross-sectional area of the river/stream [L²]; Q is flow rate of the channel [L³/T]; S_S is the man-induced source [L³/T/L]; S_R is the source of direct rainfall [L³/T/L]; S_E is the sink due to evapotranspiration [L³/T/L]; S_I is the sink due to infiltration [L³/T/L]; S_O are the source terms contributed from overland flow [L³/T/L].

In a diffusion wave approximation, the inertia terms in the momentum equation is assumed negligible and the following velocity formula is applied:

$$V = -\frac{a R^{2/3}}{n} \frac{1}{\left[1 + \left(\frac{\partial Z_o}{\partial x}\right)^2\right]^{2/3}} \frac{1}{\sqrt{\left|\frac{\partial H}{\partial x}\right|}} \frac{\partial H}{\partial x} \quad (2)$$

where n is Manning's roughness [TL^{-1/3}], a is a unit-dependent factor ($a = 1$ for SI units and $a = 1.49$ for U.S. Customary units) to make the Manning's roughness unit-independent, R is the hydraulic radius [L], Z_o is channel bottom elevation above a datum [L] and $H = h + Z_o$ is the water stage [L].

Using the definition $Q = VA$ and substituting Eq. (2) into Eq. (1), we obtain

$$B \frac{\partial H}{\partial t} - \frac{\partial}{\partial x} \left(K \left[\frac{\partial H}{\partial x} \right] \right) = S_S + S_R - S_E - S_I + S_O \quad (3)$$

in which

$$K = \frac{aAR^{2/3}}{n} \frac{1}{\left[1 + \left(\frac{\partial Z_o}{\partial x}\right)^2\right]^{2/3}} \frac{1}{\sqrt{\left|\frac{\partial H}{\partial x}\right|}} \quad (4)$$

Equation (3) contains only one unknown variable (water stage). The initial condition water depth or stage must be given for transient simulation. In addition, appropriate boundary conditions need to be specified for the channel network. These include internal boundary conditions at natural junctions, hydraulic structures (weirs, gated spillways, culverts and pump stations, etc.), and external boundary conditions (specified stage or flux boundaries or depth-dependent rating curves).

The interface condition for one-dimensional channel flow is the lateral inflow from overland (S_o) and subsurface (S_f) as source/sink terms. In a coupled model, these source/sink terms are not known *a priori*, and they are dependent not only on channel flow but also overland and subsurface flow.

4.2.2 Overland Flow

The governing equations for two-dimensional overland flow can be derived based on the conservation law of water mass and momentum. The governing equations of a diffusion wave model can be written as follows.

The continuity equation for two-dimensional overland flow is:

$$\frac{\partial h}{\partial t} + \frac{\partial(uh)}{\partial x} + \frac{\partial(vh)}{\partial y} = S + R - E - I \quad (5)$$

where h is the water depth [L]; u is the velocity component in the x -direction [L/T]; v is the velocity component in the y -direction [L/T]; S is the man-induced source [L³/T/L²]; R is the source due to rainfall [L³/T/L²]; E is the sink due to evapotranspiration [L³/T/L²]; I is the sink due to infiltration [L/T].

In the diffusion wave approximation, the momentum equations are simplified into a velocity formula by neglecting all inertia terms:

$$V = \frac{-a h^{2/3}}{n} \frac{1}{[1 + (\nabla Z_0)^2]^{2/3}} \frac{1}{\sqrt{|\nabla H|}} \nabla H \quad (6)$$

where Z_0 is land surface elevation above a datum, $H = \eta + Z_0$ is water surface elevation (stage), n is the Manning's roughness coefficient, a is unit factor ($a = 1$ for SI unit and $a = 1.486$ for US custom units).

Using Equation (5) and (6), we obtain

$$\frac{\partial H}{\partial t} - \nabla \cdot [\mathbf{K}(\nabla H)] = S + R - E - I \quad (7)$$

in which

$$k = \frac{a h^{5/3}}{n} \frac{1}{[1 + (\nabla Z_0)^2]^{2/3}} \frac{1}{\sqrt{|\nabla H|}} \quad (8)$$

Equations (7) and (8) are the governing equations of diffusion wave approximation for two-dimensional overland flow.

For transient simulations, either water depth or stage must be given as the initial condition. In addition, appropriate boundary conditions need to be specified to match the corresponding physical system. For a two-dimensional overland flow model, usually, no-flow condition is applied at the upstream watershed boundary and at the watershed outlet; instead, a specified water stage or a stage-discharge rating curve (e.g., critical flow or zero-depth gradient condition) is imposed.

For overland flow, the interface conditions are: (1) one-dimensional channel flow as part of its interfacial boundary; (2) A source/sink term from infiltration/exfiltration to/from subsurface (I) - this term is implicitly dependent on both overland and subsurface flow solutions.

4.2.3 Subsurface Flow

The governing equation of subsurface flow through saturated-unsaturated porous media can be derived based on the conservation law of water mass (Yeh et al, 2006). It is written as follows.

$$F \frac{\partial h_s}{\partial t} = \nabla \cdot [\mathbf{K} \cdot (\nabla h_s + \nabla z)] + q \quad (9)$$

where h_s is the referenced pressure head [L]; t is the time [T]; \mathbf{K} is the hydraulic conductivity tensor [L/T]; z is the potential head [L]; q is the source and/or sink [L³/L³/T]; and F is the water capacity [1/L] given by

$$F = a' \frac{\theta_e}{n_e} + \beta' \theta_e + n_e \frac{dS}{dh} \quad (10)$$

where a' is the modified compressibility of the medium [1/L], θ_e is the effective moisture content [L³/L³], n_e is the effective porosity [L³/L³], β' is the compressibility of water [1/L], and S is the degree of saturation. The Darcy's velocity is given by

$$\mathbf{V} = -\mathbf{K} \cdot (\nabla h_s + \nabla z) \quad (11)$$

It is worth noting that one-dimensional channel network and two-dimensional overland domains are part of the top boundary of three-dimensional subsurface flow that interfaces with them. In a coupled system, this part of the land surface boundary cannot be considered as global boundary and pressure head at this location is part of the numerical solution.

4.2.4 Interface Conditions

We argue that physics-based coupling should be imposed at the interface boundary. From spatial dimensionality point of view, one-dimensional and two-dimensional surface flows are part of a three-dimensional subsurface boundary. An independent subsurface flow model would consider these boundaries simply as the specified head or flux boundaries. However, surface flow becomes part of the numerical solutions in a coupled model, not specified as *a priori*.

For overland flow, the discontinuity at the interface is not justified for most watersheds when there is no present of any less permeable layer between overland flow and subsurface flow (Figure 4-1a) and both the continuity of pressure and exchange flux should be applied:

$$h^o = h^s \quad \text{and} \quad Q^o = Q^s \quad \Rightarrow \quad I = \mathbf{n} \cdot \mathbf{K} \cdot \left(\frac{\rho_o}{\rho} \nabla h^s + \nabla z \right) \quad (12)$$

where h^o and h^s are the water depth in overland flow and pressure head in subsurface flow, respectively, at the interface; Q^o and Q^s are the volumetric flow rates of overland flow and subsurface flow, respectively, through the interface.

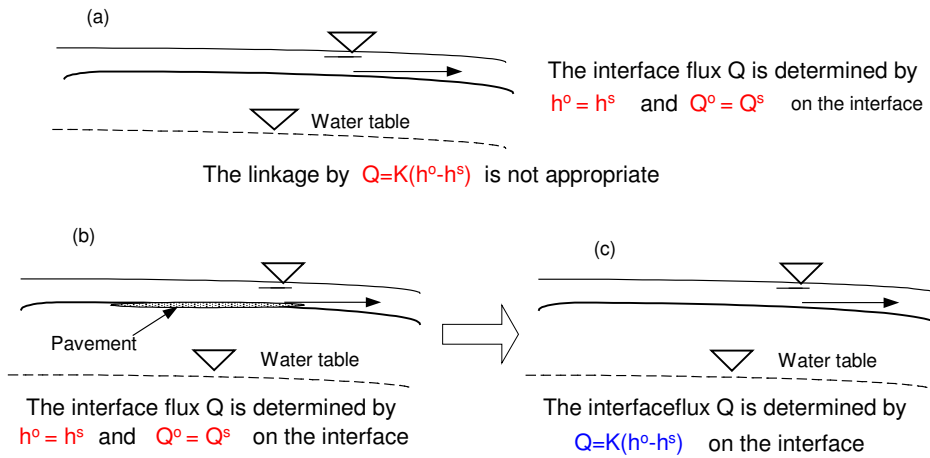


Figure 4-1: Flow interactions between overland regime and subsurface media.

Where there exists a less permeable layer separating overland flow and subsurface flow (Figure 4-1b), two coupling approaches can be taken. One is the rigorous continuity approach, with continuous pressure and fluxes. The other is the discontinuity approach, with a linkage term. If the less permeable layer is not removed (thus considered part of the subsurface media) (Figure 4-1b), the rigorous continuity approach still has to be taken; however, for this approach, numerical discretization would require excessive number of grid points.

To alleviate the problem of excessive discretization, a discontinuity approach of coupling can be taken by removing the less permeable layer from consideration (Figure 4-1c) and the ad hoc linkage term can be used

$$Q^o = Q^s \Rightarrow I = \mathbf{n} \cdot \mathbf{K} \cdot \left(\frac{\rho_o}{\rho} \nabla h^s + \nabla z \right) = \kappa(h^o - h^s) \quad (13)$$

where κ is the conductance or the exchange coefficient which is equal to K/B (where K and B are the hydraulic conductivity and thickness of the less permeable layer removed, respectively). This approach is justifiable because κ is a physical parameter representing the material property of the layer removed. This linkage term would be a good approximation as long as the storage effect of the layer is negligible.

Similarly, the explicit linkage term can be applied to stream-aquifer interaction if field evidence shows that a thin sediment layer exists at the streambed and the subsurface flow domain will not include this sediment layer.

4.3 Numerical Schemes for Surface and Subsurface Flow Coupling

We will use a simple overland/subsurface flow-coupling example for the illustration of rigorous, physics-based coupling approach. As shown in Figure 4-2, in this simple example, there are 12 overland nodes and six elements in the two-dimensional overland domain. The three-dimensional subsurface medium consists of 36 subsurface nodes and 12 elements.

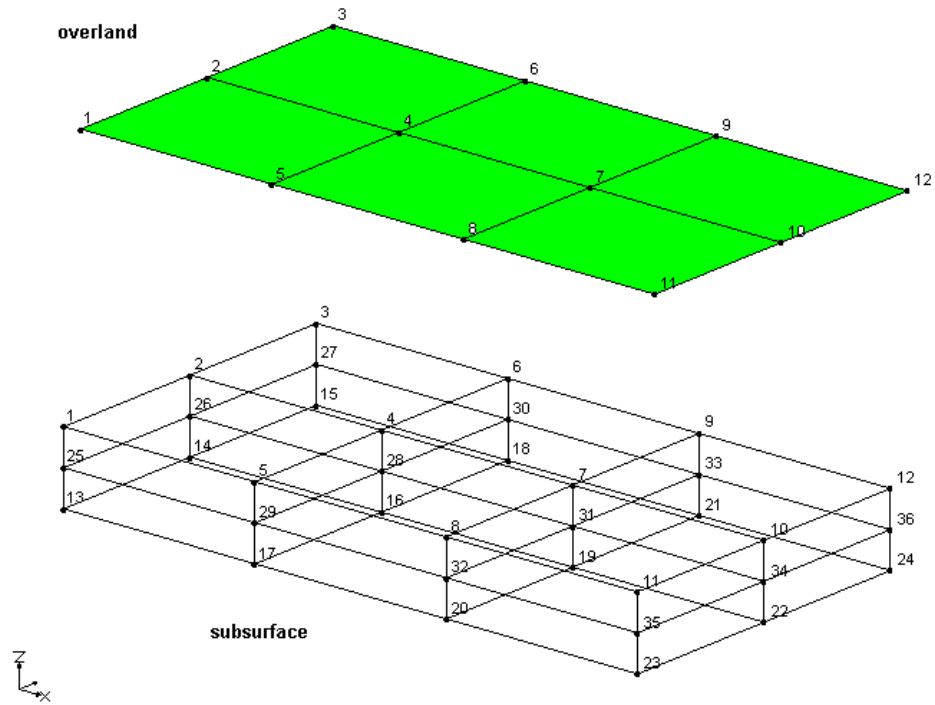


Figure 4-2: 2D overland and 3D subsurface finite element mesh for the coupling example

For decoupled flow simulations, there are 12 surface-flow equations for 12 overland unknowns (water depth) with 12 $Q^o(i)$, $i = 1, 2, \dots, 12$ considered external sources/sinks under diffusion wave approximation; and 36 subsurface-flow equations for 36 subsurface unknowns (pressure head) with 12 $Q^s(j)$, $j = 1, 2, \dots, 12$ considered external boundary fluxes. However, for a coupled flow simulation, there are 12 additional unknown overland source/sink terms $Q^o(i)$, $i=1,12$ and 12 unknown boundary fluxes for subsurface, $Q^s(j)$, $j=1,12$. In total, there are 24 new unknowns that need 24 new equations to close the mathematical formulation. These 24 equations are obtained from the interface conditions.

Obviously, the continuity of interface fluxes: $Q^o(i) = Q^s(i)$, $i = 1, 2, \dots, 12$ provide 12 equations. The additional 12 equations are based on the physical condition of the interface. For a continuous interface: $h^s(i) = h^o(i)$, $i = 1, 2, \dots, 12$. Or if a discontinuous interface exists: $Q^o(i) = Q^s(i) = k[h^o(i) - h^s(i)]$, $i = 1, 2, \dots, 12$.

In summary, there are 72 equations for 72 unknowns (12 overland water depths, h^o , 36 subsurface pressure head, h^s , and 24 exchange fluxes which compose of 12 overland source/sink terms, Q^o and 12 subsurface boundary fluxes Q^s).

Nominally, solving the coupled flow problem can be considered as the simultaneous solution of these 72 algebraic equations. The time step size of both overland and subsurface flow simulation has been assumed to be identical in the above discussion. If k sub-time steps (e.g., seconds or minutes) are used in overland flow simulation within a single subsurface flow time step (e.g., hours or days), the number of overland unknowns (water depth) will be $12k$ and the channel sources/sinks for each sub-time step are linearly interpolated in time from the sources/sink values at the beginning and end of the subsurface time steps. This will provide additional interface equations for the overland sub-time steps. Thus the total unknowns for the simultaneously coupled system would be $12k$ of h^o 's + 36 h^s 's + 12 Q^o 's + 12 Q^s 's.

(1) Time-lagged, decoupled approach

When a time lagged, decoupled approach is used; the infiltration rate is computed by using surface water flow solutions from a previous time step. In this way, it can say

that the 24 interface equations become identity equations (the right-hand side terms are known). The twelve overland algebraic equations and the 36 subsurface algebraic equations can be solved sequentially. Under this case, sub-time steps for overland flow can be easily implemented. However, the interface conditions are not strictly satisfied; therefore, the accuracy of the coupled solution is not guaranteed. The time-lagged approach can be applied to both discontinuous and continuous cases.

(2) Iterative implicit coupling approach

When the iterative coupling approach is adopted, the implicit nature is maintained by iterative updating of the exchange flux and subsurface boundary:

$$\begin{aligned} h^{s(t+\Delta t, k+1)} &= h^{o(t+\Delta t, k)} \\ Q^{t+\Delta t, k+1} &= f(h^{o(t+\Delta t, k)}, h^{s(t+\Delta t, k+1)}) \end{aligned} \quad (14)$$

For the case of discontinuous interface and a linkage-term coupling is used,

$$Q^{t+\Delta t, k+1} = k(h^{o(t+\Delta t, k)} - h^{s(t+\Delta t, k+1)}) \quad (15)$$

where k is the number of nonlinear coupling iteration for subsurface flow. Surface flow solutions can take many sub-time steps within a single subsurface time step and it will be solved within the subsurface nonlinear loop. Both continuous and discontinuous cases can be tackled with iterative implicit approach.

(3) Fully implicit coupling approach

The so-called fully implicit coupling approach is implemented in such a way that the interface equations are literally solved with other equations simultaneously within a single global matrix. The following conditions are imposed:

For continuous interface:

$$\begin{aligned} h^{s(t+\Delta t,k)} &= h^{o(t+\Delta t,k)} \\ Q^{s(t+\Delta t,k)} &= Q^{o(t+\Delta t,k)} \end{aligned} \quad (16)$$

For discontinuous interface:

$$q^{t+\Delta t,k} = c(h_c^{t+\Delta t,k} - h_s^{t+\Delta t,k}) \quad (17)$$

The simultaneous solution by a single global matrix is to make use of equations (16) or (17) to eliminate the exchange flux terms by rearranging the exchange flux terms in the algebraic equations.

In case of applying Equation (17), the flux terms in the subsurface equations and the surface equations are replaced by the explicit linkage terms, the unknown water depth of the surface water in the subsurface equations and the unknown pressure head of the subsurface in the surface equations are solved together in a single global matrix.

For the continuous case (Equation (16)), by using the interface equations, the surface equations can be added to the subsurface equations and the modified subsurface

equations are solved for the final solution. Kollet and Maxwell (2005) implemented overland flow as part of subsurface boundary and this can be considered as an example for this case. Not specifically enforcing the continuity of both pressure and fluxes, the substitution approach may yield mass errors due to numerical non-exactness. A more rigorous approach is to consider Equation (16) along with the discretized overland (surface water) flow equations (with unknowns h^o and Q^o) and the discretized subsurface flow equations (with unknowns h^s and Q_s) as a system of simultaneous algebraic equations [i.e., a single global matrix is consisting of discretized overland flow equations, discretized subsurface flow equations, and Eq. (16)]. This rigorous approach numerically ensure mass conservation across the interface.

Therefore, both cases of interface conditions can be tackled with this coupling approach; the ad-hoc assumption of discontinuous interface to apply this coupling approach seems unnecessary. However, this coupling approach is only convenient when the time steps for both surface and subsurface water flows are identical. If sub-time steps for surface flow are used, the implementation will involve more simultaneous unknowns, which can be computationally very cumbersome and involved.

4.3.1 Coupling between overland flow and subsurface flow

For two-dimensional overland flow, if the finite element method is applied to solve both subsurface and surface flow, each overland node will correspond to one subsurface node. In this case, it is obvious that infiltration is acting as a source/sink term

for overland flow, while overland regime is part of subsurface internal interfacial boundary. The detail of coupling between overland and subsurface flow has been discussed.

4.3.2 Coupling between channel flow and subsurface flow

For stream-aquifer interaction, the most accurate representation would be that the physical streambed geometry (true shape of cross-sections) is part of the subsurface top boundary. Under this condition, several subsurface nodes are connected to a single cross-section location of a stream reach (one node for stream flow). However, this is not practical for most field problems. If such a fine-scale resolution were needed, then the channel flow would be better simulated as two-dimensional overland flow. For a large-scale problem, the grid size for the subsurface domain can be several orders greater than that of channel flow; so, in a finite element model, there is only one subsurface node connected to a cross-section of a stream reach. This is similar to the case of a finite difference model, wherein a stream reach is connected to a grid cell of subsurface flow. Therefore, there is already geometry mapping approximation for stream-aquifer interaction. This means that the subsurface mesh/grid size at the stream location can have a significant impact on the coupled simulation results. With this in mind, it is not surprising that the use of a linkage term is a convenient way to compute the exchange flux for stream-aquifer interactions and, in fact, current stream-aquifer interaction modeling studies exclusively apply this approach.

In many occasions, the subsurface medium (in contact with the riverbed is continuous or the thin sediment layer at the streambed) does not extend to most part of the wetted perimeter. The leakage term is not justified. This continuous case is equivalent to imposing a changing hydraulic head at the subsurface node in direct contact with stream water. The exchange flux cannot be explicitly described as a function of stream water depth and subsurface pressure head.

4.3.3 Coupling Procedure

The Picard method or the Newton-Raphson method is usually applied for the nonlinear iteration in numerical solution of the Richards equation. A direct or iterative matrix solver can be used to solve the linearized algebraic equations. The fully implicit coupled approach is implemented in such a way to make use of the nonlinear iteration as a global coupling iteration loop. If the computation time for surface flows is only a fraction of three-dimensional subsurface flow, this is justified.

During a nonlinear iteration for subsurface flow, the numerical solution of surface flow domains are obtained with sub-time steps and boundary conditions along with computed infiltration rate (exchange flux) provided by updated subsurface flow solutions, as illustrated in Figure 4-3 for coupled overland and subsurface flow and the coupling procedure implemented in WASH123D is shown in Figure 4-4.

The calculation of infiltration rate is based on rainfall rate and water depth as potential water supply (water available for infiltration); for the time-lagged approach, overland water depth at the end of previous time step (h^n) is applied during subsurface flow computation to determine the possible infiltration rate. Then this computed infiltration rate is used in two-dimensional overland flow computation of all two-dimensional overland flow time steps within a three-dimensional time step. No feedback mechanism is provided. For iterative coupling approach, the convergence of exchange flux (infiltration rate) is checked with the updated pressure head and water depth. The fully implicit coupling approach is such that the exchange-flux terms are eliminated from the governing equations and the primary unknown variables - pressure head and water depth, are literally solved in a single global matrix.

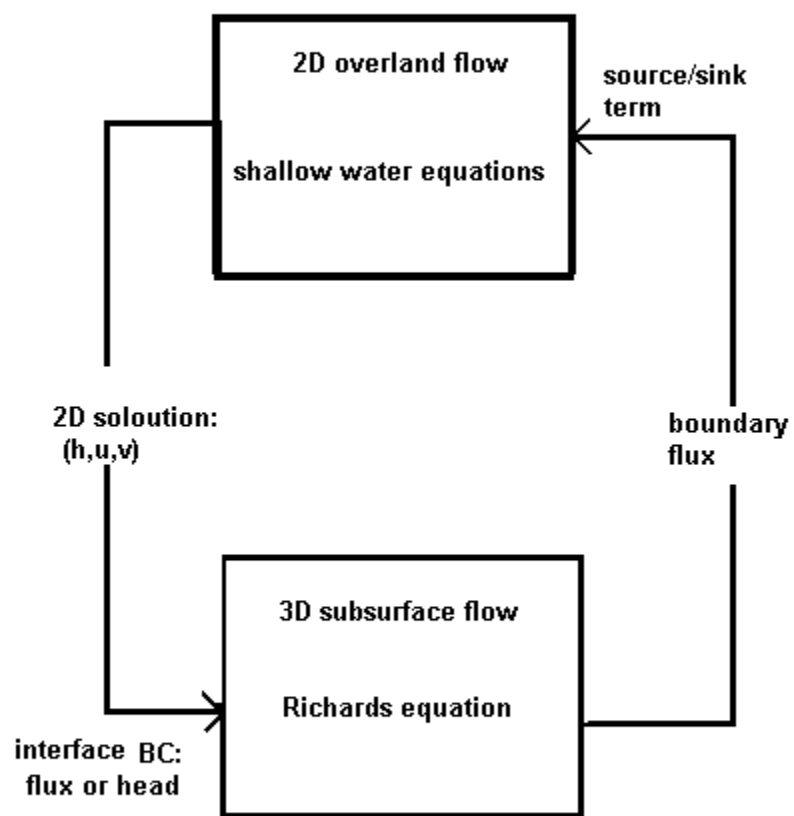


Figure 4-3: Iterative coupling loop between overland and subsurface flow

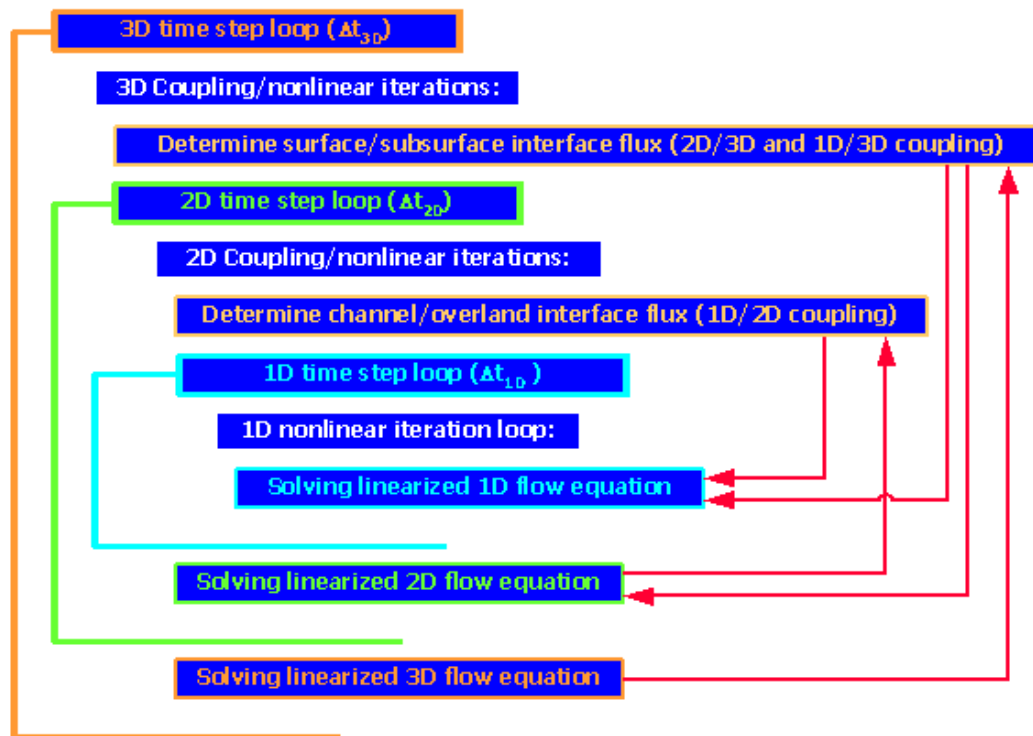


Figure 4-4: Flow coupling procedure of WASH123D

4.4 Numerical Examples

Numerical experiments for a series of coupling scheme combinations were conducted to systematically quantify the differences in simulation results. Three example problems with some preliminary simulation results are presented. One overland flow example was designed to demonstrate the inappropriate use of linkage term when there is no physical discontinuity at the interface. The field application of wetland flow shows the potential error in the time-lagged approach. The stream-aquifer interaction example demonstrates that both continuous and discontinuous coupling approaches can be applied when there is a sediment layer at the streambed.

4.4.1 Coupled overland and subsurface flow: rainfall-runoff process

The first example is a simple case of rainfall-runoff process on a horizontal surface of 500 m x 400 m. closed boundary was applied except a 100 m-outlet is located at the center of a 500 m-side (critical flow) (Figure 4-5). The Manning's n value is 0.02. A rainfall intensity of $4.0E-5$ m/s was applied for 600 minutes. The underlying porous medium has a vertical saturated hydraulic conductivity of $5.5E-5$ m/s and an effective porosity of 0.41. There is no physical discontinuity of subsurface media at the interface. Initially, the water table is 10 m below the land surface. No flow boundary was applied to subsurface domain except the top boundary, which is the interface between overland and subsurface domains. Constant time steps of 20 s and 180 s were applied for two-dimensional overland flow and three-dimensional subsurface flow, respectively. The 900-minute simulations were performed with the continuous coupling approach and the linkage-term coupling approach and the outflow discharge hydrographs were compared (Figure 4-6).

The computed outflow discharge hydrograph represents the integrated results of rainfall, surface runoff and infiltration processes. It can be seen from Figure 4-6 that the linkage-term and continuous coupling approaches resulted in different rising part of the flow hydrograph. After the subsurface domain is fully saturated and the runoff became steady, the simulation results are essentially the same. Since physically, there is no discontinuous interface, the conductance values (k) were tested for three cases ($k = 5.5E-6$, $5.5E-4$ and $3.0E-3$). A small k value constrains exchange fluxes; therefore, land surface

saturation leads to surface runoff, at which point the whole unsaturated zone gradually becomes saturated (Figure 4-6). As for enough big k values, the simulation results are very close to those of continuous coupling.

This demonstrates that the use of linkage-term coupling for this example can produce different results depending on the chosen k values. In Figure 4-7, the computed time series of total exchange fluxes were compared for all simulation cases; this is consistent with the pattern shown in the discharge hydrograph.

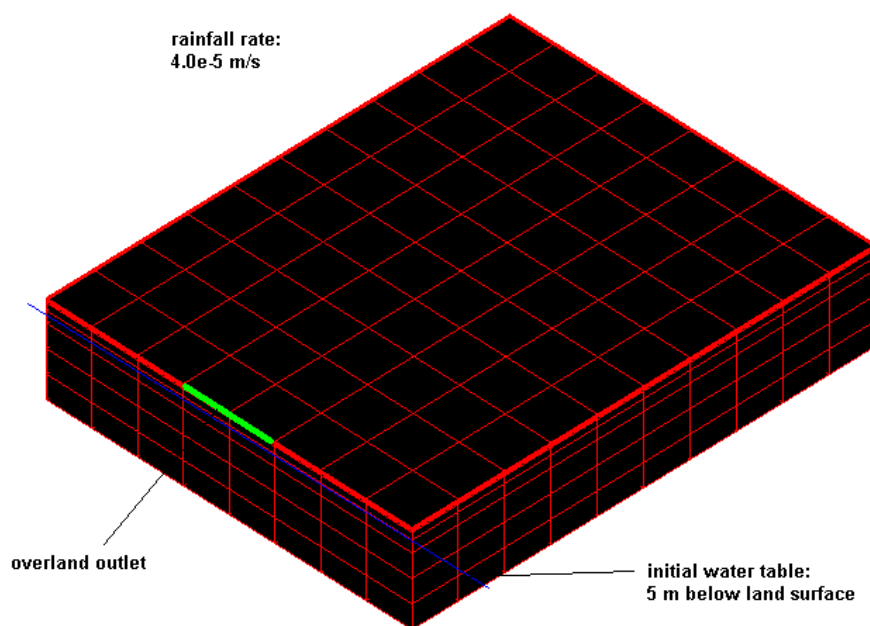


Figure 4-5: Layout of Example 1

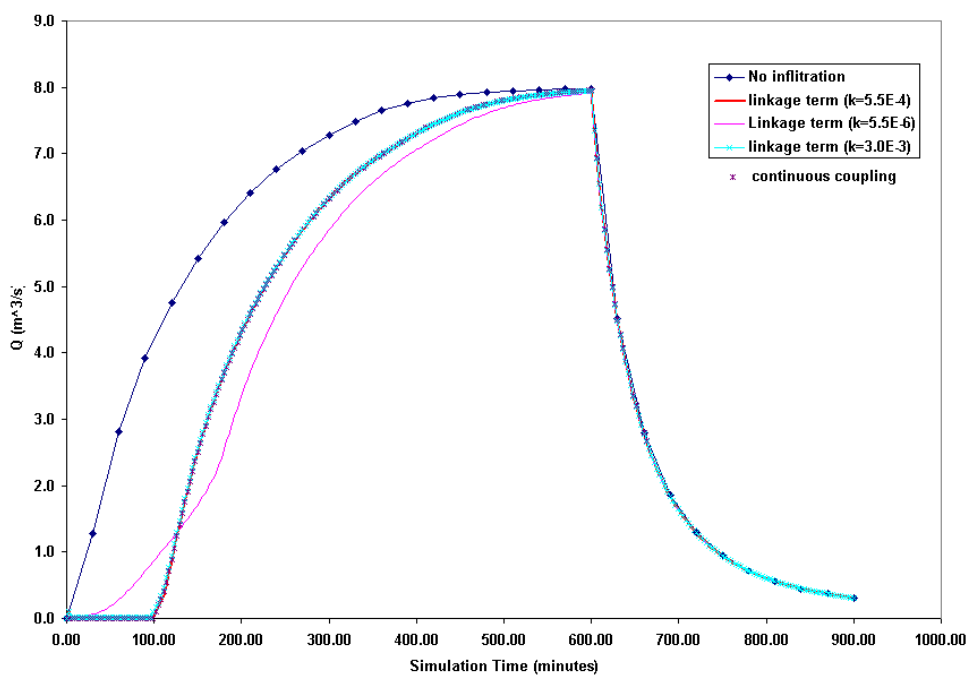


Figure 4-6: Comparison of Outflow Hydrographs

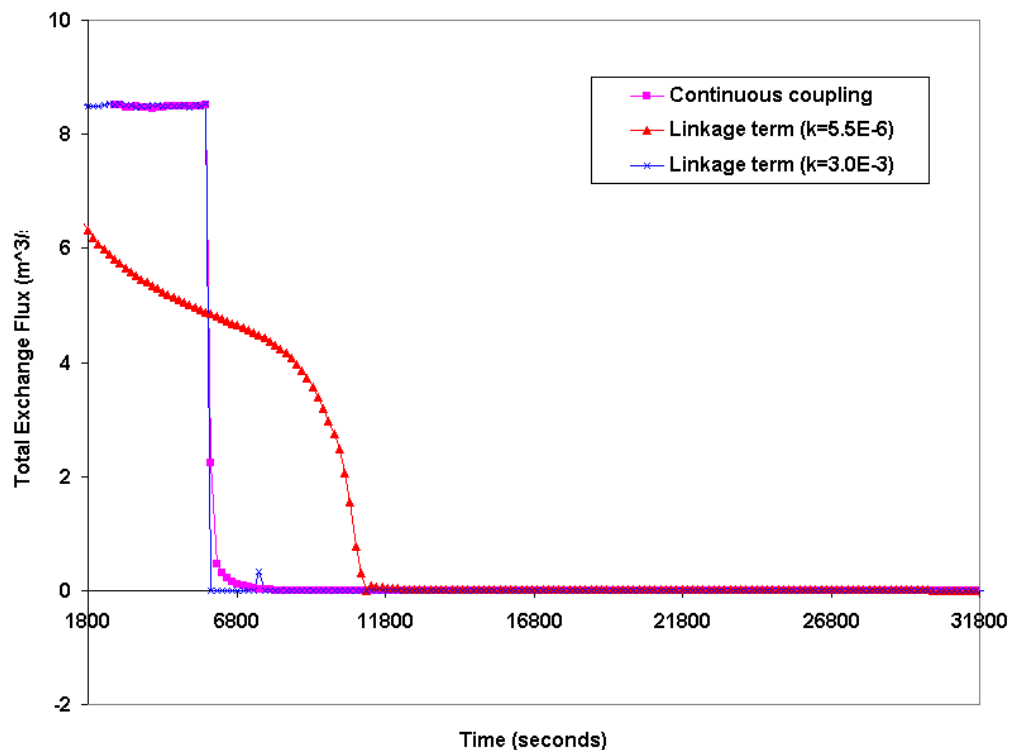


Figure 4-7: Comparison of Total Exchange Fluxes

4.4.2 Surface water-groundwater interaction in a constructed wetland

The second test example is the surface water and groundwater interaction in a constructed wetland simulated by coupled two-dimensional overland and three-dimensional subsurface flows. Both continuity of pressure and exchange flux are imposed for this example, since there is no physical discontinuous interface at the land surface.

Hydrologic processes in a treatment wetland with a total surface area of about 16 square kilometers were simulated. It consists of four treatment cells separated by interior

levees and hydraulically connected by culverts. Stormwater inflow and outflow is delivered through inflow and outflow pumping stations. Since it overlies a highly conductive surface aquifer, surface water and groundwater interaction is significant. A schematic of the model setup is shown in Figure 4-8. The subsurface flow domain vertically extends from land surface to the subsurface location of about 36.5 m deep, where vertical flow is negligible. The subsurface flow is featured with a recharge from a big surface water body at the eastern boundary and discharge into a seepage collection canal at the western boundary. The three-dimensional subsurface flow domain consists of 9,415 elements and 5,968 nodes. The peat soil made up the top three layers; the next two layers are for sandy limestone, while the bottom two, coarser layers are sand. The saturated vertical hydraulic conductivity values range from 0.09 to 20 cm/day for different subsurface materials. The two-dimensional overland flow is simulated with 1,345 linear triangular elements and 746 nodes. The Manning's n values for vegetated land surface is 0.5 ~ 1.3 based on water depth and type of vegetation.

A time period of one calendar year was selected as the simulation period. Observed historic flow and stage time series data were used. Besides structure inflow and outflow, infiltration/exfiltration, direct rainfall and evapotranspiration were the source/sinks for overland flow.

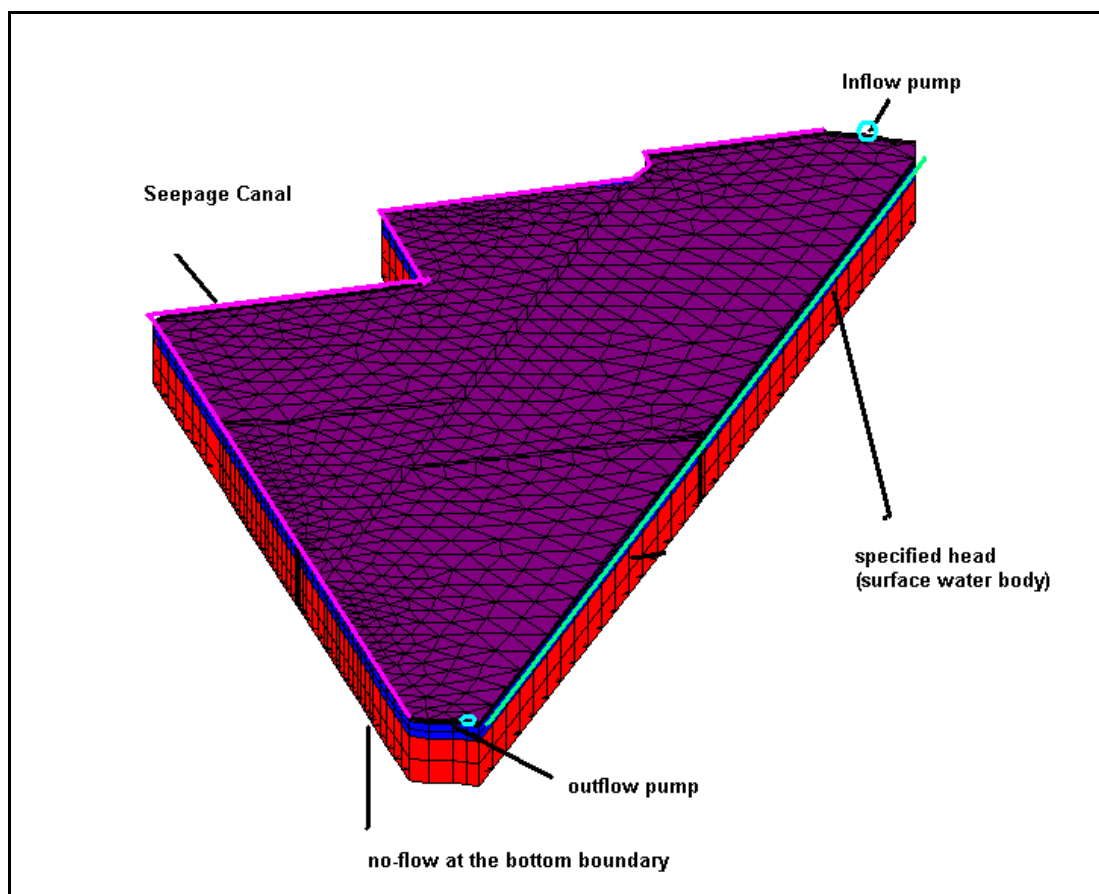


Figure 4-8: Schematic layout of the wetland example

The time step for two-dimensional overland flow is 0.25 hours and in three-dimensional subsurface flow, the time step of 24 hours was applied. And the simulation results at two surface stage-monitoring stations located at the interior of the treatment cells were compared with available observed data.

The time-lagged approach produced less accurate results, while the fully coupled approach better captured the flow dynamics and local variations at the two surface water locations (Figure 4-9). These simulation results demonstrate that the time-lagged

approach could cause significant errors.

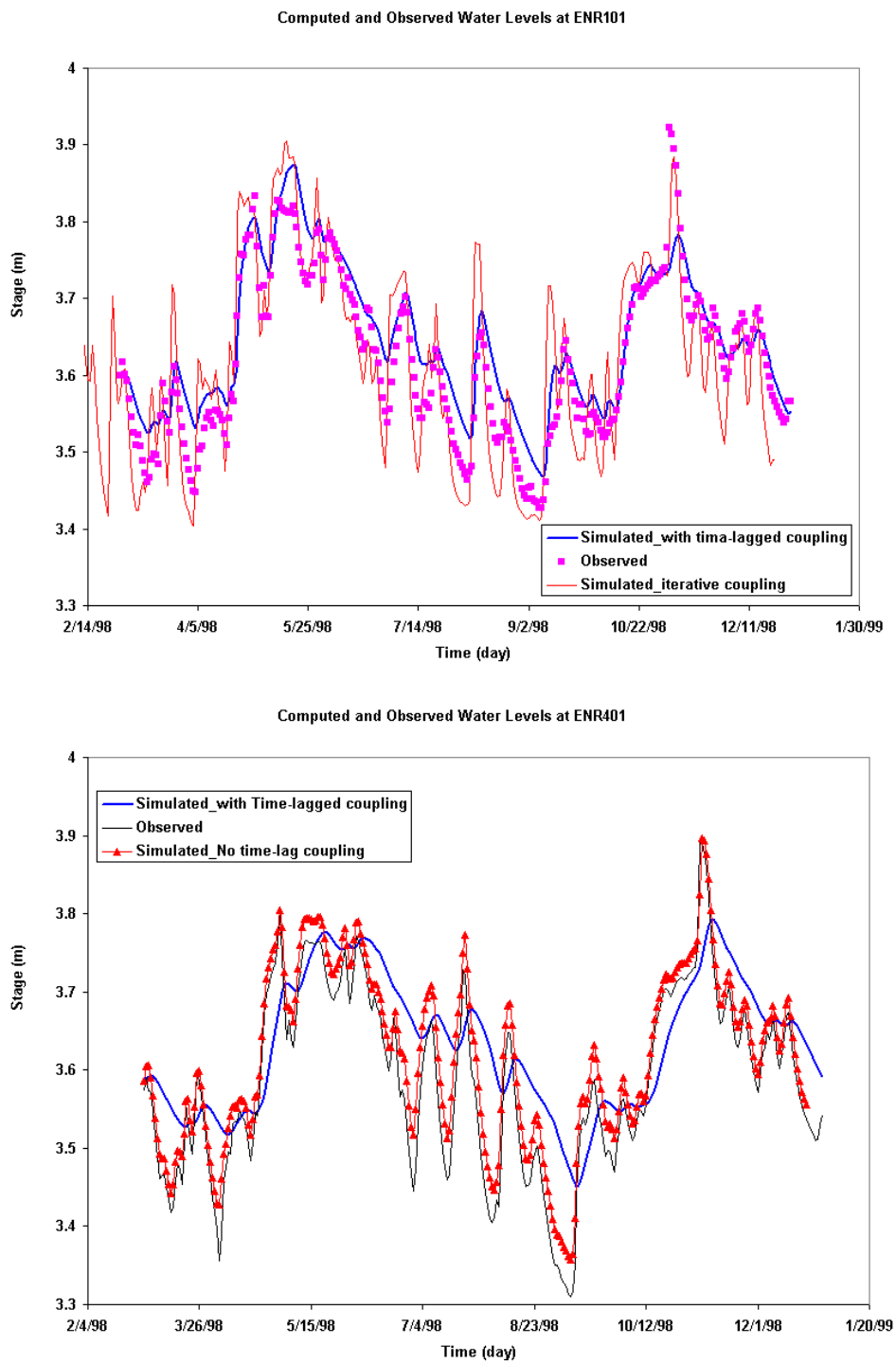


Figure 4-9: Comparison of computed water levels.

4.4.3 Stream-aquifer interaction

This hypothetical example is designed to simulate a losing stream passing through an underlying unconfined aquifer at a mountain valley (Figure 4-10). A constant total head of 20 m is applied to the aquifer in the direction of the stream and impermeable boundaries are applied to other boundary faces, except the top surface. No rainfall is applied during the simulation. The subsurface medium is homogeneous, with a domain of 800 m x 900 x 50 m. The three-dimensional finite element of the subsurface domain is shown in Figure 4-10. The saturated hydraulic conductivity is $K_{xx} = 1.0E-2$ m/s, $K_{yy} = 1.0E-2$ m/s and $K_{zz} = 1.0E-3$ m/s and the effective porosity is 0.30.

The stream bottom elevations range from 31.0 m to 26.50 along the total reach length of 900 m. The cross-sections are prismatic, rectangular with a width of 10 m. The Manning's n is 0.03. The stream is initially dry. At the beginning of the simulation, a flood discharge hydrograph is applied at the upstream end: the inflow increases linearly from 0.0 to 40.0 m³/s in 3,600 seconds, then reduces linearly to 0.0 in the next 3,600 seconds.

Weak permeable sediment exists at the streambed, with a hydraulic conductivity of 1.0E-4 m/s and a thickness of 1.0 m. Two simulations were made to compare the simulation results of continuous and discontinuous coupling approaches. For the first model run, both continuity of pressure head and exchange flux were imposed for the coupled simulation (14,200 seconds), **the streambed sediment layer was considered**

as part of subsurface media. The coupled simulation applies different time steps of 100 seconds for subsurface flow and 10 seconds for channel flow. For the second simulation, the streambed sediment layer was removed from subsurface domain, and the leakage term was applied to compute exchange rate. Figures 4-11 and 4-12 show impact of stream seepage on subsurface pressure head distribution and only saturated zones are plotted for the simulation results with continuous interface assumption. Figure 4-12 is the computed river discharge hydrograph at two different locations under coupled flow and solved with different coupling approaches. As expected, the flood peak water levels are attenuated by stream-aquifer interaction.

For this specific example, similar results were obtained with both coupling approaches; however, the differences are visible since the sediment layer was represented by only one subsurface element in the vertical direction when both continuity of state variables and exchange fluxes are imposed. Another reason for the difference is that the storage effect of the sediment layer is not considered in the discontinuity approach of a linkage term. As a result, infiltration will start earlier and the magnitude of infiltration rate will increase for the case of discontinuity approach (Figure 4-14). This would delay and decrease the magnitude of the surface runoff, i.e., the river discharge will be delayed and its magnitude will decrease. The differences also increase as the flood wave moves to the downstream boundary. Mesh refinement for the sediment layer will improve the accuracy of computed exchange fluxes. When the hydraulic conductivity of the streambed sediment is of several orders of magnitude smaller than that of the underlying

subsurface media, difficulty in obtaining convergent solutions, coupled with longer computer run-times, are the major disadvantages of using the continuous approach.

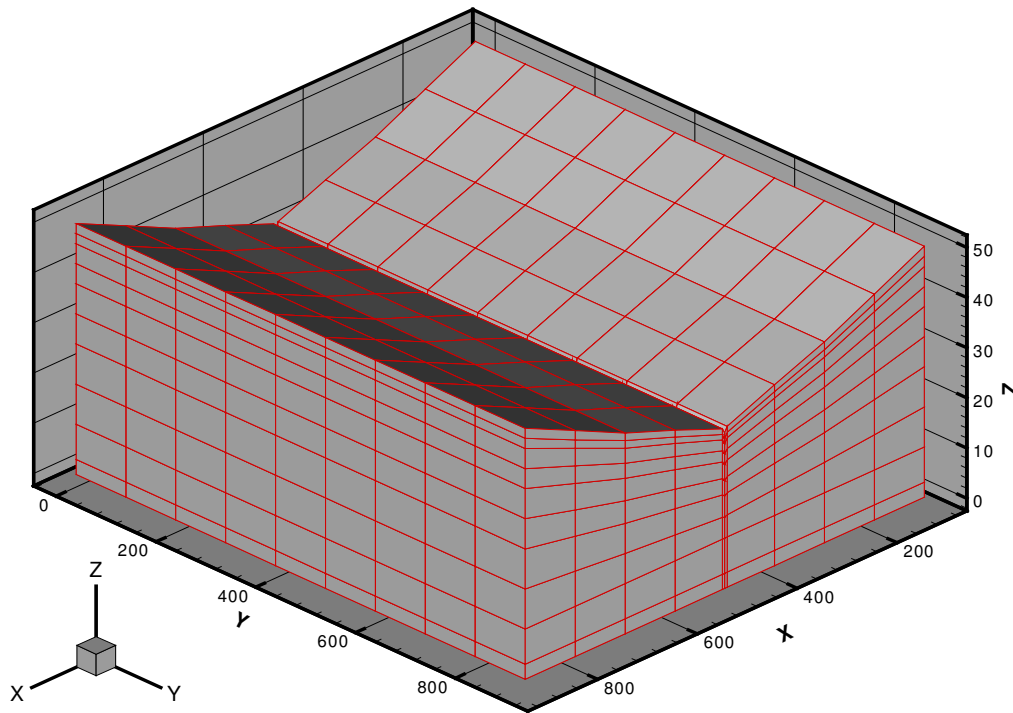


Figure 4-10: Three-dimensional finite element mesh

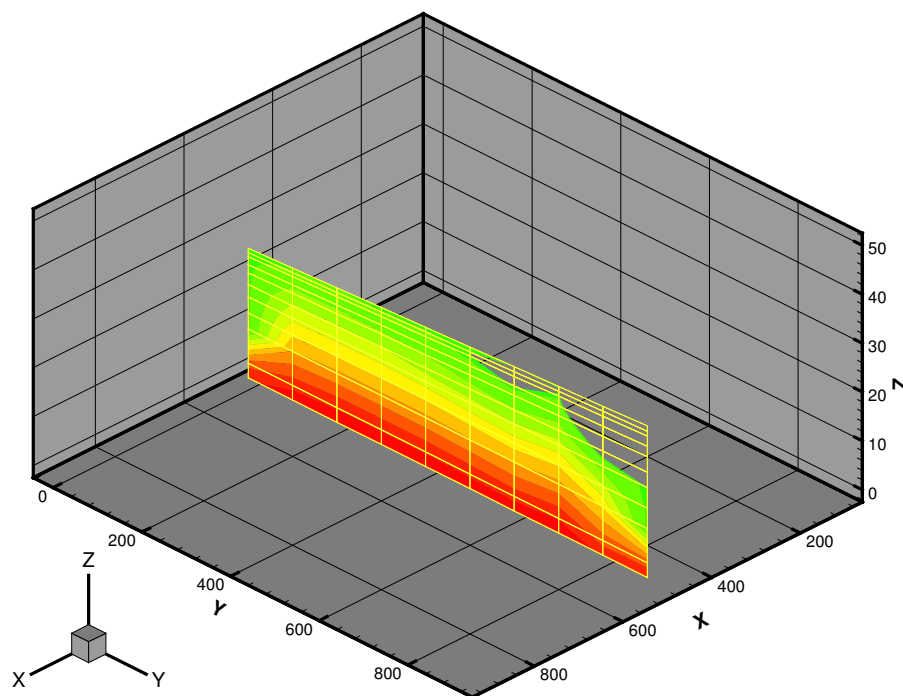


Figure 4-11: Pressure head distribution at $x=500$ m (time=14200 seconds)

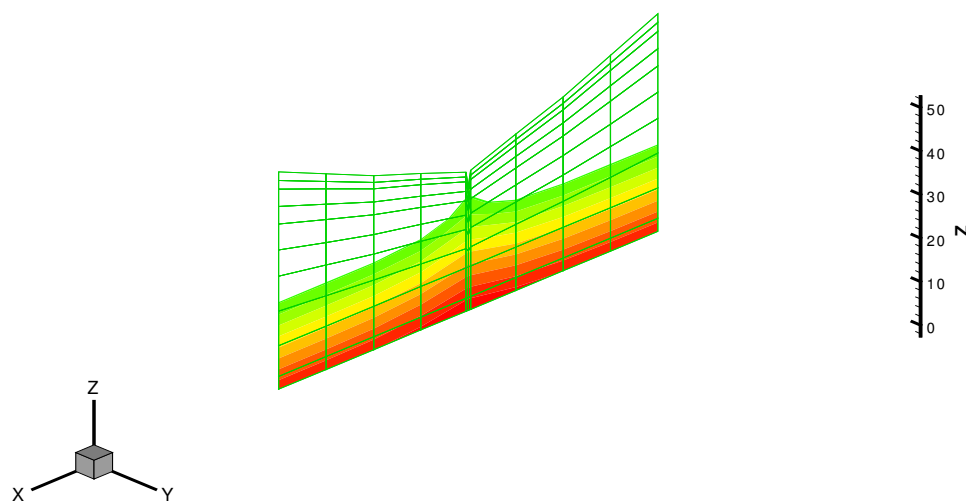


Figure 4-12: Pressure head distribution at $y=430$ m (time=14200 seconds)

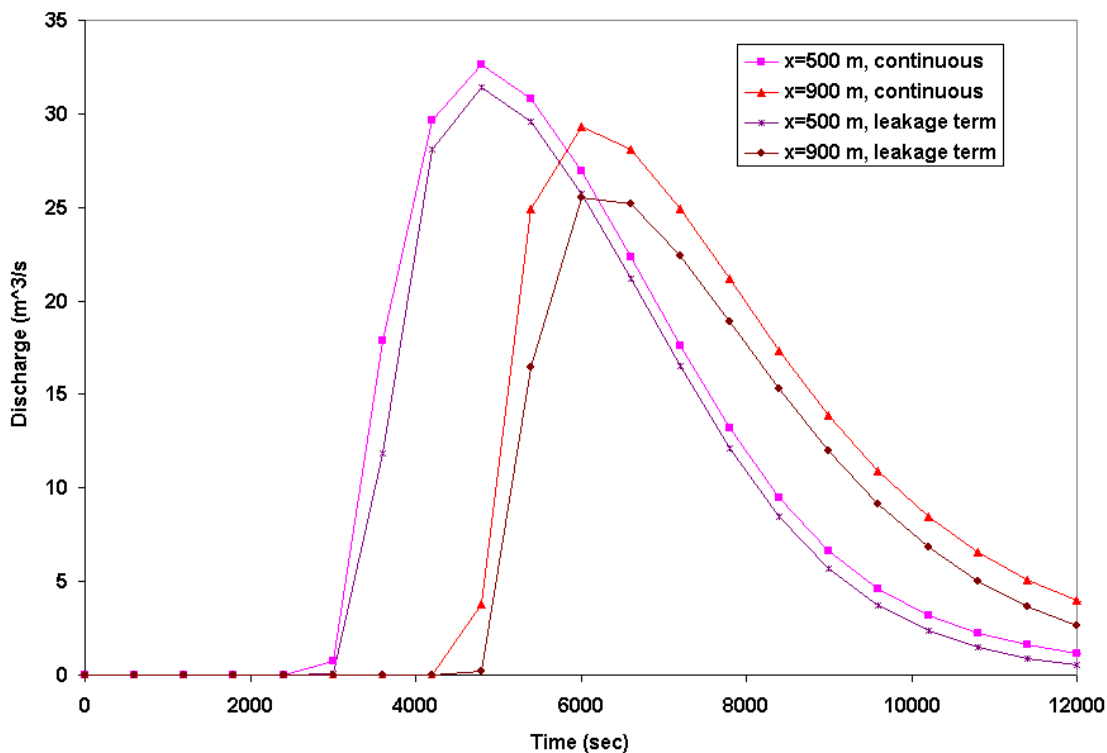


Figure 4-13: Computed Discharge hydrographs (coupled flow with different approaches)

4.5 Discussion and Conclusions

By imposing both continuity of state variables and exchange flux, an iterative or fully implicit scheme can also be similarly implemented; such is evident in the case of the linkage term approach during the coupling process. The error incurred by applying the time-lagged, decoupled approach can be significant, as demonstrated in the test examples.

There may be some numerical advantage on the simultaneous solution of a single global matrix in the linkage term-based approach; however, for practical applications,

identical time steps have to be used for both surface and subsurface flow; this paper has also demonstrated this simultaneous coupling approach can also be implemented with continuous interface conditions.

When discontinuous interface coupling is used, evidence and parameters from field observation should be able to support such an assumption. For real-world applications, many options must be provided; specifically, those that can be justified for coupled flow problems of different spatial and temporal scales and the physical setting of the interface.

Acknowledgements

This research is supported by the U.S. EPA – Science To Achieve Results (STAR) Program under Grant # R-82795602 with the University of Central Florida.

References

Abbott, M.B., J.C. Bathurst, J.A. Cunge, P.E. O’Connell, and J. Rasmussen, (1986), An introduction to the European Hydrological System- Systeme Hydrologique Europeen, “SHE”, 2: Structure of a physically-based, distributed modeling system, *Journal of Hydrology*, 87, 61-77, 1986.

A.O. Akan and B.C. Yen, (1981), Mathematical model of shallow water flow over porous media. *J. Hydraul. Div.* 107 HY4 (1981), pp. 479–494.

R.A. Freeze, Role of subsurface flow in generating surface runoff. (1972), 1. Base flow contributions to channel flow. *Water Resour. Res.* 8 (1972), pp. 609–623.

Gunduz O. and Aral M.M., (2005), River networks and groundwater flow: a simultaneous solution of a coupled system. *Journal of Hydrology.* 2005; 301: 216-34.

Hunt B., (1990), An approximation for the bank storage effect, *Water Resources Research*, Vol.26 No.11, Pages 2769-2775.

Kollet S.J. and Maxwell R.M.. (2005), Integrated surface-groundwater flow modeling: A free-surface overland flow boundary condition in parallel groundwater flow model. *Advances in Water Resources*, Volume 29, Issue 7, July 2006, Pages 945-958.

Langevin C., Swain E., and Wolfert M., (2005), Simulation of integrated surface-water/ground-water flow and salinity for a coastal wetland and adjacent estuary, *Journal of Hydrology*, Volume 314, Issues 1-4, 25 November 2005, Pages 212-234.

Morita M, Yen BC. , (2000), Numerical methods for conjunctive two-dimensional surface and three-dimensional sub-surface flows. *International Journal for Numerical Methods in Fluids* 32: 921–957.

- Morita M, Yen BC. (2002), Modeling of conjunctive two-dimensional surface–three-dimensional subsurface flows. *Journal of Hydraulic Engineering, ASCE* 128: 184–200.
- Panday S. and Huyakorn P.S., (2004), A fully coupled physically-based spatially-distributed model for evaluating surface/subsurface flow, *Advances in Water Resources*, 27 (2004) 361–382
- G.F. Pinder and S.P. Sauer, (1971), Numerical simulation of flow wave modification due to back storage effects. *Water Resour. Res.* 7 1 (1971), pp. 63–70.
- V. Singh and S.M. Bhallamudi, (1998), Conjunctive surface–subsurface modeling of overland flow. *Adv. Water Resour.* 21 (1998), pp. 567–579.
- Smith, R. E., and Woolhiser, D. A. (1971). “Overland flow on an infiltration surface,” *Water Resour. Res.*, 7(4), 899–913.
- Swain ED, Wexler EJ, (1996), A coupled surface-water and groundwater flow model for simulation of stream–aquifer interaction. *US geological survey techniques of water-resources investigations, Book 6; 1996. 125 p [chapter A6].*

VanderKwaak JE., (1999), Numerical simulation of flow and chemical transport in integrated surface–subsurface hydrologic systems, Doctorate Thesis, Department of Earth Sciences, University of Waterloo, Ontario, Canada.

Yeh, G.T., G. B. Huang, H. P. Cheng, F. Zhang, H. C. Lin, E. Edris, and D. Richards. (2006). A first principle, physics-based watershed model: WASH123D, in *Watershed Models*. Eds. By Singh VP and Frevert D.K., CRC Press, Boca Raton, FL.

Chapter 5

Integrated Modeling of Groundwater and Surface Water interactions in a constructed wetland

Abstract

As a man-made pilot wetland in south Florida, USA, the Everglades Nutrient Removal (ENR) project was modeled with a physics-based integrated approach using WASH123D. Stormwater is routed into the treatment wetland for phosphorus removal by plant and sediment uptake. It overlies a highly permeable surficial groundwater aquifer. Strong surface water and groundwater interactions are a key component of the hydrologic processes. The site has extensive field measurement and monitoring tools that provide point scale and distributed data on surface water levels, groundwater levels, and the physical range of hydraulic parameters and hydrologic fluxes. Previous hydrologic and hydrodynamic modeling studies have treated seepage losses empirically by some simple regression equations and, only surface water flows are modeled in detail. Several years of operational data are available and were used in model calibration and validation. The validity of a diffusion wave approximation for 2-D overland flow (in the region with very flat topography) was also tested. The uniqueness of this modeling study includes (1) the point scale and distributed comparison of model results with observed data; for example, the spatial distribution of measured vertical flux in the wetland is available; (2) model parameters are based on available field test data; (3) water flows in the study area consist of 2-D overland flow, hydraulic structures/levees, 3-D subsurface flow and 1-D canal

flow and their interactions. This study demonstrates the need and the utility of a physics-based modeling approach for strong surface water and groundwater interactions.

5.1 Introduction

Man-made treatment wetlands have been extensively used for wastewater treatment or stormwater nutrient removal in the USA. Typically, these surface water impoundments are built for flow-through treatment of stormwater by plant and sediment uptakes of both nutrients and pollutants. In South Florida, the Everglades restoration effort has led to the design and construction of a series of constructed wetlands, called Stormwater Treatment Areas (STAs), to reduce phosphorus levels in stormwater runoff before they can enter the Everglades protection areas. These constructed wetlands were located on former natural wetlands or farmland. The Everglades Nutrient Removal (ENR) project is a pilot constructed wetland for STAs (SFWMD, 2000).

In south Florida, the regional hydrogeology was characterized by the surficial aquifer (Fish, 1988). Wetlands in the region have strong hydraulic connections with the underlying, highly conductive surficial aquifer. Harvey et al. (2002) studied the surface and groundwater interactions in the ENR and surrounding wetlands with field investigations.

Guardo studied water budgeting in the ENR with a simple water mass balance approach (Guardo, 1999). Regression models were used to estimate groundwater

seepages in ENR and the whole ENR was treated as a point for water budget. Guardo and Tomasello (1995) simulated overland flow in ENR using a steady hydrodynamic model. Until recently, the hydraulic models applied to the design and management of constructed wetlands are quite limited in scope and detail. Most models are two-dimensional, for steady-state flow. They are good for both design purposes or as a screening tool, but lack important details [incorporating hydraulic structures, calibrated model parameters and surface/groundwater interaction]. More detailed two-dimensional hydraulic models, used in the existing treatment of wetlands, are being built for management and operation needs. They are calibrated and validated with historic time series data, considering only the two-dimensional surface flow.

Some popular hydrodynamic computer codes currently used for modeling wetland hydraulics are originally developed for coastal hydrodynamic modeling. Some limitations need to be addressed before they can be applied for wetland simulation. For instance, the incorporation of hydraulic structures, explicit representation of rainfall, and evaporation and treatment of wetting and drying are very important in a wetland hydrologic model.

Swain et al. (2004) has described their experience in adapting and modifying the USGS SWIFT2D, originally developed for coastal tidal flow, to simulate the southern Everglades wetland hydrology. A watershed model code, such as WASH123D (Yeh et al., 2006) does not have these limitations. This WASH123D application is an example of coupled surface/subsurface water flows in a constructed wetland for stormwater treatment in south Florida. Current two-dimensional hydraulic models cannot handle seepage loss

properly; therefore, an integrated surface/groundwater model is needed to study the dynamic interaction of surface flow within the treatment area and seepage loss through bottom and perimeter levees. A one-dimensional canal flow is also needed to simulate inflow/outflow and seepage collection. The impact of neglecting seepage loss is a likely distorted hydraulic model.

Wetland hydrological modeling studies have been increasingly reported in the hydrology literature. Feng and Molz (Feng and Molz, 1997) developed a surface water flow model for wetlands with the diffusion wave approximation of the 2-D shallow water equations. The model was tested with a field application. However, model calibration and history matching were not reported. Few integrated wetland hydrologic modeling studies have been reported. MIKE SHE was applied to a natural wetland in England (Thompson et al., 2004), while Langevin used a coastal natural wetland by coupling SWIFT2D and MODFLOW (Langevin et al., 2005).

The purpose of a hydraulic model for a constructed wetland is to evaluate the hydraulic performance under different flow conditions. If the transport and fate of phosphorus can be described as biogeochemical reactive transport equations, then the hydrodynamic component is also the base of the reactive transport computation. All these modeling objectives are likely to be more effectively modeled in an integrated model code such as WASH123D.

The objective of this paper, is to present a modeling study that demonstrates and validates the applicability of a physics-based, integrated modeling approach for surface water and groundwater interactions in wetlands; in addition, it seeks to show how field data from previous field studies can be used in building the integrated model with minimum model calibration. Historical time series data and field test results were applied in evaluating the model performance.

5.2 Site Description

The Everglades Nutrient Removal (ENR) project (Figures 5-1 and 5-2) was built as a prototype treatment wetland in south Florida, USA, for the Everglades restoration (SFWMD, 2000). It was operated for five years (1994 to 1999) and is now incorporated into the Stormwater Treatment Area 1 west (STA-1W).

The total surface area of the ENR is about 16 square kilometers. The land surface elevations were based on previous field survey data. Marsh area elevations range from 2.0 m NGVD29 (National Geodetic Vertical Datum of 1929) to 4.0 m NGVD29. The average land surface gradient is 0.001. The ENR basin topography is very flat that is typical in South Florida.

The vegetations in the ENR were spatially varied and changed over time. The main treatment plants were emergent cattail and submerged aquatic vegetation (SAV).

There were also some local distribution canals and remnant farm ditches in the marsh areas.

The ENR basin has been extensively monitored and studied by the South Florida Water Management District (SFWMD) and USGS (SFWMD, 2000; Harvey et al., 2002).

The measured time series data were recorded in the SFWMD corporate database DBHYDRO (SFWMD, 2005).

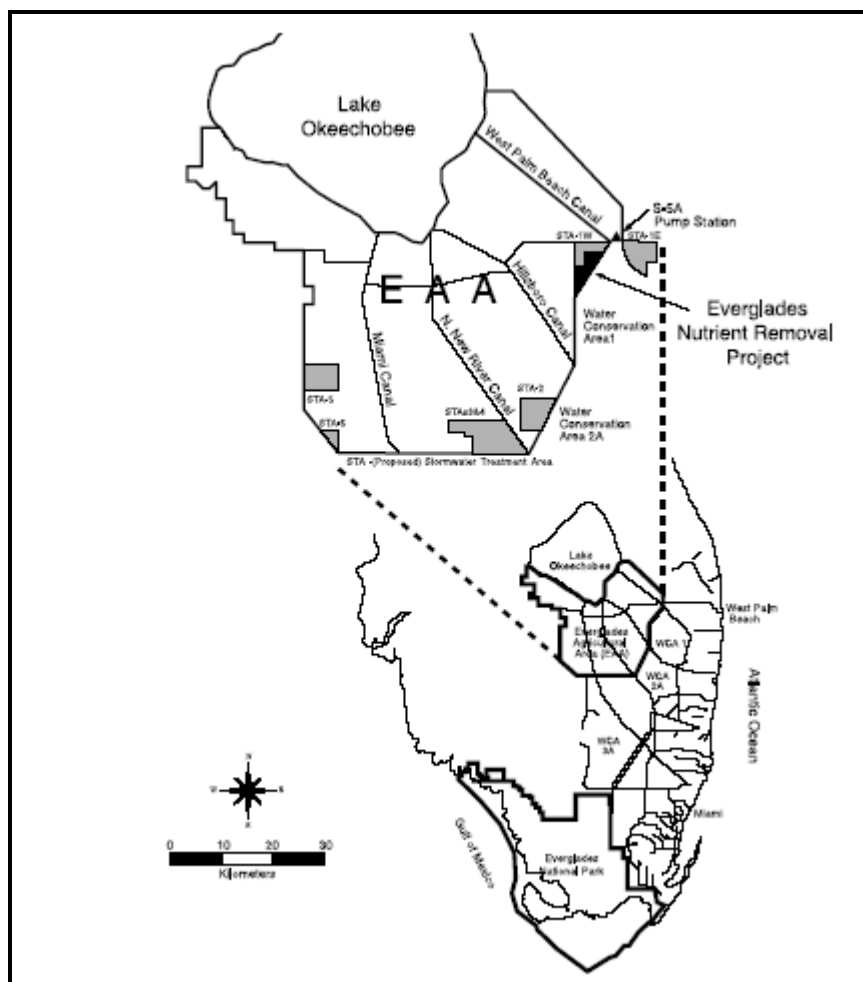


Figure 5-1: Location Map of ENR (SFWM, 2000)

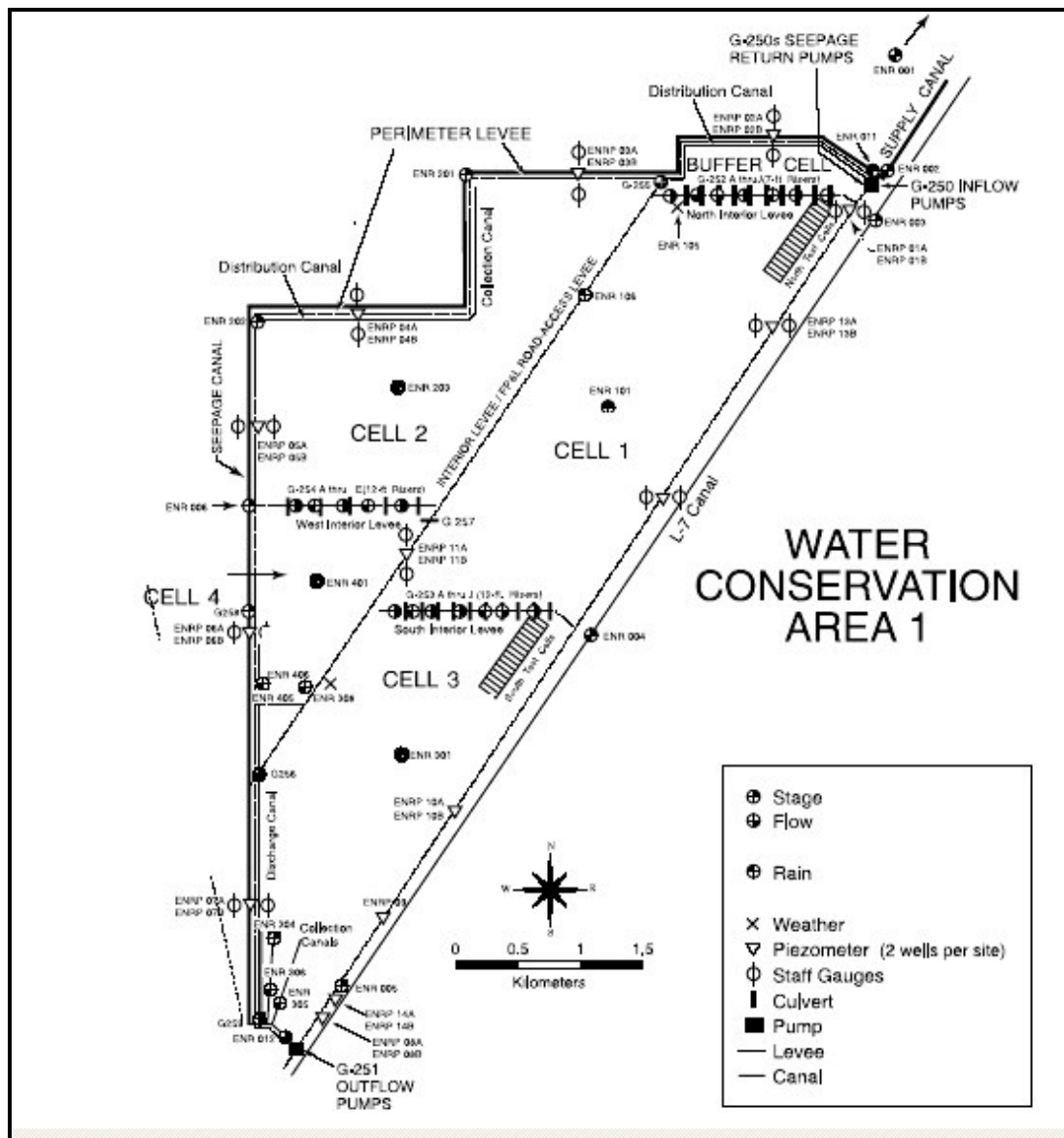


Figure 5-2 Schematic Map of ENR (Modified after SFWMD, 2000)

Subsurface Flow:

As can be seen in Figure 5-2, the ENR basin is separated from the surrounding areas by a perimeter levee. The eastern boundary of subsurface flow is controlled by water levels in the Water Conservation Area 1 (WCA-1). The Seepage Canal, running

along the western and northern boundary, controls the remaining boundaries. The bottom boundary can be considered impermeable, since the field studies have found that groundwater flow in the surficial aquifer is predominantly horizontal. Generally, groundwater received a recharge from the WCA-1, where the water levels were normally regulated between 4.88 m NGVD to 5.18 m NGVD (16 –17 ft NGVD), while discharge was mainly through the seepage canal. Subsurface flow also received recharge through overland flow infiltration.

Surface water flow in the ENR basin is controlled by a series of pump stations and gated culverts. The ENR consists of a buffer cell and four treatment cells 1-4 (Figure 5-1). Stormwater runoff was pumped into the buffer cell and distributed to the eastern flow way (Cell 1 and Cell 3) and the western flow way (Cell 2 and Cell 4). Interior levees separated each treatment cell from one another and a series of culverts with risers were built in the interior levees to control flows among cells. Treated water from the western flow way was directed to Cell 3 by the gated culverts G-256 and eventually, was discharged from ENR into WCA-1 through the outflow pump station G-251.

The major surface water inflow and outflow are through pumping stations G-250 and G-251. Structure inflows consisted of inflow pump station G-250 and seepage return pump G-250S. Structure outflow was through outflow pump station G-251. Discharge into the seepage canal could be made through gated structures G-258 and G-259. Current modeling study simulated the whole calendar year of 1998. During this time period, outflow from G-258 and G-259 was zero.

5.3 Model Tool: WASH123D

This is a generic, integrated surface water/groundwater interaction model code (Yeh et al., 2006). It can simulate a one-dimensional channel network, two-dimensional overland flows, and three-dimensional variably saturated subsurface flow, separately. When needed, it can also simulate different combinations of coupled surface water and subsurface water flows.

Some adaptations and modifications were easily implemented into the source code for this modeling effort. The original WASH123D code apply constant friction coefficient (Manning's n value) for bottom shear stresses. But the dense vegetation in the marsh area requires a water depth dependent Manning's n relationship. Different depth dependent relationships can be easily applied by a tabular (depth-n) profile input in WASH123D.

The calibrated flow rating equations for various hydraulic structures can also be coded in WASH123D that control the water transfer between different canal locations or from/to canal to overland (marsh area).

5.4 Input Data

Time series data of rainfall, evapotranspiration, structure flow, and surface and ground water levels were retrieved from the public accessible DBHYDRO database (SFWMD, 2005).

Daily rainfall was measured at a network of rain gauges throughout the ENR area and a spatially averaged daily rainfall time series was directly obtained from DBHYDRO. Daily potential evapotranspiration data was based on a regression equation derived from three lysimeters measurement (Abtew and Obeysekera, 1995; Abtew, 1996) and was also available in the database.

Structure flow data was computed by SFWMD using calibrated flow rating equations. Normally, these flow data were not as accurate as data from measured water levels.

5.5 Model Setup

The conceptualization of the study area leads to a relatively closed flow system. Stormwater runoff was pumped into the buffer cell and flow into the treatment cells through control structures. The treated water is discharged at the downstream by the outflow pump station G251 and eventually entered the Water Conservation Area 1.

The surface water flows were simulated as two-dimensional overland flow. Current model simulations applied the diffusion wave approximation of the full shallow water equations for overland flow. The entire overland flow domain was discretized into 1,345 linear triangular elements and 746 nodes. The average length of a triangular side was about 160 m. The interior levee was represented by inactive elements and water

could go only through it by structure flows. The known Inflow pumping rate was applied by a water source term in the overland domain. A specified stage boundary condition was applied at the downstream outflow location (G-251 headwater).

Vegetations were built into the treatment cells (Figure 5-3). They are categorized as emergent cattails and submerged aquatic vegetation (SAV). Previous studies have demonstrated that a water depth dependent friction coefficient is appropriate for vegetation (Yen, 1992; Wu et al., 1999). Field study at ENR showed that the Manning's n values range from 0.5 to 1.3 depending on water depth and submergence level of the plants (SFWMD, 2000).

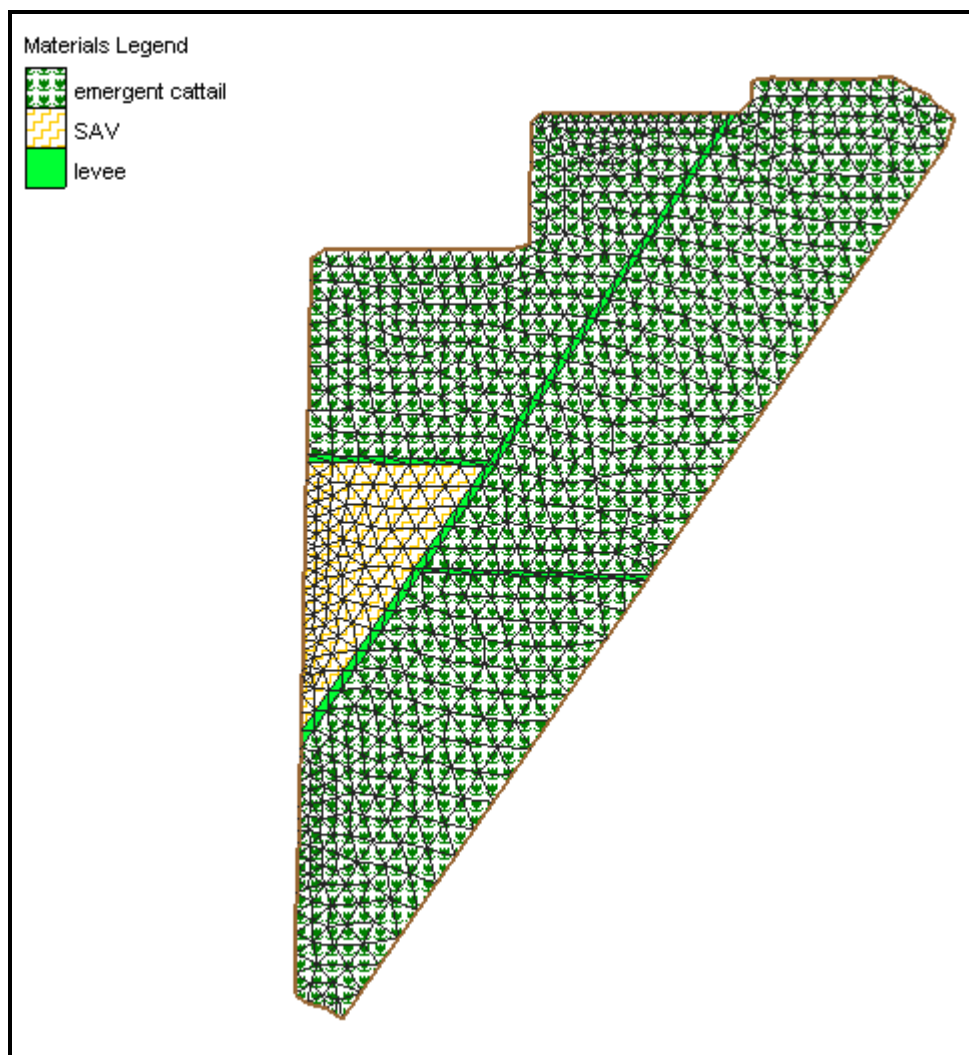


Figure 5-3: Vegetation types as simulated in the model

For subsurface flow, the surficial aquifer system was simulated with the three-dimensional Richards equation governing the variably saturated subsurface flow. The underlying surficial aquifer was vertically divided into several layers, the top layers, extending from land surface to a few feet in thickness, is the poor permeable peat; the next lower layers are composed of sand or sandy lime rock. Figure 5-4 shows the three-dimensional finite element mesh for subsurface flow. For this preliminary simulation, the

model domain was selected up to the location of the seepage canal to the west, and the L-7 canal to the east. These canals are hydraulic divides for subsurface flow.

The hydrogeology was obtained from some relevant reference sources (Fish, 1988; Harvey et al, 2002). Harvey et al. (2002) described detailed local hydro-geological data for the ENR area. The value of saturated hydraulic conductivity and effective porosity used in the model runs are listed in Table 1.

Table 5-1. Hydraulic properties for Subsurface Flow

Soil type	Porosity	Hydraulic Conductivity	
		Horizontal	Vertical
	(-)	(cm/day)	(cm/day)
Peat	0.21	9.14	0.09
Sandy limestone	0.31	271.39	2.72
Sand	0.41	2070.20	20.7

The Van Genuchten equations were used to derive the nonlinear relationships for soil hydraulic property.

The subsurface flow domain consisted of 9,415 elements and 5,968 nodes. The peat soil made up the top three layers; the next two layers were for sandy limestone and the bottom two coarser layers with the maximum depth of 36.5 m (120 ft) from land

surface. This subsurface element resolution was designed to maintain a balance between run time requirements for long-term model runs and model accuracy.

Specified head boundary conditions were applied for the WCA-1 and the seepage canal for current model simulations. The seepage canal could be simulated by the one-dimensional channel flow and coupled with subsurface flow. However, the water levels in the canal were kept below 2.4 m NGVD (8 ft NGVD) to protect farmlands adjacent to the ENR; canal flow was quite static. Therefore it was considered as a specified head boundary for subsurface flow and it had no hydraulic connection with the overland flow during model simulations. No interface sediment layers were assumed to exist between subsurface and overland or canal. So both continuity of pressure head and exchange flux were imposed for surface water and groundwater interactions.

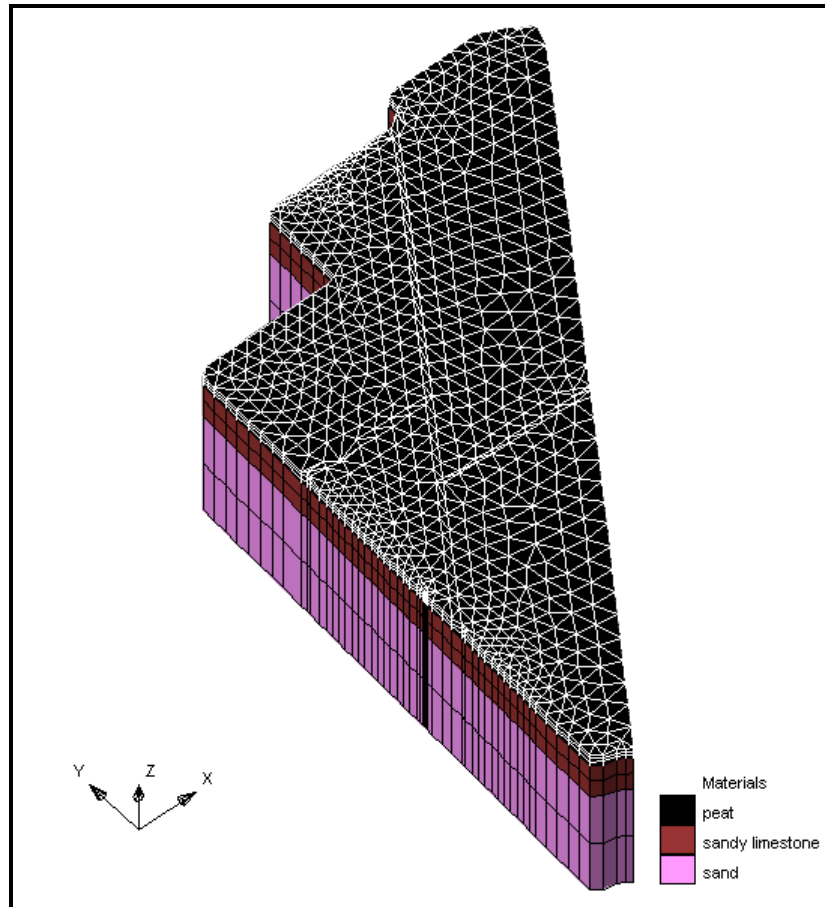


Figure 5-4: Finite Element Meshes for ENR Basin with Soil Types

5.6 Model Calibration and Validation

The integrated model was calibrated and validated with both historic stage and groundwater level data. Theoretically, most model parameters in a physics-based model are measurable physical properties and can be estimated through field studies. The ENR field studies (e.g. Harvey et al., 2002 and SFWMD, 2000) provided the physical range for saturated hydraulic conductivity and the Manning's roughness coefficient. However, due to spatial heterogeneity and limited sampling sites, minimum model calibration is still

needed to better capture historic trends and this represent the averaging and upscale uncertainty from point sampling to element level.

The split sample approach was used to calibrate and validate the ENR model. The time period from 7/1/1998 to 12/31/1998 was used for model calibration and the period from 1/1/1998 to 6/30/1998 was used in model validation. The model parameters used in model calibration were the Manning's roughness coefficient for overland flow and the hydraulic conductivity for subsurface flow. The initial conditions for model calibration and validation were estimated from observed surface water levels, flow rate and groundwater levels.

The model performance was judged by mean error, absolute mean error, and root mean square error, R^2 and U^2 , between observed and computed time-series stages and groundwater levels.

5.7 Model Simulation Results

The preliminary model simulation results (from 1/1/1998 to 12/31/1998) are presented and discussed as follows. The average hydraulic conductivity values from field studies (Table 5-1) were used for subsurface flow and no adjustment has been made. The adjusted Manning's roughness coefficients ranged from 0.3 to 0.9 for different vegetations.

5.7.1 Surface water flow

G250 inflow pumping mainly controlled two-dimensional overland flow conditions. Rainfall and evapotranspiration were a small part of the water budget. The spatial distribution of vegetation and the flow distribution among treatment cells are important factors.

The comparison of computed and observed surface water levels at the center of each treatment cell was shown in Figures 5-5 to 5-8. The variation in water levels in both flow ways was captured quite well for Cell 1 (ENR101), Cell 2 (ENR203), Cell 3(ENR301) and Cell 4 (ENR401). The R^2 values for these four locations were between 0.48 and 0.86. The mean absolute error and mean error values were relatively small for the simulation period (Table 5-2). Water levels at ENR301 are underestimated by 0.1 m. This can be attributed to the combined impact of seepage loss and downstream boundary over-drain (G251 pumping).

In Table 5-2, U^2 is Theil's inequality coefficient is defined by

$$U^2 = \frac{\sum_{i=1}^N (\Phi_F(t_i) - \Phi_M(t_i))^2}{\sum_{i=1}^N (\Phi_M(t_i))^2} \quad (1)$$

where $\Phi_M(t)$ and $\Phi_F(t)$ denote the model's prediction and field data as functions of time t , respectively. If the coefficient is equal to 0 it means that the model is perfect in its prediction and if the coefficient is equal to 1 it means that the model is not reliable.

Table 5-2. Summary of Simulation errors in Surface Water Levels

Location	Mean error (cm)	Mean absolute error (cm)	RMSE (cm)	R ²	U ²
ENR101	2.93	3.82	0.48	0.88	1.78E-4
ENR203	4.03	6.30	0.86	0.50	5.72E-4
ENR301	-11.11	11.16	1.37	0.59	1.54E-3
ENR401	4.59	6.87	0.85	0.58	5.59E-4

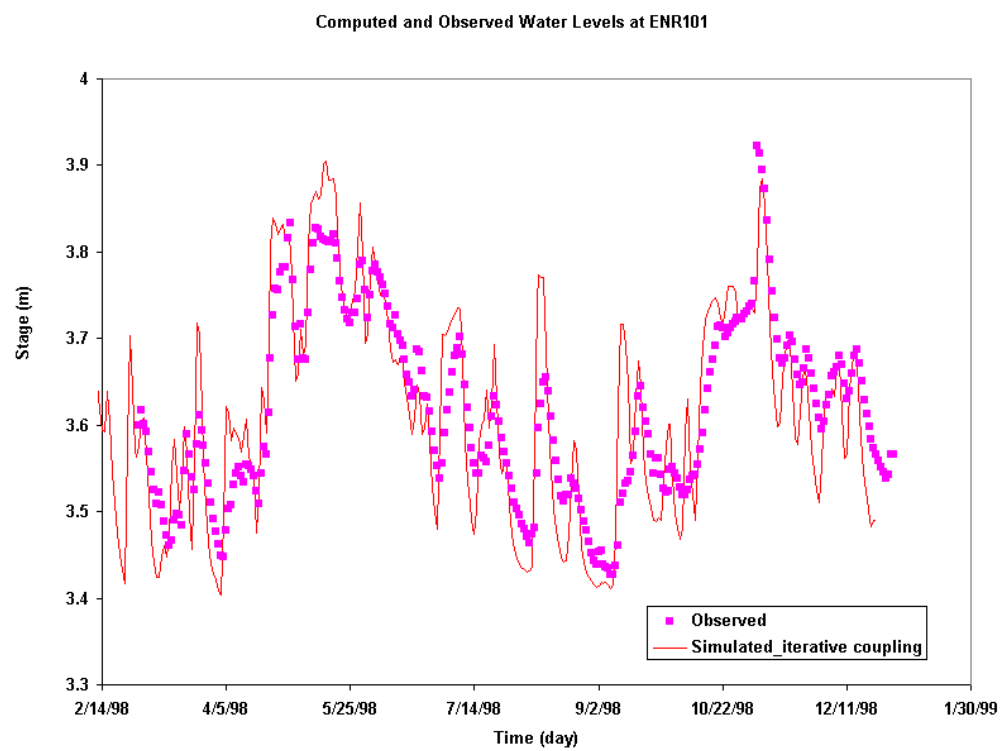


Figure 5-5: Simulated and Observed Surface Water Levels at ENR101

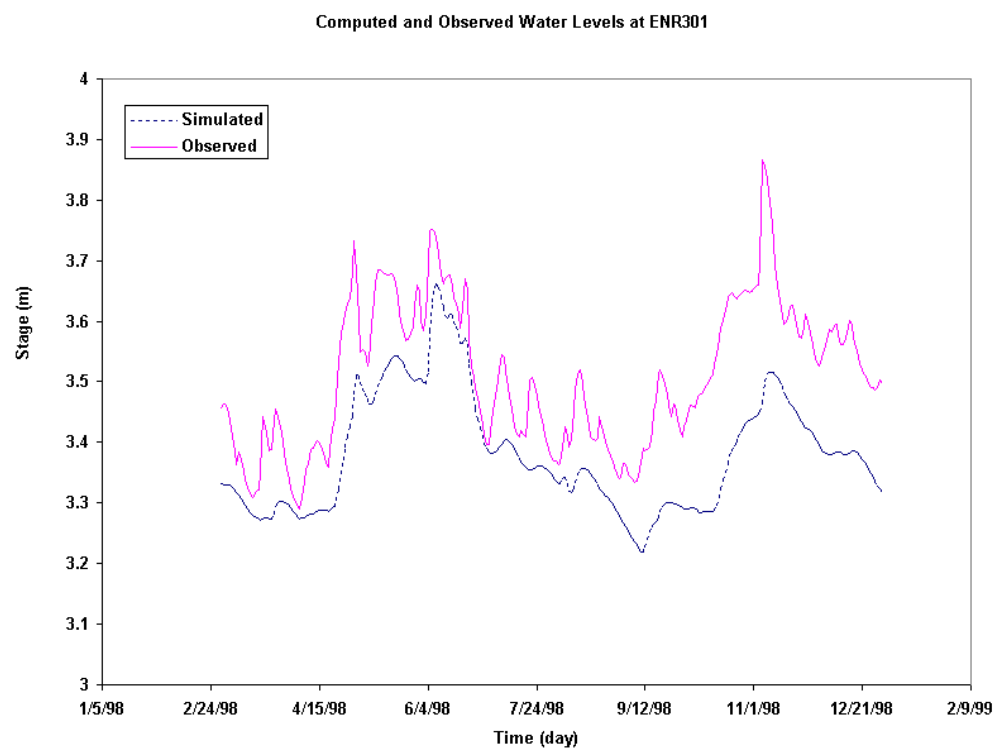


Figure 5-6: Simulated and Observed Surface Water Levels at ENR301

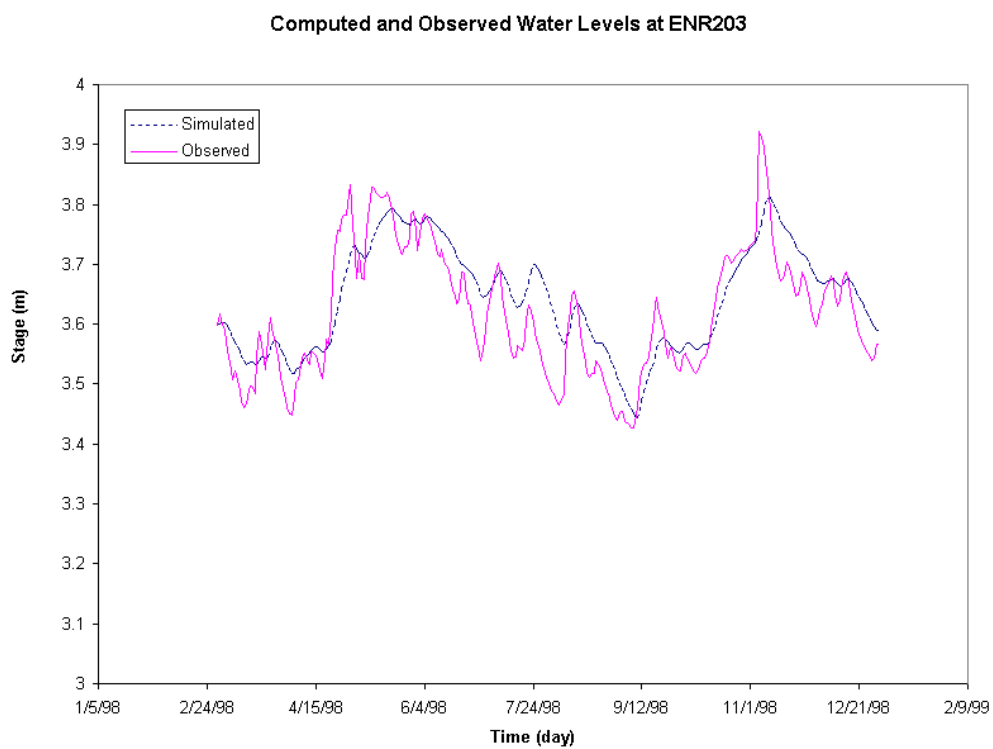


Figure 5-7: Simulated and Observed Surface Water Levels at ENR203

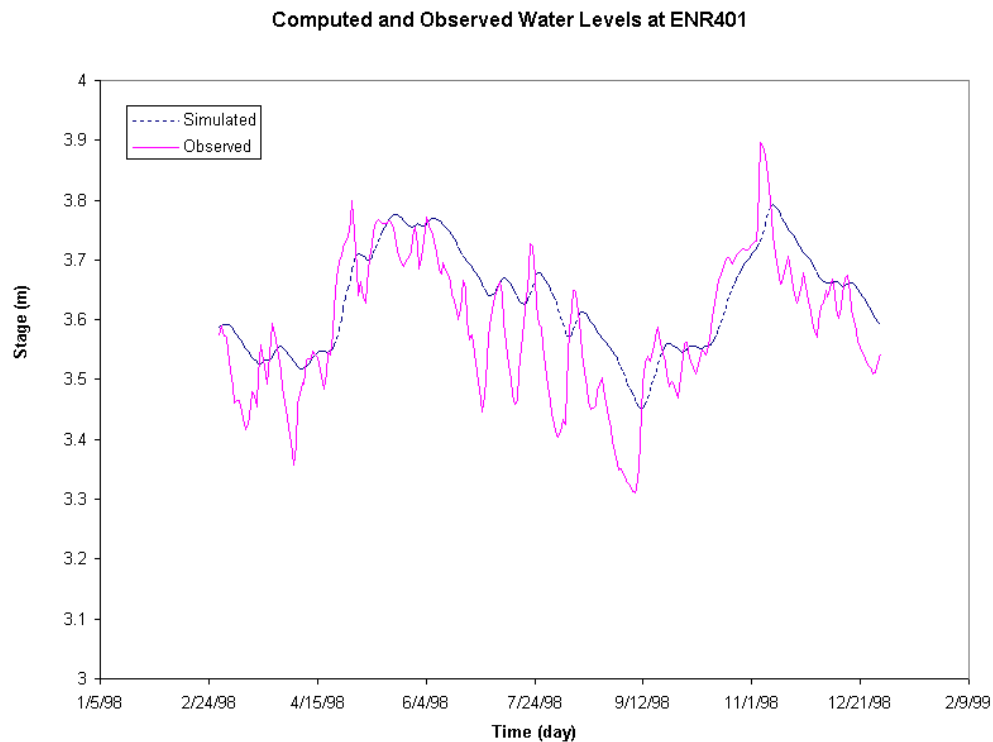


Figure 5-8: Simulated and Observed Surface Water Levels at ENR401

5.7.2 Subsurface Flow

The observed and computed groundwater levels at ENR102GW, ENR204GW, ENR401GW and ENR303GW are compared in Figures 5-9 through 5-12. The simulation results are similar to those of surface water levels. The average absolute error was less than 8.5 cm. The simulation errors are summarized in Table 5-3.

Table 5-3. Summary of Simulation errors in Groundwater Levels

Location	Mean error (cm)	Mean absolute error (cm)	RMSE (cm)	R ²	U ²
ENR102GW	7.30	7.60	0.85	0.84	5.69E-4
ENR203GW	2.74	6.33	0.80	0.51	4.92E-4
ENR303GW	1.30	6.5	0.66	0.52	5.70E-4
ENR401GW	6.40	8.20	1.01	0.49	7.89E-4

The unsaturated zone was thin and localized during the simulation period. During the dry season, a large portion of the surface area could dry up and soil moisture could be less than saturated; under this flow condition, use of the Richards equation for variably saturated subsurface flow in the model is justified. As a matter of fact, previous SFWMD STA water budget studies (Huebner, 2001) applied a regression equation to account for soil water storage during dry seasons.

The total head distribution on 2/4/1998 was plotted in Figures 5-13 through 5-15. The simulated flow pattern of subsurface flow is consistent with field studies.

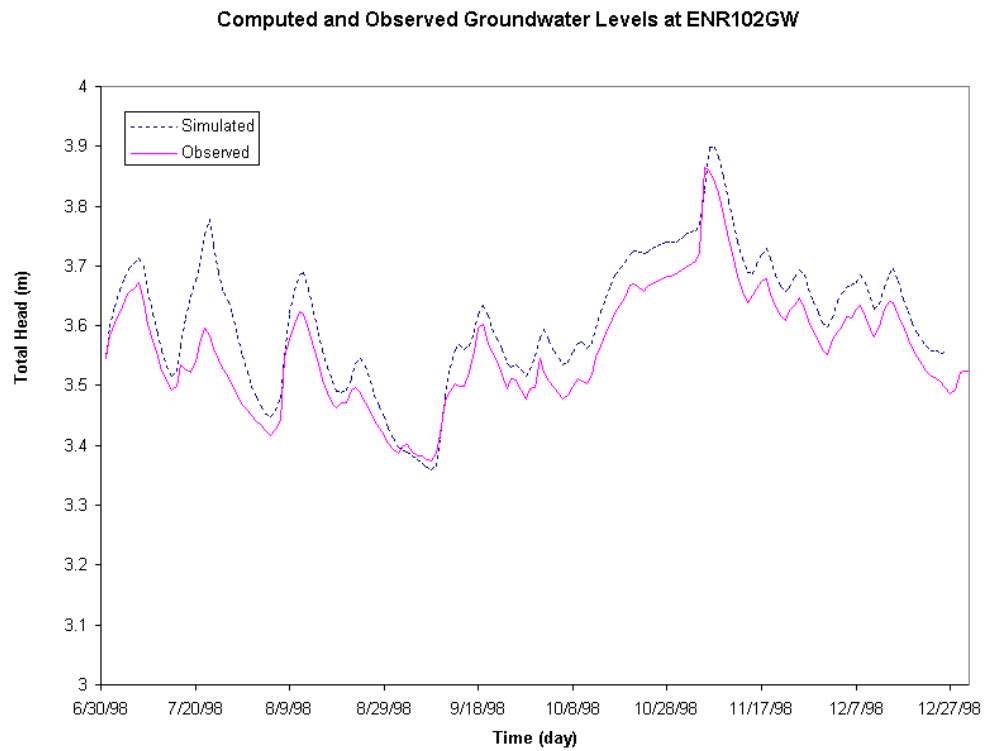


Figure 5-9: Simulated and Observed Groundwater Levels at ENR102GW

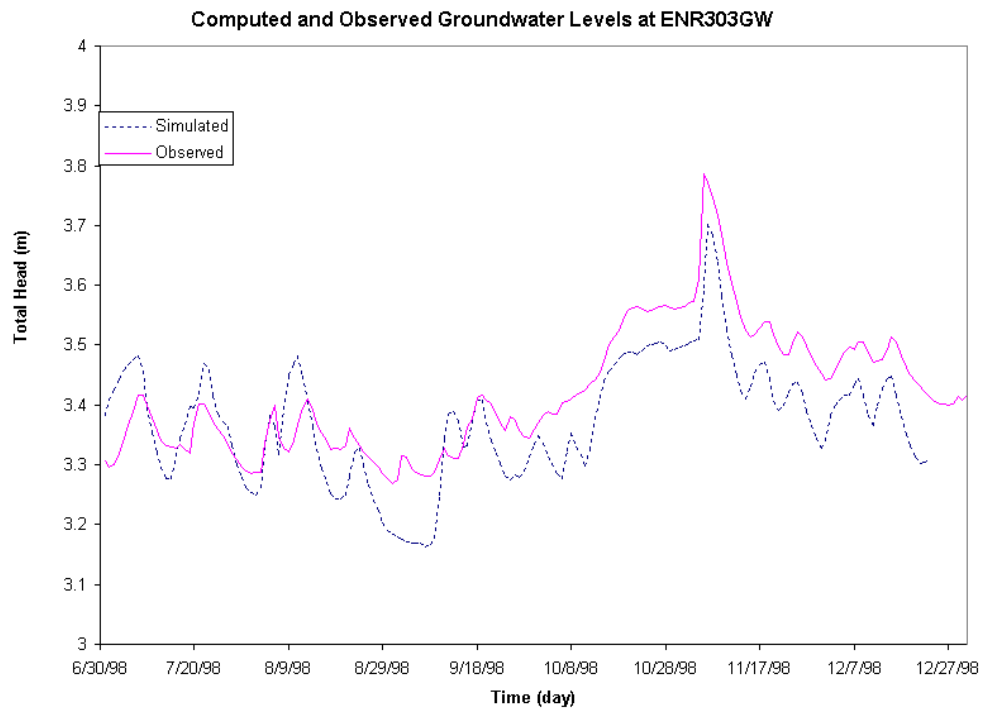


Figure 5-10: Simulated and Observed Groundwater Levels at ENR303GW

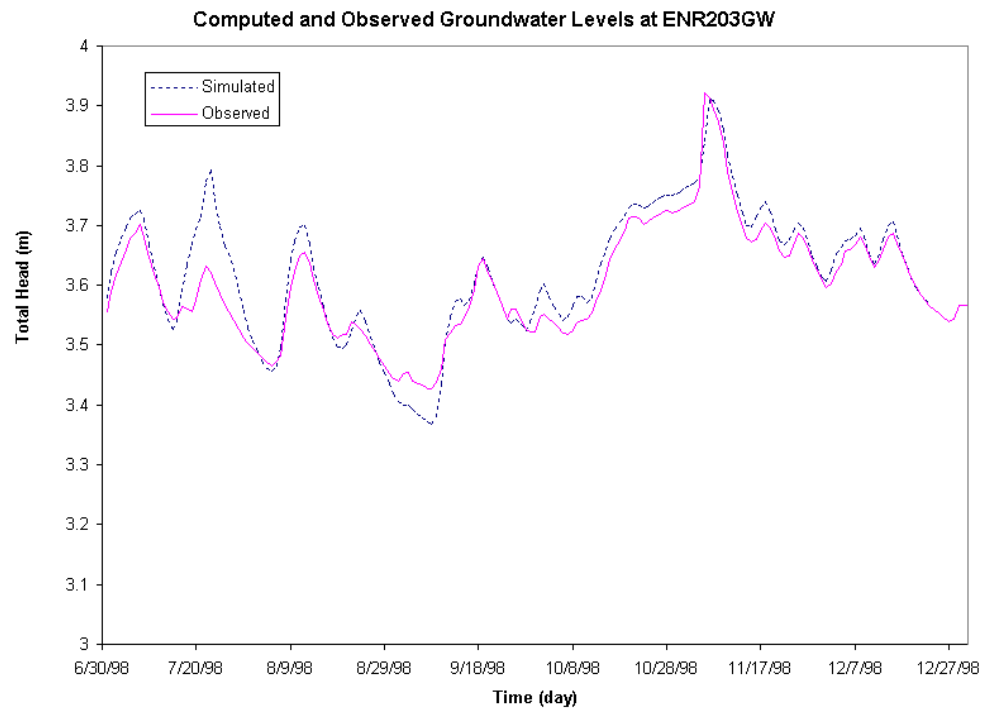


Figure 5-11: Simulated and Observed Groundwater Levels at ENR203GW

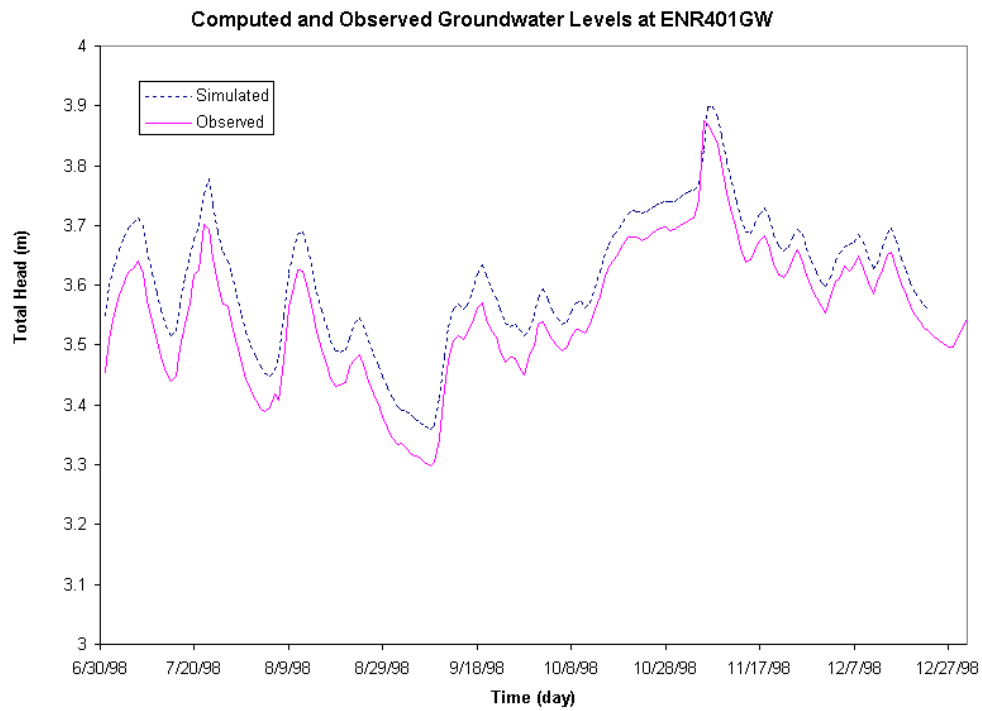


Figure 5-12: Simulated and Observed Groundwater Levels at ENR401GW

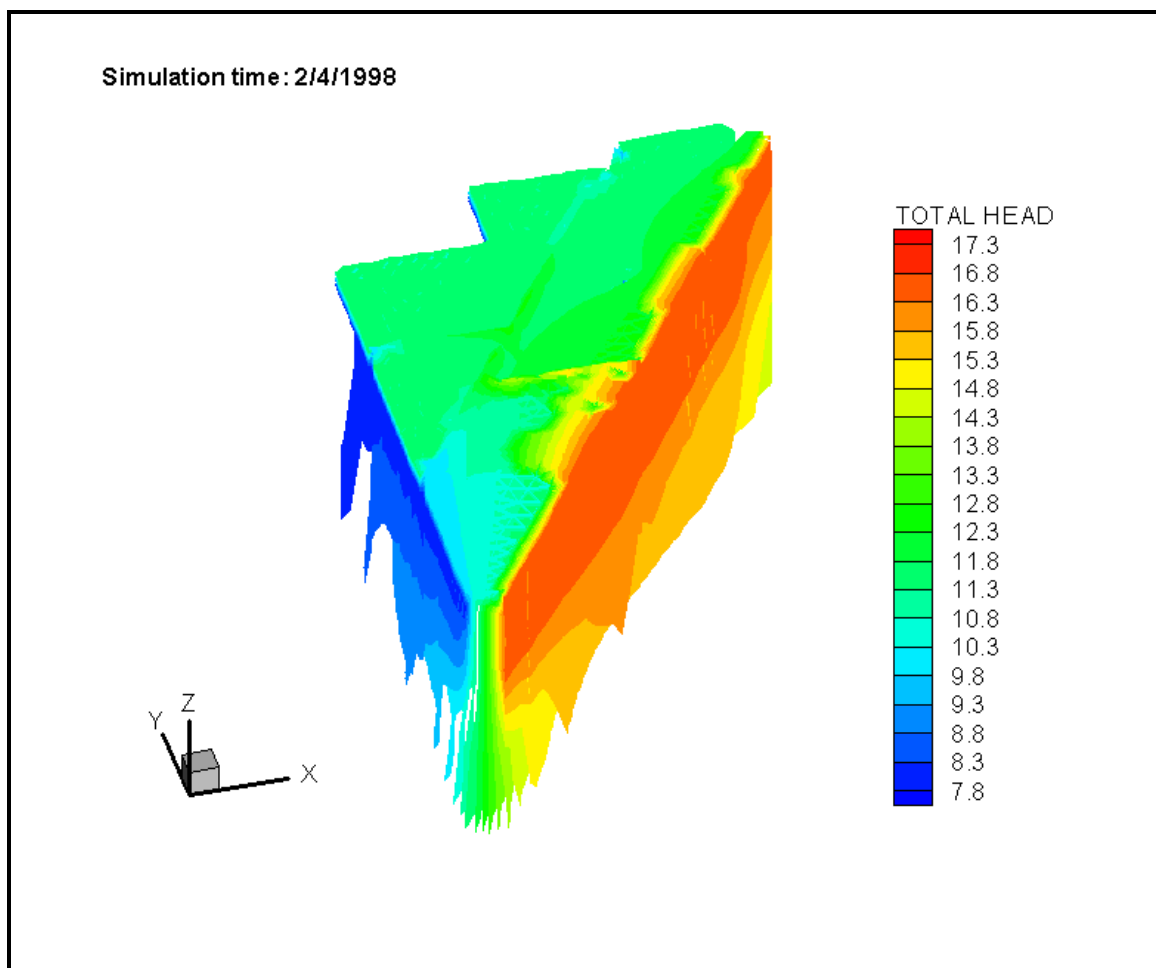


Figure 5-13: Simulated Total Head Distribution (ft NGVD) on 2/4/1998.

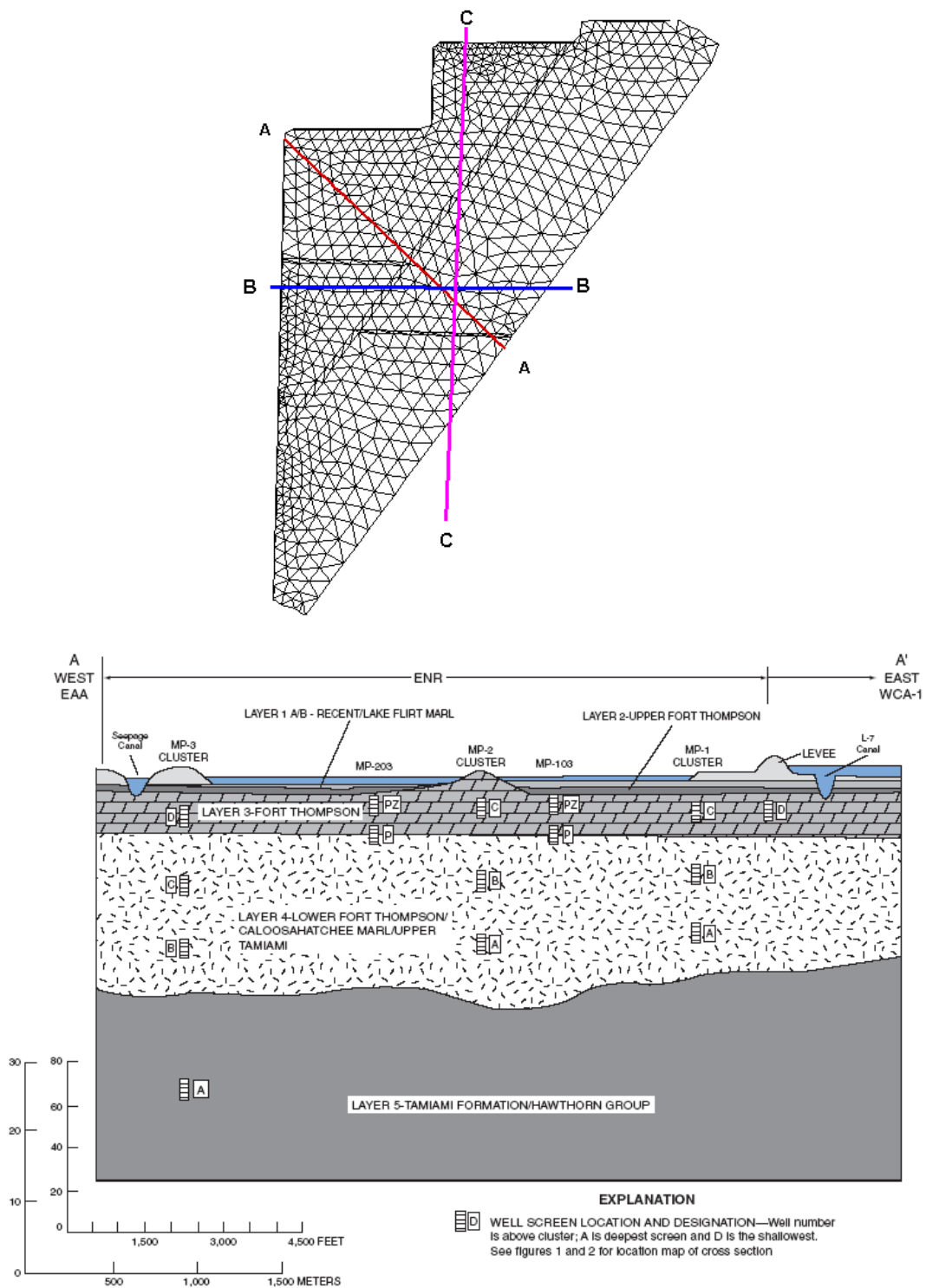


Figure 4. Lithostratigraphic cross section with formation names, Everglades Nutrient Removal (ENR) project, north-central Everglades, south Florida.

Figure 5-14: Location of Transects and Lithology of ENR (after Harvey et al., 2002)

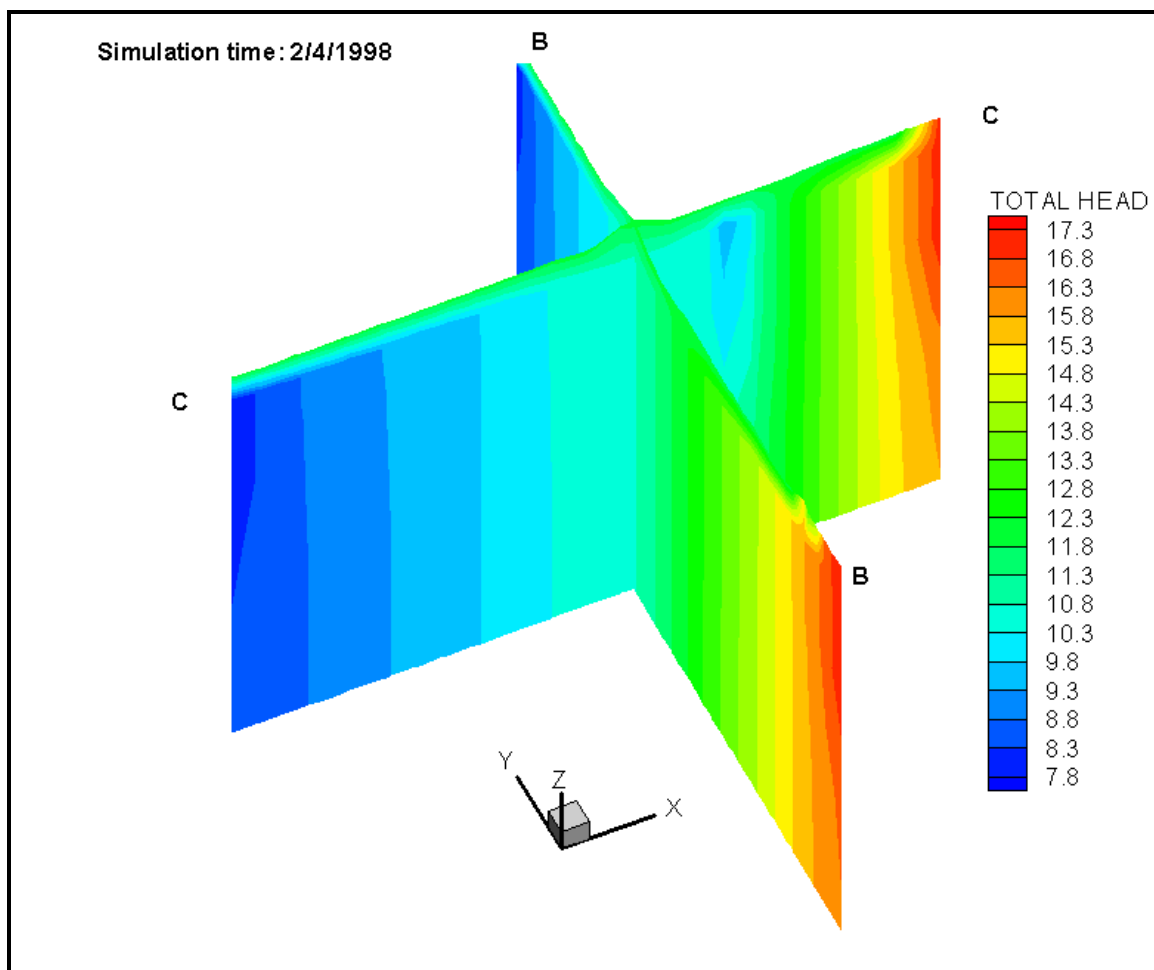


Figure 5-15: Total Head Distribution (2/4/1998) for two transects of ENR (ft NGVD).

5.7.3 Exchange Fluxes

The vertical exchange fluxes between surface water and subsurface water flows were obtained as part of the model simulation (Figure 5-16). The spatial distribution of the vertical fluxes was generally consistent with field observations of vertical hydraulic gradients distribution (Harvey et al., 2002). Groundwater discharge occurred only in the areas along the eastern boundary (L-7 canal) and groundwater recharge (infiltration of overland water) was significant along the seepage canal. Furthermore, the computed

vertical flux values ranged from -0.75 cm/day to 2.0 cm/day. These values are within the range of seepage-meter measurements during 1997-1998 at the ENR site that is documented by Harvey et al. (2002).

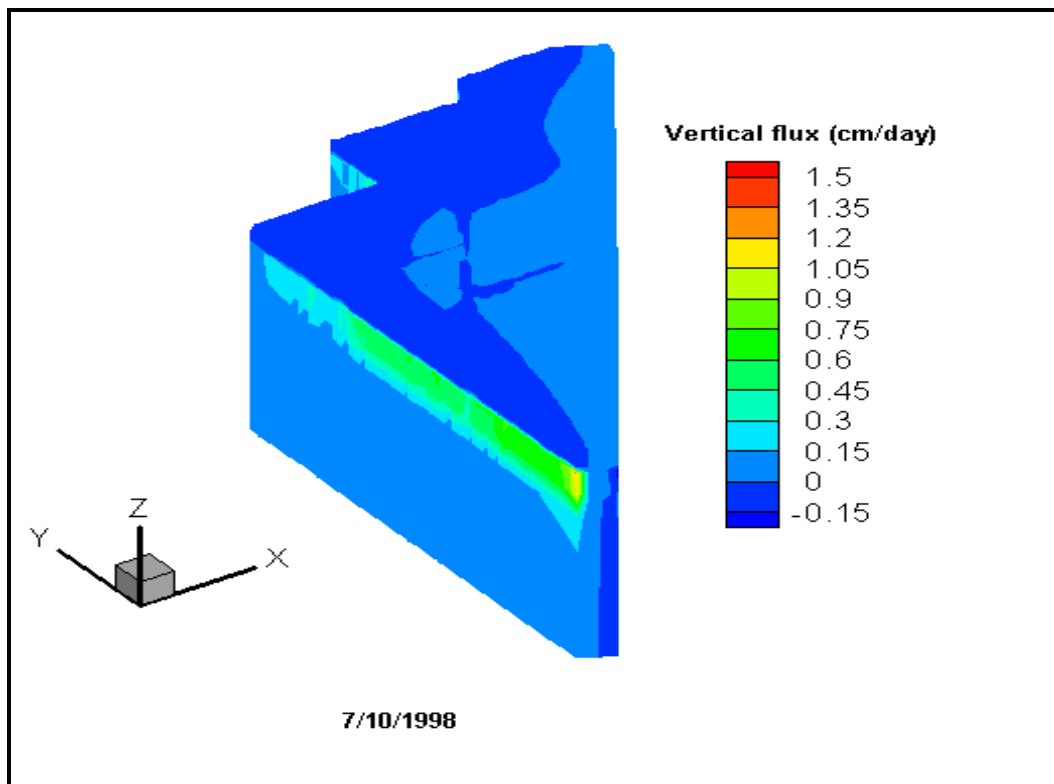


Figure 5-16: Distribution of Computed Vertical Flux (cm/day) (7/10/1998)

5.8 Discussions

Unlike some other similar integrated models, the coupling and exchange fluxes were not based on the assumption of interface discontinuity and leakage coefficient. Both continuity of pressure head and exchange flux were imposed; this avoided the calibration of the empirical leakage coefficients for overland/subsurface and canal/subsurface interfaces necessary in other models. The weak permeable peat that

restricts vertical subsurface flow was part of the subsurface domain. The model simulation results in term of surface water levels, groundwater table, exchange fluxes, etc. demonstrate that this coupling approach is aligned to the physical processes of the ENR hydrology.

Details, in terms of variables such as vegetation type, local remnant ditches in the marsh, culvert flow computation, etc., could more accurately model two-dimensional overland flow. A dynamic wave model of overland flow, to replace the diffusion wave approximation and the use of high-resolution time series data (e.g. 15 minute observed data instead of daily average data used in current model simulations), may better simulate the high-frequency dynamic variation. Although the simulation results show that diffusion wave approximation is sufficient for overland flow.

5.9 Summary and Conclusions

A physics-based, integrated model was developed to simulate complex hydrologic processes in a constructed wetland. The surface water and groundwater interactions were simulated by coupled two-dimensional overland flow and three-dimensional subsurface flow. Minimum model calibrations, combined with model parameters estimated from field studies were able to reproduce major trends in historic surface and groundwater levels. And the model provides details spatial distribution of state variables and fluxes.

Acknowledgements

The background information of STA-1W was provided by SFWMD through the contract with Sutron Corporation (C-15988-WO04-05). The second author is supported by the U.S. EPA - Science To Achieve Results (STAR) Program under Grant # R-82795602 with the University of Central Florida.

References

- Abtew, W. 1996. Evapotranspiration measurements and modeling for three wetland systems in South Florida. *Journal of the American Water Resources Association* 32: 465-473.
- Abtew, W. and J. Obeysekera. 1995. Lysimeter study of evapotranspiration of cattails and comparison of three estimation methods. *Transactions of the ASAE* 38: 121-129.
- Feng K. and Molz F.J. 1997. A 2-D, diffusion-based, wetland flow model. *Journal of Hydrology*. 196 (1997) 230–250.
- Fish, J.E., 1988, Hydrogeology, aquifer characteristics, and ground-water flow of the Surficial Aquifer system, Broward County, Florida: U.S. Geological Survey Water Resources Investigations Report 87-4034, 92 p.

Guardo, M. 1999. Hydrologic balance for a subtropical treatment wetland constructed for nutrient removal: *Ecological Engineering*, V. 12, P. 315-337.

Guardo M. and Tomasello, R.S., 1995. Hydrodynamic simulations of a constructed wetland in south Florida: *Water Resources Bullrtin*, v. 81, no.4, p. 687-701.

Huebner, S.R., 2001. Water Budget analysis for stormwater Treatment area 6, section 1, Technical Publication EMA #391. South Florida Water Management District, West Palm Beach, FL. February 2001.

Harvey, J.W., et. Al, 2002, Interactions between Surface Water and Ground Water and Effects on Mercury Transport in the North-central Everglades: U.S. Geological Survey Water Resources Investigations Report 02-4050, 91 pages.

Langevin C., Swain E., and Wolfert M., 2005. Simulation of integrated surface-water/ground-water flow and salinity for a coastal wetland and adjacent estuary. *Journal of Hydrology*. Volume 314, Issues 1-4, 25 November 2005, Pages 212-234.

South Florida Water Management District (SFWMD), 2000. 2000 Everglades Consolidated Report, Chapter 6: Stormwater Treatment Areas. West Palm Beach, FL

SFWMD. 2005. DBHYDRO: <http://www.sfwmd.gov/org/ema/dbhydro/index.html>

Thompson J.R., H. Refstrup Sørensen, H. Gavin, A. Refsgaard. (2004). Application of the coupled MIKE SHE/MIKE 11 modelling system to a lowland wet grassland in southeast England. *Journal of Hydrology*. 293 (2004) 151–179.

Swain E.D., Melinda A. Wolfert, Jerad D. Bales, and Carl R. Goodwin, 2004. Two-Dimensional Hydrodynamic Simulation of Surface-Water Flow and Transport to Florida Bay through the Southern Inland and Coastal Systems (SICS). U.S. Geological Survey Water-Resources Investigations Report 03-4287, 2004.

Wu F., Shen H.W. and Chou Y. , 1999. Variation of Roughness Coefficients for Unsubmerged and Submerged Vegetations., ASCE Journal of Hydrologic Engineering, Vol. 125, No. 9, September 1999.

Yeh, G.T., G. B. Huang, H. P. Cheng, F. Zhang, H. C. Lin, E. Edris, and D. Richards. 2006. Chapter 9: A first principle, physics-based watershed model: WASH123D, in *Watershed Models*. Eds. By Singh VP and Frevert, CRC Press, Boca Raton, FL.

Yen, B. C., 1992. "Hydraulic resistance in open channels." *Channel flow resistance: Centennial of Manning's formula*, B. C. Yen, ed., Water Resources Publications, Littleton, Colorado.

Chapter 6

Summary and Conclusions

Several critical issues in the development of a first principle, physics-based watershed model are presented in this thesis.

Firstly, the implementation of all options of dynamic wave, diffusive and kinematic wave models for surface flow in a single model code are used to investigate the applicability and accuracy of diffusion and kinematic wave approximation and from numerical experiments, it is concluded that the use of kinematic wave model should be limited to steep-slope mountainous watersheds and where downstream conditions are not important; The accuracy of diffusion wave under very mild slope is not guaranteed as flow dynamics and downstream boundary may play a key role; The dynamic wave model should be mandated for strong dynamic flow cases (e.g., dam break type flow), and when momentum fluxes are important compared to gravity force.

Secondly, the numerical solution of the fully dynamic wave model of two-dimensional overland flow is difficult. The detail and capability of a characteristics-based finite element method is discussed and demonstrated with several typical examples. Numerical simulation of a dam break problem demonstrates the numerical solution is sensitive to the choice of wave characteristic directions.

Thirdly, physics based coupling of surface water and subsurface flow is at the core of a physics-based, integrated watershed model; different combinations of coupling schemes are discussed and compared, and physics-based coupling approaches are favored. The inaccuracy and error of time-lagged, decoupled approach are demonstrated in several test examples.

Finally, the performance of the watershed model in the integrated modeling of a local-scale, field application was demonstrated through the study of surface water and groundwater interactions in a constructed wetland in south Florida.

Further work includes (1) a thorough, formal theoretical analysis of diffusive and kinematic wave approximations under two-dimensional overland flow condition; (2) full scale, rigorous test of the new integrated watershed model for hydrologic processes in a natural experiment watershed with research quality field data; (3) expand the subsurface flow module to include preferential flow in macro-pores and discrete fractures; (4) fully couple with the mechanistic based water quality and sediment transport module.

VITA

Guobiao Huang

Education

Ph.D. Civil Engineering, Pennsylvania State University, 2006
M.S. Water Resources Engineering, Hohai University, 1990
B.S. Water Resources Engineering, Tsinghua University, 1987

Professional Experience

June 2003 – present Senior Water Resources Engineer, Sutron Corporation, West Palm Beach, FL
June 2002 – June 2003 Hydrologic Modeler, Science Applications International Corporation, Miami, FL
Jan 2001 – May 2002 Graduate Research Assistant, Department of Civil and Environmental Engineering, University of Central Florida, FL
June 1999 – Dec 2000 Graduate Research Assistant, Department of Civil and Environmental Engineering, Pennsylvania State University, PA
Aug 1990 – May 1999 Senior Engineer (after 1995), Nanjing Research Institute of Hydrology and Water Resources, Ministry of Water Resources, Nanjing, China

Selected Publications

Gour-Tsyh Yeh and Guobiao Huang, Hwai-Ping Cheng, Fan Zhang, Hsin-Chi Lin, Earl Edris and David Richards. 2005. "A first principle, physics based watershed model: WASH123D", chapter 9 in the book: Watershed Models, eds. by Vijay Singh and Donald Frevert, CRC Press, Boca Raton, FL. September 2005.

Guobiao Huang, Gour-Tsyh Yeh, "Modeling coupled surface water and groundwater flows from storm events using WASH123D", Proceedings of the 1st annual stormwater management research symposium at Orlando, Florida, p.107-117. October 2004.

Guobiao Huang and Gour-Tsyh Yeh, 2002. "Numerical Simulation of Surface runoff with Coupled Two- Dimensional Overland Flow and One-Dimensional Stream Network Flow", proceedings of the XIV International Conference on Computational Methods in Water Resources (CMWR2002), Netherlands. June 2002.

Guobiao Huang and Gour-Tsyh Yeh, "Development of a Numerical Watershed Model", Proceedings of the XIII International conference on Computational Methods in Water Resources (CMWR2000), Calgary, Canada, June 2000.